Periodic Brake Orbits in the N-Body Problem

A THESIS
SUBMITTED TO THE FACULTY OF THE GRADUATE SCHOOL
OF THE UNIVERSITY OF MINNESOTA
BY

Nai-Chia Chen

IN PARTIAL FULFILLMENT OF THE REQUIREMENTS
FOR THE DEGREE OF
DOCTOR OF PHILOSOPHY

Richard Moeckel, Advisor

August, 2014

Acknowledgements

My deepest thanks go to my advisor, Prof. Richard Moeckel. I thank him for being a great teacher, who answers my questions patiently, explains things in a way that I can understand, and gives me many insightful ideas. Besides his brilliance, his liberality and great sense of humour make working with him a pleasure. I also thank him for promptly reading my writings and providing helpful suggestions for my first conference presentation.

I am indebted to Prof. Richard Montgomery, who has been generous with his ideas and time. From him, I've learned to not be afraid to ask questions. I also thank him for his hospitality during my short visit to Santa Cruz and his help in my job application.

I thank Prof. Richard McGehee, who welcomed me with a Gopher sticker on the orientation day and has shown genuine care to all students in our program. I also thank him for vividly telling the story of Poincaré and the three body problem in a real analysis class that aroused my interest in history.

I thank Professors Richard McGehee, Peter Poláčik, and Peter Rejto for serving in my thesis committee.

I thank Prof. Kuo-Chang Chen for introducing the N-body problem to me and making my study abroad possible.

I thank Ms. Bonny Fleming for her personal warmth and for taking care of my paperwork. I thank Ms. Diane Trager and Ms. Jan Minette for handling my mails.

Finally, I thank my family and my husband for their constant love and support.

Abstract

The thesis is devoted to finding periodic brake orbits in the N-body problem. We consider certain subsystems of the N-body problem that have two degrees of freedom, including the isosceles three-body problem and other highly symmetric sub-problems. We prove the existence of several families of symmetric periodic orbits, including "Schubart-like" orbits and brake orbits, by using topological shooting arguments.

Contents

List of Tables

List of Figures

Chapter 1

Introduction

In this chapter, we introduce the N-body problem and some of its fundamental questions. Then we explain the motivation and results of our thesis research.

1.1 The N-Body Problem

The (Newtonian) N-body problem concerns the motion of N particles moving in $\mathbf{R}^3$. The motion of these particles are governed by the Newton's law of gravitation. Let $m_i > 0$ denote the masses and $\mathbf{q}_i \in \mathbf{R}^3$ the positions of the particles, then the equation of motions can be written as

$$m_i \ddot{\mathbf{q}}_i(t) = \sum_{j \neq i}^{N} m_i m_j \frac{\mathbf{q}_j - \mathbf{q}_i}{|\mathbf{q}_j - \mathbf{q}_i|^3}, \quad 1 \leq i \leq N. \tag{1.1}$$

Another way to write the equations of motion is the Hamiltonian formulation of the N-body problem. Let $\mathbf{p}_i := m_i \dot{\mathbf{q}}_i \in \mathbf{R}^3$, $\mathbf{q} = (\mathbf{q}_1, \mathbf{q}_2, \cdots, \mathbf{q}_N) \in \mathbf{R}^{3N}$, $\mathbf{p} = (\mathbf{p}_1, \mathbf{p}_2 \cdots, \mathbf{p}_N) \in \mathbf{R}^{3N}$, and

$$H(\mathbf{q}, \mathbf{p}) = \frac{1}{2} \mathbf{p}^T M^{-1} \mathbf{p} - U(\mathbf{q}),$$

where $M = \mathrm{diag}(m_1, m_1, m_1, m_2, m_2, m_2, \cdots, m_N, m_N, m_N)$, and

$$U(\mathbf{q}) = \sum_{i<j} \frac{m_i m_j}{|\mathbf{q}_j - \mathbf{q}_i|^3}.$$

The Hamilton's differential equations are:

$$\begin{aligned} \dot{\mathbf{q}} &= M^{-1}\mathbf{p} \\ \dot{\mathbf{p}} &= \nabla U(\mathbf{q}). \end{aligned} \tag{1.2}$$

In general, given a dynamical system, the ultimate is goal is to classify all possible behaviours of solutions. The following questions are fundamental and arise immediately:

(Q1) How far can one reduce the number of equations, by using symmetries or constant of integrals? How many integrals does the system have?

(Q2) Is the flow complete? In other words, do solutions exist for all time?

(Q3) Can we locate the landmarks in the phase space: equilibrium points, periodic orbits, and other invariant sets?

For $N = 2$, the two-body problem can be reduced to the Kepler's problem, a completely integrable system. The solutions of the two-body problem can be expressed analytically: when viewed in the center of mass frame, which is an inertia frame, the trajectories of the two bodies are two similar conic sections—circles, ellipses, parabolas, and ellipses.

The cases $N \geq 3$ are far more complicated than the two-body problem. Here we briefly discuss the three questions listed above.

Reduction: Without any reductions, the dimension of the N-body equation (1.2) is $6N$; it is too many to work on. Fortunately, the N-body problem possesses ten well-known integrals: three from the total linear momentum $\sum \mathbf{p}_i$, three from the linear motion of the center of mass $\sum m_i\mathbf{q}_i - t\mathbf{p}_i$, another three from the angular momentum $\sum \mathbf{q}_i \times \mathbf{p}_i$, and one from the energy function $H(\mathbf{q}, \mathbf{p})$. Bruns proved the non-existence of any other algebraic integrals [5].

Non-completeness of the flow: We say that a solution experiences a singularity at time $t = t_{max} < \infty$ if the solution can not be extended beyond t_{max}. Observe that the equation (1.1) is not defined when $\mathbf{q}_i = \mathbf{q}_j$ for some $i \neq j$, which represents the collision of the i-th and j-th masses. More or less trivially, collisions may occur in finite time, and therefore the flow is not complete. What about solutions without collisions? Can they experience singularities as well? A theorem of von Zeipel [21]

showed the only possible non-collision singularities occur when the moment of inertia (a measurement of the size of the configuration) of a solution approaches infinity as time approaches t_{max}. Whether non-collision singularities exist is far from trivial. In 1897, Painlevé proved that non-collision singularities do not exist in the three-body problem [30]. In 1974, Mather and McGehee proved the existence of solutions in the collinear four-body problem that become bounded in finite time after the occurrence of infinitely many binary collisions [20]. In 1988, Xia constructed the first example of non-collision singularities in the spatial five-body problem [48]. The existence of non-collision singularities in the four-body problem remains an open problem.

Invariant sets: There is no equilibrium point in the N-body problem. As for periodic orbits, finding them is an active research topic. Already known in 1763, Euler's collinear solution consists of three masses moving along confocal ellipses, while the three masses are always collinear. Another famous solution to the three-body problem is Lagrange's equilateral solution, in which the configuration of the three masses always forms an equilateral triangle with varying size. Both Euler's and Lagrange's solutions belong to a class of periodic solutions, namely **relative equilibria**. Relatively equilibria are the simplest periodic orbits, yet we know very little about the number of relative equilibria, counted up to rotations, translations and dilations; in fact, Smale included the following question in his list of problems for the 21st century [44]: "*Given positive real numbers $m_1, m_2, \cdots, m_n$ as the masses in the n-body problem of celestial mechanics, is the number of relative equilibria finite?*" Hampton and Moeckel in 2006 proved that the number of the class of relative equilibria is finite for the case $N = 4$ [15]; Albouy and Kaloshin in 2008 proved the finiteness in the planar problem for generic choices masses for the case $N = 5$ [1]. The problem is still wide open for the case $N > 5$.

Besides the relative equilibrium solutions, many periodic solutions in the N-body problem have been found by using various mathematical techniques. Classical methods include continuation, averaging, normal forms, majorants, fixed-point theorems, and symbolic dynamics; see Poincaré [31], Moser [29], Lyaupunov [17], Siegel [38], Schmidt [36], Birkhoff [2], Meyer [23], and many others. Another approach, the calculus of variation, has made a breakthrough progress in the recent fifteen years. Two pioneering works are Chenciner-Venturelli's "hip-hop" orbits [10] and Chenciner-Montgomery's figure-eight orbit [9]. First numerically discovered by C. Moore, the figure-eight orbit is

a periodic orbit consists of three masses chasing each other along a eight-shape curve. Chenciner and Montomery's work opens an industry of finding (choreographic) periodic solutions to the N-body problems; for example, see Simo [43], Ferrario-Terracini [14], Chen [6], and many others.

1.2 Motivation and Results

This thesis will focus on finding a special type of periodic orbits—the so called **periodic brake orbits**—in the N-body problem. A solution to the N-body problem is called a **brake orbit** if the initial velocities of all masses are zero. There are abundant reasons that brake orbits appeal to us. Here we list four of them:

The first motivation comes from the reminiscences of our early science classes. We recall that, under the assumption of conservation of energy, dropping a ball without giving it any initial velocity, the ball will hit the ground, bounce back, and resume its initial state, leading to periodic motion. We ask the question for the N-body problem: dropping N bodies with zero initial velocities—what can happen? For N=2, as will be shown in Chapter 2, every brake orbit in the two-body problem is periodic, if we allow bodies to bounce back after collisions. What about the case $N \geq 3$?

Second, a naive and numerical way to search for periodic orbits is to use a numerical N-body integrator, which allows the users to enter arbitrary masses, initial positions, and initial velocities of the bodies, to simulate the evolution of orbits. Provided with such an integrator and very little knowledge about how to select initial velocities properly (such that they lead to periodic orbits), the simplest way to select initial velocities is perhaps to set them equal to zero. We are curious about whether this is a feasible way to obtain periodic orbits. Do periodic orbits with zero-initial velocities even exist?

Third, brake orbits have played a significant role in the study of Hamiltonian systems. Besides the celebrated Lyapunov center theorem, theorems about the existence of periodic orbits have been lacking. According to a survey on periodic solutions of Hamiltonian systems by Rabinowitz, "*the first work we know of (about the existence in the large of periodic solutions) in a global setting is due to Seifert.*"[32]. Published in 1948, Seifert's pioneering work proved the existence of periodic solutions in a class of Hamiltonian systems in a fixed energy level surface. (While he did not call these

solutions brake orbits, they are indeed brake orbits; it was Ruiz who coined the term brake orbit [35].) Subsequent work that generalizes Seifert's to a wider class of Hamiltonian systems has been carried on by Weinstein [47], Rabinowitz [33], Bolotin [3], van Groesen [45], Liu and Zhang [16], and others. Their results, however, do not apply to the N-body problem, as they require the energy level surface to be either compact or convex and the Hamiltonian function needs to be at least C^1. We wonder whether periodic brake orbits exist in the N-body problem as well.

The last reason is more involved than the others. An interesting fact, proved by Montogomery, states that, in the three-body problem with zero angular momentum, all but one solution have syzygies [27, 28]. (A "syzygy", also known as an eclipse, means a configuration at which the three masses are collinear.) Furthermore,Moeckel, Montogmery, and Venturelli studied the brake-to-syzygy map; by following solutions with zero initial velocities until a syzygy occurs, they obtained a continuous, flow-induced Poincaré map [24]. A question of interest is: does any of these solutions meet the syzygy set orthogonally? If a solution does meet the syzygy set orthogonally, from symmetry and reversibility of the problem, the solution is a periodic brake orbit.

In a word, we are motivated to to investigate into periodic brake orbits in the N-body problem. A difficulty that we immediately encounter is the large number of variables, even after reduction. Therefore, we will focus on sub-systems of the N-body problems that have only two degrees of freedom, including the isosceles three-body problem and some highly-symmetric N-body problems. Another issue is the occurrence of collisions. Imagine in the two-body problem, two masses are released with zero initial velocities—the two masses attract and move toward each other until they collide. Collisions are unavoidable for brake orbits not only in the two-body problem but also in all the problems that we study. Two types of collisions: regularizable and non-regularizable collisions, occur in our problems; to deal with them, we perform two standard techniques, Levi-Civita regularization and McGehee blow-up transformation, which include changes of variables and a rescaling of time. We then obtain a complete flow in a three-dimensional manifold, called the **energy manifold**.

For the isosceles three-body problem, three subsets of the energy manifold play an important role: the set of brake initial conditions, which is an one-dimensional curve and is called the **zero-velocity curve**; the set of collinear configurations, which is a

two-dimensional plane and abbreviated as the **syzygy plane** herein; and the set of binary collision configurations, which is a two-dimensional plane and abbreviated as the **binary collision plane** herein.

Due to certain symmetries of the flow, a solution that starts at the zero-velocity curve and orthogonally cross the syzygy plane is necessary a periodic brake orbit. A previous paper, "*From brake to syzygy*" by Moeckel, Montgomery, and Venturelli, proves the existence of such solutions by using a topological shooting argument, which shoots from the zero-velocity curve and targets to orthogonally hit the collinear plane [24]. Before reaching the plane of collinear configurations, their solutions cross the binary collision plane only once. Several questions arise naturally: (1) Do there exist brake orbits that cross the binary collision plane multiple times before reaching the syzygy plane? (2) Do there exist brake orbits that non-orthogonally cross the syzygy plane multiple times before orthogonally crossing the syzygy plane? (3) Do there exists brake orbits orthogonally cross the binary collision plane, rather than the syzygy plane? (4) Do there exists periodic orbit cross neither the binary collision plane nor the syzygy plane orthogonally?

We answer the questions proposed affirmatively. As a result, we prove that in the isosceles three-body problem, there exist six infinite families of periodic brake orbits, parametrized by the number of binary collisions. Our method is an extension of the shooting argument used in [24]. We then furthermore generalize our shooting arguments to other highly symmetric N-body problems that share similar properties with the isosceles problem. In addition to periodic brake orbits, we prove the existence of other families of periodic orbits, including the "Schubart-like" periodic orbits.

The thesis is organized as follows. In Chapter 2, we review the well-understood two-body problem, with a focus on the Levi-Civita regularization. In Chapter 3, we look for periodic brake orbits in the isosceles three-body problem; this part has been published in [7]. Finally, in Chapter 4, we extend the technique used in Chapter 3 to other highly symmetric N-body problems; this part has been published in [8].

Chapter 2

Two-Body Problem

The objectives of this chapter are to rigorously treat the collision of two masses, to classify all possible motions in the two-body problem, and to show that every brake orbit in the two-body problem is periodic.

For readers who are familiar with the two-body problem, an intuitive way to think about a brake orbit is to consider it as the limit orbit of its nearby (periodic) elliptic orbits, as shown in figure 2.1. When the eccentricity of the ellipses increases to 1, periodic motion of two bodies degenerates to periodic rectilinear motion. Below, we will use Levi-Civita regularization to legitimately "take the limit".

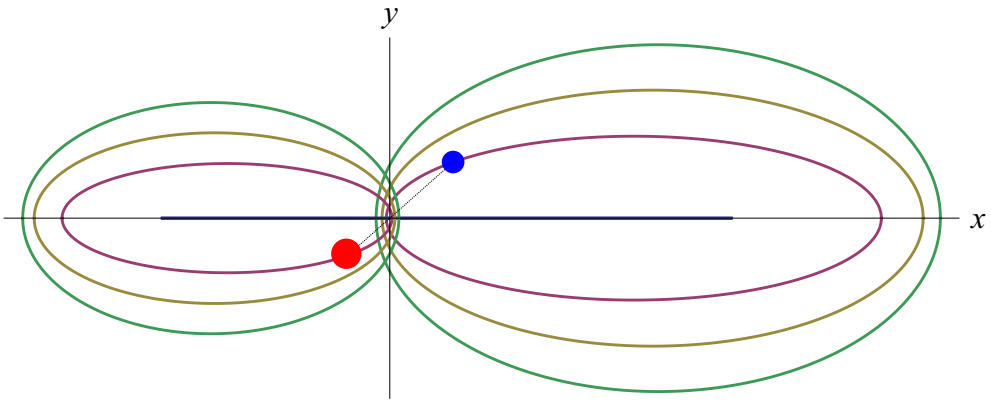

Figure 2.1: Elliptic orbits of the two-body problem: The trajectories of two masses describe two similar ellipses, having a focus at their center of mass.

2.1 Reduction to the Kepler's Problem

The Newtonian two-body problem consists of two point masses $m_1, m_2 > 0$ moving in $\mathbf{R}^3$, with the only force acting on them being their mutual gravitation attraction. Let $\mathbf{r_1}, \mathbf{r_2} \in \mathbf{R}^3$ denote the positions of the masses; then the equations of motion are

$$m_i \ddot{\mathbf{r}}_i(t) = \sum_{j \neq i}^{N} m_i m_j \frac{\mathbf{r}_j - \mathbf{r}_i}{|\mathbf{r}_j - \mathbf{r}_i|^3}, \quad i = 1, 2. \tag{2.1}$$

The two-body problem can be decomposed to two one-body problems as follows. Let $\mathbf{R}(t)$ be the center of masses of m_1, m_2 and $\mathbf{q}(t)$ be the difference vector from $\mathbf{r}_1$ to $\mathbf{r}_2$, i.e.,

$$\begin{aligned} \mathbf{R} &= \frac{m_1 \mathbf{r}_1 + m_2 \mathbf{r}_2}{m_1 + m_2}, \\ \mathbf{q} &= \mathbf{r}_2 - \mathbf{r}_1. \end{aligned} \tag{2.2}$$

Then we find that the center of mass moves at constant velocity, i.e., $\ddot{\mathbf{R}} = 0$, and that the difference vector $\mathbf{q}(t)$ satisfies

$$\ddot{\mathbf{q}}(t) = -(m_1 + m_2) \frac{\mathbf{q}}{|\mathbf{q}|^3}.$$

By a scaling of time: $t \mapsto t\sqrt{m_1 + m_2}$, we may assume without loss generality that $m_1 + m_2 = 1$ and hence obtain the so-called Kepler's problem:

$$\ddot{\mathbf{q}} = -\frac{\mathbf{q}}{|\mathbf{q}|^3}. \tag{2.3}$$

Defining the angular momentum $\mathbf{L}(t)$ by $\mathbf{L}(t) = \mathbf{q}(t) \times \dot{\mathbf{q}}(t)$, one may easily verify that $\mathbf{L}(t)$ is a constant vector. This implies that the trajectory of $\mathbf{q}(t)$ is planar—it always lies on the plane containing $\mathbf{q}(0)$ with normal vector $\mathbf{L}(\mathbf{0})$. Therefore, without loss of generality, we may assume that $\mathbf{q}(t)$ lies on the xy-plane.

Next, we classify all possible trajectories of $\mathbf{q}(t)$.

2.2 Levi-Civita Regularization

We notice that the equation (2.3) is not defined when $\mathbf{q} = 0$, which corresponds to the collision of m_1 and m_2. To extend solutions that pass the singularity $\mathbf{q} = 0$, we apply

the Levi-Civita regularization, which consists of a double covering map and a rescaling of time.

We first write $\mathbf{q}(t) = (q_1(t), q_2(t)) \in \mathbf{R}^2$ and define $\mathbf{p}(t) = (p_1(t), p_2(t)) := (\dot{q}_1(t), \dot{q}_2(t))$. Then the equation (2.3) is equivalent to the Hamiltonian equation defined by the Hamiltonian function

$$H(\mathbf{q}, \mathbf{p}) = \frac{1}{2}|\mathbf{p}|^2 - \frac{1}{|\mathbf{q}|}.$$

Define $\phi : \mathbf{R}^2 \to \mathbf{R}^2$ by $\phi(\mathbf{Q}) = (Q_1^2 - Q_2^2, 2Q_1Q_2)$. When one identifies $\mathbf{R}^2$ with the complex plane, the map ϕ is equivalent to the z^2 map, a double covering branched at the origin; see figure (2.2).

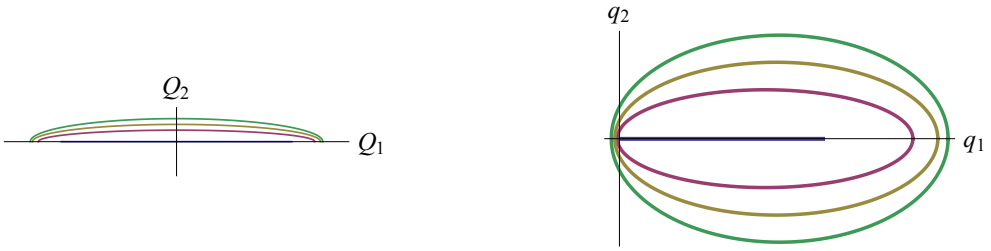

Figure 2.2: The z^2 maps a half ellipse centered at the origin to an ellipse with one focus at the origin.

Extend ϕ to $\Phi : \mathbf{R}^2 \times \mathbf{R}^{2*} \to \mathbf{R}^2 \times \mathbf{R}^{2*}$ by

$$\Phi(\mathbf{Q}, \mathbf{P}) = (\phi(\mathbf{Q}), \mathbf{P}D\phi(\mathbf{Q})^{-1}),$$

where $\mathbf{Q}$ is a column vector and $\mathbf{P}$ is a row vector. Then Φ is a canonical transformation, and we obtain a new Hamiltonian system with Hamiltonian function

$$K(\mathbf{Q}, \mathbf{P}) := H(\Phi(\mathbf{Q}, \mathbf{P})) = \frac{1}{|\mathbf{Q}|^2}(\frac{1}{8}|\mathbf{P}|^2 - 1).$$

Additionally, we rescale the time by

$$\frac{dt}{d\tau} = 4|\mathbf{Q}(t)^2|.$$

Then one obtains, on the fixed energy set $H = h$,

$$\begin{aligned} \frac{d\mathbf{Q}}{d\tau} &= \mathbf{P} \\ \frac{d\mathbf{P}}{d\tau} &= 8h\mathbf{Q}. \end{aligned}$$

Therefore, $\frac{d^2\mathbf{Q}}{d\tau^2} = 8h\mathbf{Q}$. We discuss the solution $\mathbf{Q}(\tau)$ (and hence $\mathbf{q}(t)$) according to the values of h:

Case 1: $h < 0$. Then

$$\mathbf{Q}(\tau) = A \begin{bmatrix} \cos\sqrt{-8h}\tau \\ \sin\sqrt{-8h}\tau \end{bmatrix},$$

where A is a two-by-two constant matrix. Therefore, $\mathbf{Q}(\tau)$ is periodic, and the trajectory of $\mathbf{Q}(\tau)$ is either an ellipse, a circle, or a segment, centered at the origin. Consequently, $\mathbf{q}(t)$ is periodic, and the trajectory of $\mathbf{q}(t)$ is either an ellipse (with one focus at the origin), a circle, or a segment.

Case 2: $h = 0$. Then

$$\frac{d^2\mathbf{Q}}{d\tau^2} = 0$$

Therefore, the trajectory of $\mathbf{Q}(\tau)$ is a straight line, which may or may not pass the origin. Consequently, the trajectory of $\mathbf{q}(t)$ is either a ray starting at the origin or a parabola.

Case 3: $h > 0$. Then

$$\mathbf{Q} = \mathbf{A} \begin{bmatrix} e^{\sqrt{8h}\tau} \\ e^{\sqrt{-8h}\tau} \end{bmatrix},$$

where $\mathbf{A}$ is a two-by-two constant matrix. Therefore, the trajectory of $\mathbf{Q}(\tau)$ is either a hyperbola centered at the origin or a straight line passing the origin. Consequently, the trajectory of $\mathbf{q}(t)$ is either a hyperbola or a ray starting at the origin.

2.3 Brake orbits

A brake orbit has negative energy, i.e., $h < 0$, since its initial velocity vanishes and its potential energy contributes negative values. From the discussion above, we conclude that every brake orbit in the two-body problem is periodic.

Chapter 3

Isosceles Three-Body Problem

A brake orbit is an orbit that starts with zero initial velocity. The purpose of this chapter is to find periodic brake orbits in the isosceles three-body problem. We use various shooting arguments; we follow a curve of brake initial conditions under the flow until it reaches a suitable surface, and show that the image curve includes a point that corresponds to a periodic orbit. As a result, we prove the existence of six types of periodic brake orbits.[1]

3.1 Introduction

The classical three-body problem studies the motion of three masses in the Euclidean space moving according to Newton's law of gravitation. In the isosceles three-body problem, two of the masses are equal and the shape of the three bodies forms an isosceles triangle at every instant. A *brake orbit* is a solution to the three-body problem for which, at some instant, all three bodies have zero velocity. Our goal in this paper is to find periodic brake orbits in the planar isosceles three-body problem.

The three-body problem has singularities that correspond to binary collisions and triple collision. McGehee [22] studied the collinear three-body problem, introducing a transformation to blow up the triple collision singularity, which he replaced with an invariant manifold called the *triple collision manifold*. Later, Devaney [12] extended McGehee's technique to the planar isosceles three-body problem. He considered the

[1] The content in this chapter has been published in [7].

flow on a fixed level of negative energy, called an *energy manifold*.

Simó and Martínez [42] extensively studied the energy manifold including its boundaries – the triple collision manifold and the infinity manifold. Their study characterizes orbits that pass near triple collision and near infinity with symbolic dynamics. Two kinds of spirals are obtained by considering the intersection of some unstable manifolds with suitable cross sections. One of these spirals is near the Euler collinear configurations, and it only exists when the mass-ratio is in a certain range; the other spiral is near infinity. The spiraling property could be proved only locally by analytical means. Based on local spiraling properties, several types of periodic orbits are proved to exist; some of these orbits are periodic brake orbits.

Recently in [24], the authors gave a different proof for the existence of a periodic brake orbit. The main idea is to follow a curve of brake initial conditions along the flow and show that at least one initial condition leads to a periodic orbit. We extend their idea here. By further following the same curve, we obtain six types of periodic brake orbits, parametrized by the numbers of binary collisions. See figure 3.13.

Now we briefly describe the six types of orbits. Let T denote the period of any periodic orbit. For each orbit of Type 1 to 4, the *fundamental domain* is the time interval $[0, T/4]$, i.e., one can recover the entire orbit from the first quarter of period of the orbit. Here we describe the motions of the three bodies in only the first quarter of period. For Type 1 orbits, the two symmetric bodies have n binary collisions, and then a collinearity occurs at $t = T/4$. For Type 2 orbits, the two symmetric bodies have n binary collisions, then the three bodies become collinear, and then a binary collision occurs again at $t = T/4$. For Type 3 and 4 orbits, binary collisions and collinearities occur alternately; at $t = T/4$, Type 3 orbits have a collinearity, while Type 4 orbits have a binary collision. On the other hand, the fundamental domain of Type 5 and 6 orbits is $[0, T/2]$. Both Type 5 and 6 orbits start with zero velocity and reach zero velocity again at $t = T/2$. During the half period, Type 5 orbits have one collinearity, and have i and j binary collisions before and after the collinearity respectively. Type 6 orbits have two collinearities with i binary collisions before the first collinearity, one binary collision in between the two collinearities, and j binary collisions after the second collinearity.

Compared with [42], we do not assume the spiraling property, and the concerned region stays away from infinity. Most of the periodic orbits proved in [42] must have a

sufficiently large number of syzygies, while ours do not. In detail, they have our Type 1 and 2 orbits only for large n, and our Type 5 and 6 orbits only for large i and j. Our Type 3 and 4 orbits are newly found. In addition, our Type 2 and 6 orbits are proved in a wider range of mass ratios ϵ, that is, we do not require $\epsilon < 55/4$.

This paper proceeds as follows: In Section 3.2, we state the planar isosceles three-body problem and the equations of motion in Jacobi coordinates. In Section 3.3, we write the equations of motion in Devaney's coordinates and review the dynamics on the energy manifold. We also include the classification of the behaviour of stable manifolds on the collision manifold from [42]. In Section 3.4, we review the coordinates used in [24] and relevant results. Finally in Sections 3.5 and 3.6, we prove the existence of six types of periodic brake orbits.

3.2 Planar Isosceles Three-Body Problem

The planar isosceles three-body problem consists of three mass points, with masses $m_1 = m_2$, positioned symmetrically as shown in figure 1. Initially the two equal masses have position and velocity symmetric with respect to the y-axis, and the third mass lies on the $y-$axis with velocity parallel to the y-axis. So initially the shape the three masses form is an isosceles triangle; due to the symmetry of the problem, the shape will remain isosceles.

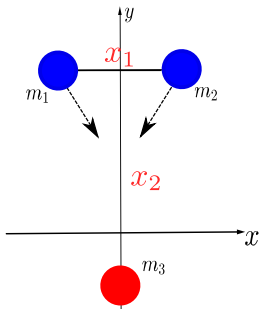

Figure 3.1: Configuration of the planar isosceles problem.

We introduce Jacobi coordinates. Let x_1 be the distance between m_1 and m_2, and x_2 be the signed distance from the midpoint of m_1 and m_2 to m_3. Note that $x_1 \geq 0$,

and $x_2 < 0$ when m_3 is below the midpoint of m_1 and m_2. Now we derive the equations for x_1 and x_2.

The Lagrangian is

$$\begin{aligned} L(x_1, x_2, \dot{x}_1, \dot{x}_2) =& \text{Kinetic energy - Potential energy} \\ =& \frac{1}{4} m_1 \dot{x}_1^2 + \frac{m_1 m_3}{2m_1 + m_3} \dot{x}_2^2 + \frac{m_1^2}{x_1} + \frac{2m_1 m_3}{\sqrt{\frac{x_1^2}{4} + x_2^2}}. \end{aligned} \tag{3.1}$$

Using the Euler-Lagrange equations, $\frac{d}{dt}\frac{\partial L}{\partial \dot{x}_1} = \frac{\partial L}{\partial x_1}$ and $\frac{d}{dt}\frac{\partial L}{\partial \dot{x}_2} = \frac{\partial L}{\partial x_2}$, we obtain

$$\begin{aligned} \ddot{x}_1 =& \frac{-2m_1}{x_1^2} - \frac{8m_3 x_1}{(x_1^2 + 4x_2^2)^{\frac{3}{2}}} \\ \ddot{x}_2 =& \frac{-8(2m_1 + m_3)x_2}{(x_1^2 + 4x_2^2)^{\frac{3}{2}}}. \end{aligned} \tag{3.2}$$

The energy integral is given by the function

$$H(x_1, x_2, \dot{x}_1, \dot{x}_2) = \frac{1}{4} m_1 \dot{x}_1^2 + \frac{m_1 m_3}{2m_1 + m_3} \dot{x}_2^2 - \frac{m_1^2}{x_1} - \frac{2m_1 m_3}{\sqrt{\frac{x_1^2}{4} + x_2^2}}.$$

It is known that for all initial conditions with non-negative energy, the three masses escape to infinity. Since our goal is to find periodic orbits, we only study the case when $H < 0$. Without loss of generality, we study the level set $H = -1$, and the center of mass is fixed at the origin.

Notice that the equation (3.2) is singular when $x_1 = 0$. Physically "$x_1 = 0, x_2 \neq 0$" represents the binary collisions between m_1 and m_2, and "$x_1 = x_2 = 0$" represents triple collision.

3.3 Devaney's Coordinates [12]

Now we introduce "polar" coordinates (r, ϕ). Write

$$x_1 = r\sqrt{\frac{2}{m_1}}\cos\phi, \;\; x_2 = r\sqrt{\frac{2m_1 + m_3}{2m_1 m_3}}\sin\phi, \quad r \geq 0, \phi \in \left[-\frac{\pi}{2}, \frac{\pi}{2}\right],$$

where $r^2 = \frac{m_1}{2}x_1^2 + \frac{2m_1 m_3}{2m_1 + m_3}x_2^2$. Then the Lagrangian becomes

$$L(r, \dot{r}, \phi, \dot{\phi}) = \frac{1}{2}\dot{r}^2 + \frac{1}{2}r^2\dot{\phi}^2 - \frac{1}{r}U(\phi),$$

where

$$U(\phi) = -\frac{m_1^2}{\sqrt{\frac{2}{m_1}}\cos\phi} - \frac{4m_1m_3}{\sqrt{\frac{2}{m_1}\cos^2\phi + \frac{2(2m_1+m_3)}{m_1m_3}\sin^2\phi}}. \tag{3.3}$$

Note that the system of differential equations for $(r, \dot{r}, \phi, \dot{\phi})$ has singularities at $r = 0$ and at $\phi = \pm\frac{\pi}{2}$. To regularize the singularities, Devaney introduces a change of time scale $\frac{dt}{ds} = r^{\frac{3}{2}}\frac{\cos\phi}{\sqrt{W(\phi)}}$, where $W(\phi) = -\cos(\phi)U(\phi)$.

Let $v = r^{\frac{1}{2}}\frac{dr}{dt}$ and $w = \frac{d\phi}{ds}$, then the system of differential equations becomes

$$\begin{aligned}
\frac{dr}{ds} =& \frac{dr}{dt}\frac{dt}{ds} = rv\frac{\cos\phi}{\sqrt{W(\phi)}} \\
\frac{dv}{ds} =& \sqrt{W(\phi)}(1 - \frac{\cos\phi}{2W(\phi)}(v^2 - 4rh)) \\
\frac{d\phi}{ds} =& w \\
\frac{dw}{ds} =& \sin\phi(-1 + \frac{\cos\phi}{W(\phi)}(v^2 - 2rh)) - \frac{vw\cos\phi}{2\sqrt{W(\phi)}} + \frac{dW}{d\phi}\frac{\cos\phi - \frac{w^2}{2}}{W(\phi)},
\end{aligned} \tag{3.4}$$

and the energy equation is

$$\frac{w^2}{2\cos\phi} - 1 = \frac{\cos\phi}{W(\phi)}(rh - \frac{v^2}{2}). \tag{3.5}$$

Now we study the dynamics for the system. First observe that this system has two symmetries [39]. Let

$$\begin{aligned}
&R_1 : (r, v, \phi, w) \to (r, -v, \phi, -w) \\
&R_2 : (r, v, \phi, w) \to (r, -v, -\phi, w) \\
&\mathrm{Fix}(R_i) = \{(r, v, \phi, w) : R_i(r, v, \phi, w) = (r, v, \phi, w)\}, \quad i = 1, 2.
\end{aligned}$$

Then $\xi(t)$ is a solution if and only if $R_i\xi(-t)$ is a solution for $i = 1, 2$. A solution $\xi(t)$ is called R_i-*symmetric* with time t_1 if $\xi(t_1 + t) = R_i\xi(t_1 - t)$. One can show that an orbit is R_i-symmetric with time t_1 if and only if it intersects the space $\mathrm{Fix}(R_i)$ at $t = t_1$.

Our next observation is that $\{r = 0\}$ is an invariant manifold for the flow. (Devaney's Words: Thus we have removed the singularity which corresponds to triple collision. In its place we have pasted a smooth manifold which is called the triple collision manifold. Orbits which previous began or ended at triple collision in finite time are now slowed down so that they tend to the triple collision manifold at $t \to -\infty$ or $t \to \infty$. And

orbits which pass close to triple collision now behave very much like orbits on the triple collision manifold itself. Hence understanding the flow on this manifold gives a good deal of information about these near-collision orbits.)

The *energy manifold* (with $h = -1$) is defined as the set

$$\{(r, v, \phi, w) \in [0, \infty) \times \mathbf{R} \times [-\frac{\pi}{2}, \frac{\pi}{2}] \times \mathbf{R} : \frac{w^2}{2\cos\phi} - 1 = \frac{\cos\phi}{W(\phi)}(-r - \frac{v^2}{2})\}.$$

The *triple collision manifold* is defined as the set

$$\{(r, v, \phi, w) \in [0, \infty) \times \mathbf{R} \times [-\frac{\pi}{2}, \frac{\pi}{2}] \times \mathbf{R} : r = 0, \frac{w^2}{2\cos\phi} + \frac{v^2\cos\phi}{2W(\phi)} = 1\}.$$

The triple collision manifold is a two-dimensional invariant manifold and is topologically equivalent to a sphere with four holes (see figure 3.2).

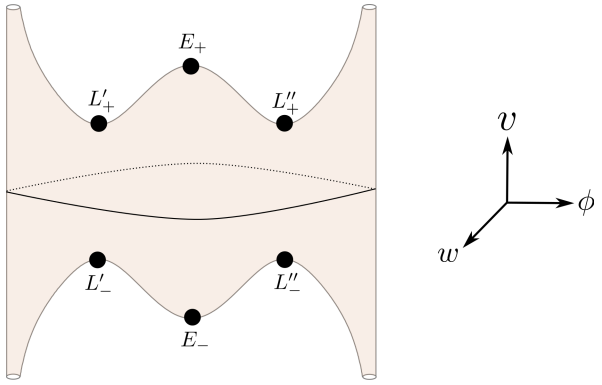

Figure 3.2: The triple collision manifold is topologically a two-dimensional sphere with four holes. The energy manifold is enclosed by the triple collision manifold.

The flow on the triple collision manifold is determined by the system of differential equations

$$\begin{aligned}
\frac{dv}{ds} &= \sqrt{W(\phi)}(1 - \frac{\cos\phi}{2W(\phi)}v^2) \\
\frac{d\phi}{ds} &= w \\
\frac{dw}{ds} &= \sin\phi(-1 + \frac{\cos\phi}{W(\phi)}v^2) - \frac{vw\cos\phi}{2\sqrt{W(\phi)}} + \frac{dW}{d\phi}\frac{\cos\phi - \frac{w^2}{2}}{W(\phi)}.
\end{aligned} \tag{3.6}$$

Now we summarize some properties of the flow on the energy manifold (with $h = -1$):

Proposition 3.3.1. *[12]*

(i) $U(\phi)$ *has exactly three critical points for* $\phi \in (-\frac{\pi}{2}, \frac{\pi}{2})$. *These are a non-degenerate minimum at* $\phi = 0$ *and two non-degenerate maximum at* $\phi_* = \arctan(\pm\sqrt{\frac{3m_3}{2m_1+m_3}})$.

(ii) The system has exactly six equilibrium points: the Lagrange equilibria $L'_\pm = (0, \pm v_*, -\phi_*, 0)$, $L''_\pm = (0, \pm v_*, \phi_*, 0)$, *and the Euler equilibria* $E_\pm = (0, \pm v_0, 0, 0)$, *where* $v_* = \sqrt{-2U(\phi_*)}$, $v_0 = \sqrt{-2U(0)}$.

(iii) When using (v, ϕ, w) *as local coordinates at rest points, the eigenvalues of the Jacobian matrix of any equilibrium, say* $(\bar{v}, \bar{\phi}, 0)$, *are* $\lambda = \frac{\bar{v}\cos\bar{\phi}}{\sqrt{W(\bar{\phi})}}, \lambda_1, \lambda_2$ *with eigenvectors* $(1,0,0)^T$,$(0,1,\lambda_1)^T$,$(0,1,\lambda_2)^T$, *where*

$$\lambda_{1,2} = \frac{1}{\sqrt{8}}(-sgn(\bar{v})\sqrt{\cos\bar{\phi}} \pm \sqrt{\cos\bar{\phi} - \frac{8\cos^2\bar{\phi}}{W(\bar{\phi})}\frac{d^2U}{d\phi^2}(\bar{\phi})}\ ).$$

(iv) For every mass ratio $\epsilon = m_3/m_1$, *the Lagrange equilibria are saddles with real characteristic exponents; the Euler equilibrium with* $v > 0$ *is a sink, and the Euler equilibrium with* $v < 0$ *is a source. For* $\epsilon \geq 55/4$, *the characteristic exponents of the Euler equilibria are real, and for* $\epsilon < 55/4$, *the characteristic exponents of the Euler equilibria are complex.*

(v) The stable manifold $W^s(L''_-)$ *has dimension two. The unstable manifold* $W^u(L''_-)$ *has dimension one. Once we have* $W^{s,u}(L''_-)$, *we may find the stable/unstable manifolds of other Lagrange equilibria from symmetries:* $W^{s,u}(L''_+) = R_1W^{u,s}(L''_-)$, $W^{s,u}(L'_+) = R_2W^{u,s}(L''_-)$, *and* $W^{s,u}(L'_-) = R_1R_2W^{s,u}(L''_-)$.

(vi) The stable manifold $W^s(E_-)$ *has dimension one. The unstable manifold* $W^u(E_-)$ *has dimension two. From symmetries,* $W^{s,u}(E_+) = R_1W^{u,s}(E_-) = R_2W^{u,s}(E_-)$.

Now we summarize some properties of the flow on the triple collision manifold:

Proposition 3.3.2. *[12]*

(i) The flow has six equilibrium points. They are exactly the equilibrium points for the flow in the energy manifold.

(ii) For all mass ratios, the Lagrange equilibria are saddles with real characteristic exponents; the Euler equilibrium with $v > 0$ is a sink, and the Euler equilibrium with $v < 0$ is a source. For $\epsilon \geq 55/4$, the characteristic exponents of the Euler equilibria are real, and for $\epsilon < 55/4$, the characteristic exponents of the Euler equilibria are complex.

(iv) When restricted to the triple collision manifold, both $W^u(L''_-)$ and $W^u(L'_-)$ are one-dimensional.

(iii) The flow is gradient-like, that is, v is strictly increasing along all non-equilibrium orbits.

On the triple collision manifold, let γ' and γ'' denote the branches of $W^u(L'_-)$ and $W^u(L''_-)$ respectively with initial $w \geq 0$. The following theorem classifies the behaviour of γ' and γ'' according to mass ratios. See figure 3. Without loss of generality, we assume $m_1 = m_2 = 1$ and $m_3 = \epsilon$.

Theorem 3.3.3. *[41, 42] There exists two critical values of ϵ: $\epsilon_1 \approx 0.378532$ and $\epsilon_2 \approx 2.661993$ such that*

(i) For $0 < \epsilon < \epsilon_1$, the branch γ' intersects $\{v = 0\}$ with $\phi > 0$ and $w > 0$; the branch γ'' intersects $\{v = 0\}$ with $\phi > 0$ and $w < 0$. Then γ' dies at E_+, and γ'' escapes around the upper branch of binary collision with $\phi = -\pi/2$.

(ii) For $\epsilon = \epsilon_1$, the branch γ' intersects $\{v = 0\}$ with $\phi = \pi/2$ and $w = 0$; the branch γ'' intersects $\{v = 0\}$ with $\phi > 0$ and $w < 0$. Then γ' connects L'_- and L'_+, and γ'' escapes around the upper branch of binary collision with $\phi = -\pi/2$.

(iii) For $\epsilon_1 < \epsilon < \epsilon_2$, both γ' and γ'' intersect $\{v = 0\}$ with $\phi > 0$ and $w < 0$. Then γ' and γ'' turn around the upper branch of $\phi = -\pi/2$.

(iv) For $\epsilon = \epsilon_2$, the branch γ' intersects $\{v = 0\}$ with $\phi > 0$ and $w < 0$; the branch γ'' intersects $\{v = 0\}$ with $(\phi, w) = (0, -\sqrt{2})$. Then γ' turns around the upper branch of $\phi = -\pi/2$, and γ'' connects L''_- and L'_+,

(v) For $\epsilon > \epsilon_2$, the branch γ' intersects $\{v = 0\}$ with $\phi > 0$, $w < 0$, and γ'' intersects $\{v = 0\}$ with $\phi < 0, w < 0$. Then γ' escapes through the upper branch of $\phi = -\pi/2$ and γ'' ends at E_+.

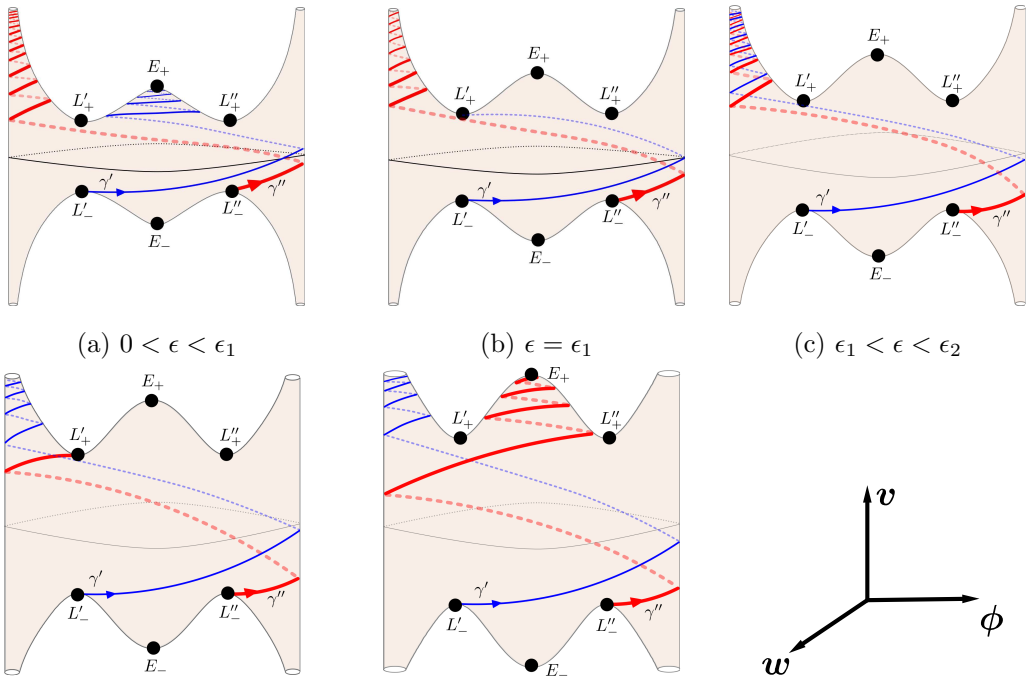

(a) $0 < \epsilon < \epsilon_1$ (b) $\epsilon = \epsilon_1$ (c) $\epsilon_1 < \epsilon < \epsilon_2$

(d) $\epsilon = \epsilon_2$ (e) $\epsilon > \epsilon_2$

Figure 3.3: Evolution of γ' and γ'' with the mass ratio ϵ.

3.4 New Coordinates [24]

In this section, we review the coordinates (referred to as "new coordinates" here) and relevant results from Section 5 of [24].

Recall that we have assumed $m_1 = m_2 = 1$. The new coordinate system uses the same size variable r as in Devaney's coordinates and a different shape variable θ. We write $r^2 = \frac{1}{2}x_1^2 + \frac{2m_3}{2+m_3}x_2^2$, then $(\bar{x}_1, \bar{x}_2) := (\frac{x_1}{r\sqrt{2}}, \frac{x_2}{r\sqrt{\frac{2+m_3}{2m_3}}})$ lies on the right half unit circle. See figure 3.4. To parametrize this half unit circle, we first parametrize the diameter segment $\{(0, \bar{x}_2), -1 \le \bar{x}_2 \le 1\}$ by $\bar{x}_2 = \sin\theta$, and then consider the projection of the segment from $(\bar{x}_1, \bar{x}_2) = (-1, 0)$ onto the half unit circle. We obtain

$$x_1 = r\sqrt{2}\frac{\cos^2\theta}{1+\sin^2\theta}, \quad x_2 = r\sqrt{\frac{2+m_3}{2m_3}}\frac{2\sin\theta}{1+\sin^2\theta}, \quad r \ge 0.$$

We allow the θ-variable to vary from $-\infty$ to ∞; this gives a multiple cover of the half unit circle, and hence the isosceles shapes. Note that the isosceles binary collision shape

corresponds to $\theta = \pm\pi/2 \mod 2\pi$, where θ-variable locally gives a branched double cover.

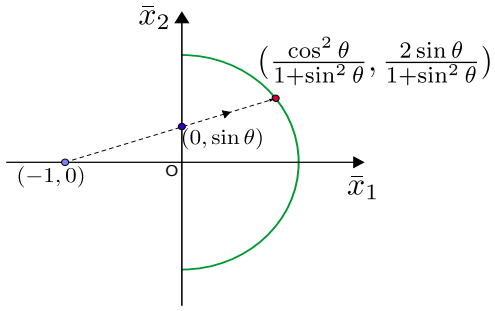

Figure 3.4: The shape variable θ.

Now we introduce two new variables: v, w, and another change of time scale $\frac{dt}{ds} = r^{\frac{3}{2}}\cos^2\theta$, where

$$v = r^{\frac{1}{2}}\dot{r}, \quad w = 4\frac{\theta'}{(1+\sin^2\theta)^2}.$$

(Here the dot mark "." means taking derivative with respect to t, and the prime mark " $'$ " means taking derivative with respect to s.)

Remark on the relation between Devaney's coordinates and the new coordinates. The size variables r are equal. The v-variables, which are directly related to r and $\dot{r}$, are also equal. Note that Devaney's ϕ-variable parametrizes the right half unit circle by polar coordinates, so the relation between the ϕ-variable and the θ-variable is $\frac{\cos^2\theta}{1+\sin^2\theta} = \cos\phi$, $\frac{2\sin\theta}{1+\sin^2\theta} = \sin\phi$. As for the w-variables, to avoid confusion, let w_{old} and w_{new} denote the w-variables in the two coordinates respectively. There is no simple algebraic relation between w_{old} and w_{new}. Nonetheless, one may determine the sign of the w_{new}-variable by inspecting the change of the ϕ-variable. Note that w_{new} is directly related to the change rate of θ. Assume $\theta(t_0) \in (-\pi/2, \pi/2) \mod 2\pi$ and $w_{new}(t_0) \geq 0$, (for example, the unstable branches γ' and γ'' in Theorem 3.3.3 satisfy these assumptions), then $w_{new}(t)$ remains positive if $\theta(t)$ remains strictly increasing; unless $\theta(t)$ converges, this is equivalent to that $\bar{x}_2(t)$ remains monotonically bouncing between -1 and 1 with the moving direction only changes at the endpoints $\bar{x}_2 = \pm 1$. This is also equivalent to that $\phi(t_0) \in (-\pi/2, \pi/2)$ and $\phi(t)$ remains monotonically bouncing between $-\pi/2$ and $\pi/2$ with the moving direction only changes at the endpoints $\phi = \pm\pi/2$.

In the new coordinates the Lagrangian becomes

$$L(r,\dot{r},\theta,\dot{\theta}) = \frac{\dot{r}^2}{2} + \frac{2r^2\cos^2\theta\dot{\theta}^2}{(1+\sin^2\theta)^2} + \frac{1}{r}V(\theta),$$

where $V(\theta) = (1+\sin^2\theta)(\frac{1}{\sqrt{2}\cos^2\theta} + \frac{2\sqrt{2}m_3}{\sqrt{(1+\sin^2\theta)^2+\frac{8}{m_3}\sin^2\theta}})$. We remark that $V(\theta) = -U(\phi)$.

The energy equation becomes

$$\frac{1}{2}v^2\cos^2\theta + \frac{1}{8}w^2(1+\sin^2\theta)^2 - \mathcal{W}(\theta) = rh\cos^2\theta, \tag{3.7}$$

where $\mathcal{W}(\theta) = \cos^2\theta V(\theta)$.

As before we fix the energy at $h=-1$. The *energy manifold* is defined as

$$P_1 = \{(r,\theta,v,w) : r \geq 0, \frac{1}{2}v^2\cos^2\theta + \frac{1}{8}w^2(1+\sin^2\theta)^2 - \mathcal{W}(\theta) = -r\cos^2\theta\},$$

and the *(triple) collision manifold* is defined as the invariant set $\{r=0\}$. Note that in the energy manifold P_1, the coordinate w can be solved as a two-valued function of (r,θ,v). So P_1 can be visualized through its projection to the (r,v,θ)-space, which is given by the inequality $r + v^2/2 \leq V(\theta)$. See figure 3.5 for the projection. The top boundary surface is given by $\{w=0, r+v^2/2 = V(\theta)\}$, and the lower boundary surface is the collision manifold.

In the new coordinates, the system of differential equations (with $h=-1$) becomes

$$\begin{aligned}
r' =& vr\cos^2\theta \\
v' =& \frac{1}{2}v^2\cos^2\theta + \frac{1}{4}w^2(1+\sin^2\theta)^2 - \mathcal{W}(\theta) \\
\theta' =& \frac{1}{4}w(1+\sin^2\theta)^2 \\
w' =& \frac{d\mathcal{W}}{d\theta} - \frac{1}{2}vw\cos^2\theta + \sin\theta\cos\theta(2r+v^2-\frac{1}{2}w^2(1+\sin^2\theta)).
\end{aligned} \tag{3.8}$$

Proposition 3.4.1. *[24]*

(i) The function $V(\theta)$ is a π-periodic even function. $V(\theta)$ has exactly three critical points in $(-\pi/2,\pi/2)$, including $\theta=0$. Denote the critical point in $(0,\pi/2)$ by θ^*.

(ii) The equilibrium points of the system (3.8) are the Lagrange equilibria $(r, \theta, v, w) = (0, \pm\theta^* + k\pi, \pm v^*, 0)$ *and the Euler equilibria* $(r, \theta, v, w) = (0, k\pi, \pm\sqrt{2V(0)}, 0)$, *where* $k \in \mathrm{Z}$ *and* $v^* = \sqrt{2V(\theta^*)}$.

(iii) Denote the equilibrium points used later in our proof by

$$L_\pm = (0, \theta^* - \pi, \pm v^*, 0), \quad L'_\pm = (0, -\theta^*, \pm v^*, 0),$$
$$E_\pm = (0, 0, \pm\sqrt{2V(0)}, 0), \quad L''_\pm = (0, \theta^*, \pm v^*, 0).$$

Then L_+ *and* L_- *are connecting by the Lagrange homothetic orbit; so are* L'_+ *and* L'_-. *Also* E_+ *and* E_- *are connecting by the Eulerian homothetic orbit.*

(iv) When restricted to the energy manifold P_1, $W^s(L_-)$ *has dimension two and* $W^u(L_-)$ *has dimension one.*

Next we divide the energy manifold P_1 into several regions and analyze the flow in them. Define

$$\begin{aligned}
R_I &= P_1 \cap \{\theta \in [\theta^* - \pi, -\pi/2], w \geq 0\}, \quad Q_I = P_1 \cap \{\theta \in [\theta^* - \pi, -\pi/2], w \leq 0\},\\
R_{II} &= P_1 \cap \{\theta \in [-\pi/2, -\theta^*], w \geq 0\}, \qquad Q_{II} = P_1 \cap \{\theta \in [-\pi/2, -\theta^*], w \leq 0\},\\
R_{III} &= P_1 \cap \{\theta \in [-\theta^*, 0], w \geq 0\},\\
R_{IV} &= P_1 \cap \{\theta \in [0, \theta^*], w \geq 0\},\\
R_V &= P_1 \cap \{\theta \in [\theta^*, \pi/2], w \geq 0\}.
\end{aligned}$$

The planes $\theta = \theta^* - \pi$ and $\theta = -\pi/2$ will be called the left and right walls of R_I respectively with similar definitions for the other regions.

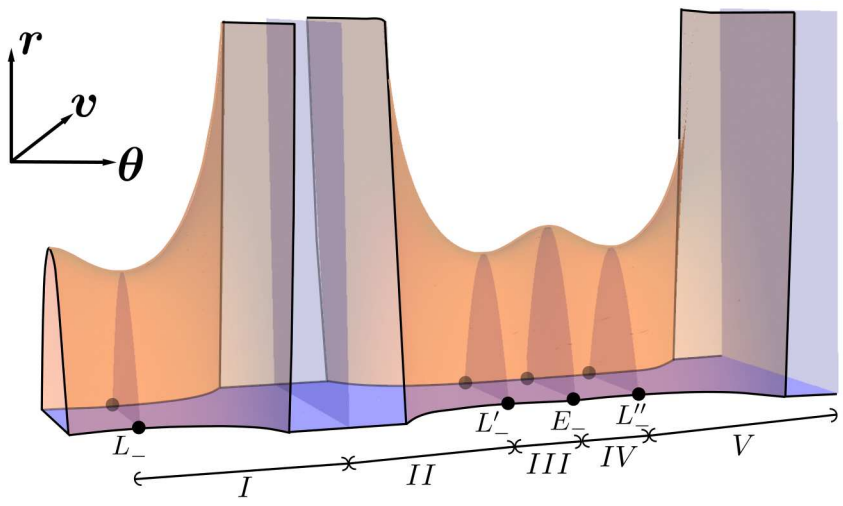

Figure 3.5: The projection of the energy manifold to the (r, v, θ)-space.

Lemma 3.4.2. *[24]*

(i) Regions R_I, R_{III}, R_V are flowing-rightward. With the exception of the Lagrange homothetic orbits and orbits in the stable manifold of E_+, orbits cross theses regions as follows: every orbit beginning in the left wall of $R_I(R_{III}, R_V)$ crosses region $R_I(R_{III}, R_V)$ and exits at the right wall.

(ii) Region $R_{II}(R_{IV})$ is flowing-leftward in backward-time. Except for the Lagrange homothetic orbits, any backward-time orbit beginning in the right wall of $R_{II}(R_{IV})$ can be followed back to the left wall. Furthermore, forward orbits beginning in the left wall of R_{II} either leave $R_{II}(R_{IV})$ through the right wall, leave $R_{II}(R_{IV})$ through the surface $\{w = 0\}$, or converge to one of the Lagrange restpoints $L'_\pm(L''_\pm)$ in the right wall. In other words, forward orbits would not stay in $R_{II}(R_{IV})$ forever unless they belong to $W^s(L'_\pm)(W^s(L''_\pm))$.

(iii) Region Q_I is flowing-rightward in backward-time. Except for the Lagrange homothetic orbit, every backward-time orbit beginning in the left wall of Q_I can be followed back to the right wall. Region Q_{II} is flowing-leftward; except for the Lagrange homothetic orbit, every forward orbit beginning in region Q_{II} crosses the region and exits at the left wall.

(***Remark.*** *The term "flowing-rightward" replaces the term "positively invariant" used in [24].)*

Proof. Here we review the proof for (i) about region R_I only. Similar arguments work for the other regions.

First, we show that the only way an orbit may leave region R_I is through the right wall. This is done by showing that orbits cannot leave R_I through the lower boundary or the top boundary. For the lower boundary surface of R_I, i.e., $R_I \cap \{r = 0\}$, note that $\{r = 0\}$ is an invariant set for the flow, so orbits cannot leave R_I by crossing the lower boundary. As for the top boundary surface, from the definition of R_I, we have $w \geq 0$ in R_I. The top boundary surface of R_I has $w = 0$ and $w' = cos^2\theta(dV/d\theta) \geq 0$, so orbits cannot leave R_I through the top boundary either.

Second, we show that if an orbit, say $\varphi(t) = (r(t), v(t), \theta(t), w(t))$, stays in R_I forever, then $\varphi(t)$ must be bounded. Obviously, $\theta(t)$ is bounded by $\theta^* - \pi$ and $-\pi/2$. As for $w(t)$, from the definition of R_I, we have $0 \leq w(t)$; from the energy equation, we have $w(t) \leq \sqrt{8\mathcal{W}(\theta(t))}$. Since $\mathcal{W}(\theta)$ is analytic and periodic, $w(t)$ is bounded. Now we consider r and v. Let $\lambda = \sqrt{2r + v^2}$. From (3.8) we obtain $\lambda\lambda' = \frac{1}{8}vw^2(1 + \sin^2\theta)^2$ and $\theta' = \frac{1}{4}w(1+\sin^2\theta)^2$. Since $\theta(t)$ is increasing, we can reparametrize λ by θ to obtain $|\frac{d\lambda}{d\theta}| = |\frac{1}{2}\frac{vw}{\lambda}| \leq \frac{1}{2}w$. Since θ and w are bounded in R_I, λ is bounded, therefore r and v are also bounded.

Third, we show that orbits cannot stay in R_I forever by contradiction. Assume there is an orbit other than the Lagrange homothetic orbit, say $\varphi(t)$, that remains in R_I for all time $t \geq 0$, then $\varphi(t)$ must be bounded as proved in the previous paragraph. Moreover, $\theta(t)$ must converge monotonically to some limit $\theta_\infty \in (\theta^* - \pi, -\pi/2)$. The omega limit set of the orbit $\varphi(t)$ must be empty; otherwise, it will be included in $\{\theta = \theta_\infty\}$ which does not contain any nontrivial invariant sets. The emptiness of the omega limit set implies that the orbit is not included in any compact subset of R_I. This is impossible because the orbit is bounded and R_I is closed.

□

3.5 Finding Symmetric Periodic Brake Orbits

In this section, we prove the existence of Type 1 to 4 periodic brake orbits. We have described these orbits in the configuration space in the introduction section. Here we describe the projection of these orbits to the (r, θ)-plane in the new coordinates. See figure 3.12. Type 1 to 4 orbits all start with zero velocity. When projected to the (r, θ)-plane, these orbits are symmetric with respect to either the line $\theta = k\pi$, which represents the Euler collinear shape, or the line $\theta = (2k + 1)\pi/2$, which represents the binary collision shape, for some $k \in Z$. The orbits meet their symmetric lines at $t = T/4$, where T denotes the periods, and their full orbits are determined by one quarter of the periods. On one hand, in a quarter of period, Type 1 and 2 orbits can cross either $\theta = \pi/2$ or $\theta = -\pi/2$ successively without crossing the lines representing Euler collinear shape; the variable θ is not monotonically changing with respect time. At $t = T/4$, Type 1 orbits reach the collinear shape, while Type 2 orbits reach the binary collision shape. On the other hand, in a half period, the variable θ of every Type 3 and 4 orbits is monotonically increasing with respect to time. At $t = T/4$, Type 3 orbits reach the Euler collinear shape, while Type 4 orbits reach the binary collision shape.

We now introduce additional notations used throughout the paper.

When considering the projection to the (r, v, θ)-space, for any $k \in \mathbf{Z}$, we define the *Lagrange plane*, the *Euler plane*, and the *binary collision plane* as follows:

$$
\begin{aligned}
&Lagrange(\bar{\theta}, +) = \{(r, v, \bar{\theta}, w) : w \geq 0\}, \quad \text{where } \bar{\theta} = \pm\theta^* + k\pi. \\
&Lagrange(\bar{\theta}, -) = \{(r, v, \bar{\theta}, w) : w \leq 0\}, \quad \text{where } \bar{\theta} = \pm\theta^* + k\pi. \\
&Euler(\bar{\theta}, +) = \{(r, v, \bar{\theta}, w) : w \geq 0\}, \quad \text{where } \bar{\theta} = k\pi. \\
&Euler(\bar{\theta}, -) = \{(r, v, \bar{\theta}, w) : w \leq 0\}, \quad \text{where } \bar{\theta} = k\pi. \\
&Binary(\bar{\theta}, +) = \{(r, v, \bar{\theta}, w) : w \geq 0\}, \quad \text{where } \bar{\theta} = \pi/2 + k\pi. \\
&Binary(\bar{\theta}, -) = \{(r, v, \bar{\theta}, w) : w \leq 0\}, \quad \text{where } \bar{\theta} = \pi/2 + k\pi.
\end{aligned}
$$

When considering the projection to the (r, θ)-plane, we call the line $\theta = k\pi$ the *Euler line*, and the line $\theta = \pi/2 + k\pi$ the *binary collision line* for any $k \in \mathbf{Z}$.

Next, we find sufficient conditions for a symmetric orbit to be periodic. The system

(3.8) has three symmetries. Let

$$R_1 : (r, v, \theta, w) \to (r, -v, \theta, -w)$$
$$R_2 : (r, v, \theta, w) \to (r, -v, -\theta, w)$$
$$T_1 : (r, v, \theta, w) \to (r, v, \theta + \pi, w)$$
$$\mathrm{Fix}(R_i) = \{(r, v, \theta, w) : R_i(r, v, \theta, w) = (r, v, \theta, w)\}, \quad i = 1, 2.$$

Then $\xi(t)$ is a solution to (3.8) if and only if $R_i\xi(-t)$ and $T_1\xi(t)$ are solutions to (3.8) for $i = 1, 2$. A solution $\xi(t)$ is called *R_i-symmetric* with time t_1 if $\xi(t_1+t) = R_i\xi(t_1-t)$. One can show that an orbit is R_i-symmetric with time t_1 if and only if it intersects the space $\mathrm{Fix}(R_i)$ at $t = t_1$. Note that every brake orbit is R_1-symmetric.

The following lemma will be used to find periodic brake orbits.

Lemma 3.5.1. *Let $\varphi(t) = (r(t), v(t), \theta(t), w(t))$ be a solution to the system (3.8) with brake initial condition, i.e., $v(0) = w(0) = 0$. Then any of the following conditions implies that $\varphi(t)$ is periodic with period T.*

(i) The orbit starts with zero velocity and reaches zero velocity again at t=T/2, i.e, $v(T/2) = w(T/2) = 0$.

(ii) The orbit reaches an Euler collinear line orthogonally at t=T/4, i.e., $v(T/4) = 0$ and $\theta(T/4) = k\pi$ for some $k \in \mathbf{Z}$.

(iii) The orbit reaches a binary collision line orthogonally at t=T/4, i.e., $v(T/4) = 0$ and $\theta(T/4) = (2k-1)\pi/2$ for some $k \in \mathbf{Z}$.

*(**Remark.** We will use condition (i) to find Type 5 and 6 orbits, condition (ii) to find Type 1 and 3 orbits, and condition (iii) to find Type 2 and 4 orbits.)*

Proof. We prove (i) first. Since $v(T/2) = w(T/2) = 0$, $\varphi(t)$ is R_1-symmetric with time $T/2$. Thus $\varphi(T/2+t) = R_1\varphi(T/2-t)$; by plugging in $t = T/2$ and using $v(0) = w(0)$, we obtain $\varphi(T) = R_1\varphi(0) = \varphi(0)$. The proofs for (ii) and (iii) are similar. One may show that $\varphi(T/4 + t) = T_1^{2k}R_2\varphi(T/4 - t)$ for (ii), and that $\varphi(t + T/4) = T_1^{2k-1}R_2\varphi(T/4 - t)$ for (iii).

□

We now are ready to find periodic brake orbits.

Theorem 3.5.2. *[24] For any m_3 in an open set of mass parameters, including $m_3 = 1$, there exists a periodic brake orbit. In a quarter of period, the orbit starts at a brake time, and hits the Euler collinear line orthogonally after crossing the double collision line. See figure 3.12(a) for the orbit. (**Remark.** We will show that the open set includes $(0, \epsilon_2)$.)*

Proof. (Idea of the proof:) Let Z be the part of the zero velocity curve in R_I. The proof uses a shooting argument that starts from Z and targets at $Euler(0, +)$. The main idea is to show that part of Z can be followed across regions from R_I to R_{III}. See figure 3.6(b). The image curve in $Euler(0, +)$, say Z_{III}, will include a point satisfying the condition (ii) in Lemma 3.5.1; the point corresponds to the desired period orbit. We will prove this theorem during the proof of Theorem 3.5.3. □

By extending the idea of the proof of Theorem 3.5.2, one can follow part of the zero velocity curve under the flow to cross more regions, and prove the existence of period brake orbits that hit the binary collision line $\theta = \pi/2$ orthogonally.

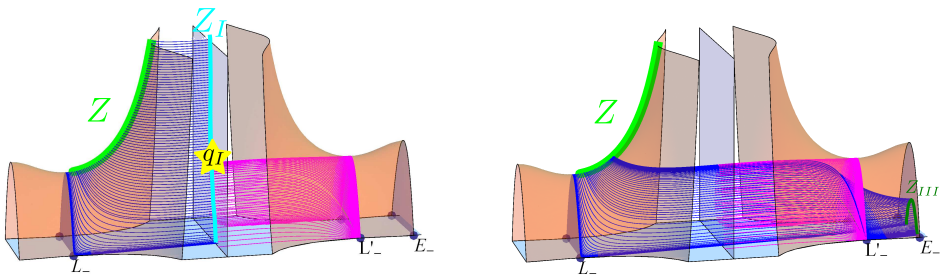

(a) q_I is the first intersection of Z_I with the "quadrant" of the surface $W^s(L'_-)$.

(b) Part of Z can be followed across regions from R_I to R_{III} to form Z_{III}.

Figure 3.6: This figure illustrates the proof of Theorem 3.5.2 and the third to sixth paragraphs of the proof for Theorem 3.5.3.

Theorem 3.5.3. *For any $m_3 > \epsilon_1 \approx 0.378532$, there exists a T-periodic brake orbit. In a quarter of period, the orbit starts at a brake time, then crosses the binary collision line $\theta = -\pi/2$, and then hits another binary collision line orthogonally, i.e., $\theta(T/4) = \pi/2$ and $v(T/4) = 0$. See figure 3.12(d).*

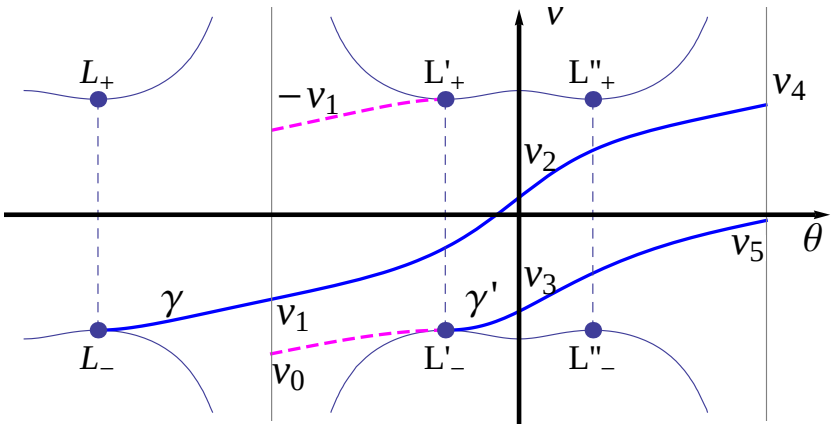

Figure 3.7: For $m_3 > \epsilon_1$, the branches γ and γ' of $W^u(L_-)$ and $W^u(L'_-)$ are shown. Two branches of $W^s(L'_-)$ and $W^s(L'_+)$ are also shown in thicker dashed curves.

Proof. We use a shooting argument that starts from a zero velocity curve and targets at $Binary(\pi/2, +)$. The main idea is to follow a zero velocity curve across regions from R_I to R_V. The image curve in $Binary(\pi/2, +)$ will include a point with $v = 0$, which corresponds to a period brake orbit by Lemma 3.5.1(iii).

On the collision manifold, denote the branches of $W^u(L_-)$ and $W^u(L'_-)$ with initial $w > 0$ by γ and γ' respectively. See figure 3.7. Note that both L_- and L'_- in figure 3.7 correspond to L'_- in figure 3.3 (i.e., in Devaney's coordinates). Moreover, the curve γ of figure 3.7 corresponds to the branch of $W^u(L'_-)$ with initial $w_{old} < 0$, that is to say, to the image by R_1R_2 of the curve denoted by γ'' in figure 3.3. Another way to think about γ is to consider its translation by $\theta \to \theta + \pi$, then the image curve $T_1\gamma$ is an unstable branch of $W^u(L''_-)$ with initial $w > 0$, which corresponds to γ'' in figure 3.3. By Theorem 3.3.3, for $m_3 > \epsilon_1$, in Devaney's coordinates, the ϕ-variable of γ'' first monotonically increases to $\phi = \pi/2$ and then monotonically decreases at least until it reaches $\phi = -\pi/2$; the ϕ-variable of γ' first monotonically increases to $\phi = \pi/2$ and then monotonically decreases at least until it reaches $\phi = -\pi/2$. This implies that, in the new coordinates, γ' and γ'', and hence γ, stay in $\{w \geq 0\}$ at least until they crosses two binary collisions lines. Moreover, recall that the flow on the collision manifold is gradient-like with respect to the variable v by Proposition 3.3.2. The fact that γ'' intersects $\phi = -\pi/2$ after it intersects $v = 0$ in Devaney's coordinates implies that γ''

has $v > 0$ at the second time it crosses a binary collision line; in the new coordinates, this means γ intersects $\theta = \pi/2$ at $v = v_4 > 0$. The the fact that γ' intersects $\phi = \pi/2$ before it intersects $v = 0$ implies that γ' has $v < 0$ at the first time it crosses a binary collision line; i.e., γ' intersects $\theta = \pi/2$ at $v = v_5 < 0$. Additionally, we denote the intersections of $\theta = -\pi/2$ with γ and with $W^s(L'_-)$ by v_1 and v_0 respectively.

We start from region R_I, which is flowing-rightward. Let Z be the curve of brake initial conditions in R_I whose shapes vary from equilateral to binary collision, i.e., $Z = \{(r, 0, \theta, 0) : \theta^* - \pi < \theta < -\pi/2\} \cap P_1$. See figure 3.6. Let Z_I be the image curve of Z in the right wall of R_I. Now we consider the two endpoints of Z. At one endpoint, $\theta = \theta^* - \pi$ corresponds to the Lagrange homothetic orbit (a heteroclinic connection between L_+ and L_-); orbits start near this endpoint will follow the Lagrange homothetic orbit to a neighborhood of L_-, and then follow γ to meet the right wall of R_I arbitrarily close to $(r, v, \theta) = (0, v_1, -\pi/2)$. On the other hand, the other end point of Z has infinitely large λ-value. From the estimate of $|d\lambda/d\theta|$ in the proof of Lemma 4.2, Z_I also has infinitely large λ-value. Hence Z_I is an arc in the right wall of R_I (which is also the left wall of R_{II}), connecting $(r, v, \theta) = (0, v_1, -\pi/2)$ with infinity.

Region R_{II} is not flowing-rightward; orbits can leave R_{II} by w becoming negative, that is, θ begins to decrease. Nonetheless, we will construct part of Z_I, call Z'_I, that is trapped inside R_{II} by an invariant surface, namely, the stable manifold $W^s(L'_-)$, such that Z'_I can be followed to cross region R_{II}. (This idea of construction will be used for all the following proofs.) Recall that from Theorem 3.4.1, $W^s(L'_-) \cap P_1$ has dimension two. Consider the "quadrant" surface of $W^s(L'_-)$ in R_{II}; one edge of the surface is the Lagrange homothetic orbit connecting L'_+ to L'_-, and the other edge is the branch of $W^s(L'_-)$ on the collision manifold with $w > 0$. Since R_{II} is flowing-leftward in backward time, with the exception of the Lagrange homothetic orbit, orbits in this quadrant surface can be followed backward under the flow to reach the left wall of R_{II}. The backward image forms a curve in the left wall of R_{II}, having one endpoint at $(0, v_0, -\pi/2)$, which arises from the branch of $W^s(L'_-)$ in the collision manifold, and the other endpoint at $(0, -v_1, -\pi/2)$, which arises from the branch of $W^s(L'_+)$ in the collision manifold; moreover, this curve has $r > 0$ except at its two endpoints, since $\{r = 0\}$ is an invariant set. We have finished describing the trapping surface.

Now we construct Z'_I as follows. Recall that Z_I is an arc in the left wall of R_{II},

connecting $(r, v) = (0, v_1)$ with infinity. Since the flow on the collision manifold is gradient-like with respect to the variable v, we have $v_0 < -v^* < v_1 < -v_1$, where recall that $-v^*$ is the v-coordinate of L'_-. Therefore, Z_I and $W^s(L'_-)$ must intersect. Let q_I be the "first" intersection of Z_I with the backward image of $W^s(L'_-) \cap R_{II}$ in the left wall of R_{II}; choose Z'_I to be part of the Z_I that connects $(0, v_1, -\pi/2)$ with q_I. Then the surface $W^s(L'_-) \cap R_{II}$ serves as a roof preventing the points on Z'_I from leaving through the top boundary $\{w = 0\} \cap R_{II}$. Therefore, Z'_I can be followed across region R_{II} and forms a curve, say Z_{II}, in the left wall of R_{III}. (**Remark.** Here, "first" is in the sense when one imagines moving along Z_I starting from the root point $(0, -v_1, -\pi/2)$. Although figure 3.5.3(a) shows that Z_I and $W^s(L'_-)$ have only one intersection, it is unknown and is irrelevant to the proof whether there might be multiple intersections.)

Region R_{III} is flowing-rightward, so Z_{II} can be followed across region R_{III}, with its endpoints following the branches γ and γ', to the right wall of R_{III}, and forms an arc, called Z_{III}, connecting $(r, v, \theta) = (0, v_2, 0)$ with $(0, v_3, 0)$ in the left wall of R_{IV}. (**Remark.** The only distinction between our proof so far and the proof for Theorem 3.5.2 is that we do not require $v_2 > 0$ here. Note that if we replace the assumption $m_3 > \epsilon_1$ with the assumption $0 < m_3 < \epsilon_2$, then by Theorem 3.3.3, we have $v_3 < 0 < v_2$; therefore, by intermediate value theorem, Z_{III} includes a point with $v = 0$. This proves Theorem 3.5.2.)

Region R_{IV} is not flowing-rightward. To construct the part of Z_{III}, called Z'_{III}, that can be followed across region R_{IV}, we consider a trapping surface. More precisely, we consider the backward image of $W^s(L''_-) \cap R_{IV}$ in the left wall of R_{IV}, which is an arc, whose endpoints arise from $W^s(L''_+)$ and $W^s(L''_-)$ on the collision manifold. Moreover, the two points $(0, v_2, 0)$ and $(0, v_3, 0)$ must lie strictly inside the two endpoints just mentioned, otherwise γ and γ' will not be able to reach $\theta = \pi/2$, which makes a contradiction to the second paragraph of the proof. Now, to construct Z'_{III}, we discuss two cases depending on the position of Z_{III} relative to the arc. The first case is that Z_{III} is below this arc; in this case, $W^s(L''_-) \cap R_{IV}$ serves as a roof preventing the points in Z_{III} from leaving through the top boundary $\{w = 0\} \cap R_{IV}$. So Z_{III} will be followed across regions R_{IV} and R_V, with its endpoints following γ and γ', to the right wall of R_V and form an arc connecting $(0, v_4, \pi/2)$ with $(0, v_5, \pi/2)$. The second case is that only part of Z_{III} is below this arc; for this case, we use the same idea of the construction of

Z'_I as follows. Let p_{III} be the first intersection of Z_{III} and $W^s(L''_-)$, and let Z'_{III} be the part of Z_{III} connecting $(r, v, \theta) = (0, v_2, 0)$ with p_{III}. The surface $W^s(L''_-) \cap R_{IV}$ serves as a roof here; Z'_{III} can be followed across regions R_{IV} and R_V, with its endpoints following γ and $T_1(\gamma) \subseteq W^u(L''_-)$, and then form an arc connecting $(0, v_4, \pi/2)$ with $(0, v_1, \pi/2)$ in the right wall of R_V. Note that $v_1 < 0$, $v_4 > 0$, and $v_5 < 0$, so in both cases there is a point of the zero velocity curve Z which can be followed through all five regions to reach $\{\theta = \pi/2\}$ with $v = 0$.

□

Next we have the Type 1 periodic orbits.

Theorem 3.5.4. *(Type 1 periodic brake orbits) For any $0 < m_3 < \epsilon_2$ and $n \in N$, there exists a T-periodic brake orbit with the following properties: In a quarter of period, the orbit starts at a brake time, then crosses the binary collision line $\{\theta = -\pi/2\}$ n times, and then hits the Euler collinear line orthogonally at $t = T/4$, i.e., $(\theta(T/4), v(T/4)) = (0, 0)$. See the first row in figure 3.12. (**Remark.** The orbits in Theorem 3.5.2 are Type 1 with $n = 1$)*

Proof. Theorem 3.5.2 proves the case $n = 1$. Here, we prove the case $n = 2$ in detail; the proof can be generalized to prove the general case $n \in N$.

We use a shooting argument which starts from the zero velocity curve Z and targets at $Euler(-\pi, -)$. The main idea is to follow the zero velocity curve going between the two regions $\{w \geq 0\}$ and $\{w \leq 0\}$ and show that part of the zero velocity curve can cross R_I to enter R_{II}, then leave R_{II} through the top boundary surface $\{w = 0\}$, then enter Q_{II}, then cross Q_I, and then form an arc in $Euler(-\pi, -)$ with one end point that has $v > 0$ and the other end point that has $v < 0$. See figure 3.8.

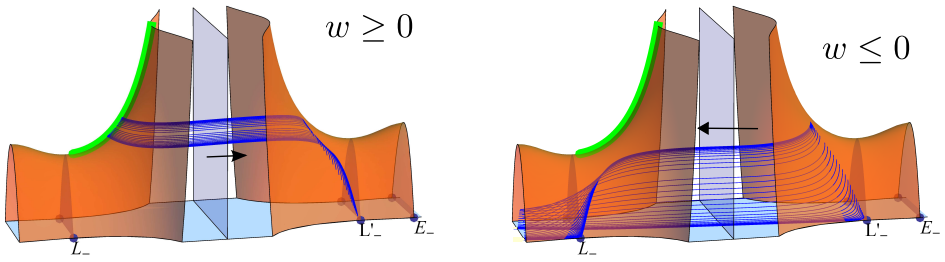

(a) Part of Z will cross R_I and leave R_{II} through the surface $\{w = 0\}$.

(b) Then enter Q_{II}, then cross Q_I, and then reach $Euler(-\pi, -)$.

Figure 3.8: For Theorem 3.5.4 with $n = 2$.

Again the branches γ and γ' play a key role here. By Theorem 3.3.3, for $0 < m_3 < \epsilon_2$, in Devaney's coordinates, the ϕ-variable of γ'' (which corresponds to $T_1\gamma$), first monotonically increases to $\phi = \pi/2$ and then monotonically decreases at least until it reaches $\phi = -\pi/2$; the ϕ-variable of γ' first monotonically increases to $\phi = \pi/2$ and then monotonically decreases at least until it reaches $\phi = 0$. This implies that, in the new coordinates, γ'' (respectively γ') stays in $\{w > 0\}$ at least until it crosses the second binary collision line (respectively the first Euler collinear line $\theta = 0$). The fact that γ'' intersects $\phi = 0$ after it intersects $v = 0$ implies that γ'' has $v > 0$ at the intersection in Devaney's coordinates; in the new coordinates, this means γ intersects $\theta = 0$ at $v = v_2 > 0$. The fact that γ' intersects $\phi = 0$ before it intersects $v = 0$ implies that γ' has $v < 0$ at the intersection; in the new coordinates, this means γ' intersects $\theta = 0$ at $v = v_3 < 0$.

Additionally, we denote the branches of $W^u(L_-)$ and $W^u(L'_-)$ on the collision manifold with initially $w < 0$ by γ_- and γ'_- respectively. Note that from symmetry, one may reflect γ and γ' with respect to the line $\theta = -\pi/2$ to obtain γ_- and γ'_-. It is worth marking that both γ and γ'_- intersect $\theta = -\pi/2$ with $v = v_1$. See figure 3.9 for these branches.

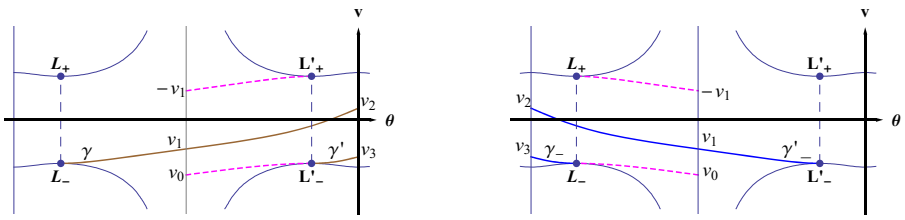

(a) $w \geq 0$ (b) $w \leq 0$

Figure 3.9: For $0 < m_3 < \epsilon_2$, the branches γ,γ_- of $W^u(L_-)$ and γ',γ'_- of $W^u(L'_-)$ are shown. Note that γ and γ' lie in $\{w \geq 0\}$ while γ_- and γ'_- lie in $\{w \leq 0\}$. The thicker dashed curves represent stable manifolds.

We start from region R_I, which is flowing-rightward. Let Z and Z_I be defined as in the third paragraph of the proof for Theorem 3.5.3. Recall that Z_I is an arc in the left wall of R_{II}, connecting $(r, v, \theta) = (0, v_1, -\pi/2)$ with infinity. Also recall that we have defined $\lambda = \sqrt{2r + v^2}$ in the proof of Lemma 3.4.2.

Region R_{II} is not flowing-rightward but is flowing-leftward in backward-time. We will construct Z''_I such that all points on Z''_I leave R_{II} through the top boundary, enter the region Q_{II}, cross the region, and then form a curve connecting the floor with infinity in the left wall of Q_{II}. First, we show that points on Z_I with a sufficiently large λ-value cannot reach the right wall of R_{II}. In the proof of Lemma 3.4.2, it is shown that for an orbit with θ monotone increasing, we have $|d\lambda/d\theta| \leq w/2$. Note that w is bounded in the energy manifold, so there is a uniform bound of the change of λ-value for all orbits that stay in R_{II}. On the other hand, in the right wall of R_{II}, we have $\lambda \leq \sqrt{2V(\theta)} = \sqrt{2V(\theta^*)}$. So points on Z_I with a sufficiently large λ-value cannot reach the right wall of R_{II}. Second, we consider the "quadrant" of the surface $W^s(L'_-)$ in R_{II}. As described in the proof of Theorem 3.5.3, this surface can be followed backward to reach the right wall of R_I and form an arc connecting $(0, v_0, -\pi/2)$ with $(0, -v_1, -\pi/2)$. Let p_I be the last point of Z_I that intersects this surface. Let Z''_I be the part of Z_I that is above p_I. Then all points on Z''_I cannot reach the right wall of R_{II}; instead, they leave R_{II} from the top surface $\{w = 0\}$, and then they enter Q_{II}. (Note that R_{II} and

Q_{II} can be glued together along their common boundary in $\{w = 0\}$.)

Region Q_{II} is flowing-leftward. Let Z_{II} be the image of Z_I'' in the left wall of Q_{II}. The curve Z_{II} has one end point at $(r, v, \theta) = (0, v_1, -\pi/2)$ with $w < 0$, which arises from γ'_-, and the other end point at infinity.

Region Q_I is not flowing-leftward but is flowing-rightward in backward-time; not all of Z_{II} can be followed to the left wall of Q_I. Using the same trick as before, we consider only part of Z_{II}, i.e., let Z'_{II} be part of the Z_{II} that is below the backward image of $W^s(L_-)$. Then Z'_{II} can be followed to $Euler(-\pi, -)$. The image of Z'_{II} in $Euler(-\pi, -)$, say Z_{III}, is a curve connecting $(r, v, \theta) = (0, v_2, -\pi)$ and $(0, v_3, -\pi)$. Recall that $v_2 > 0$ and $v_3 < 0$, so Z_{III} includes the point $(r, v, \theta) = (0, 0, -\pi)$. This point yields a brake periodic orbit that hits $\theta = -\pi$ orthogonally at $t = T/4$; after translating this orbit by $\theta \to \theta + \pi$ and reversing the orbit, we obtain the case $n = 2$.

Furthermore, if instead of considering Z'_{II}, we consider Z''_{II} to be the part of Z_{II} that is above the backward image of $W^s(L_-)$, then all points on Z''_{II} will leave Q_I through the top surface $\{w = 0\}$, enter R_I, and then reach the right wall of R_I, forming a curve connecting $(r, v, \theta) = (0, v_1, -\pi/2)$ and infinity; the situation now is exactly the same as that when we have Z_I. By repeating the same arguments as before, one may construct orbits that go between $\{w \geq 0\}$ and $\{w \leq 0\}$ as many times as desired and then reach $Euler(0, +)$ or $Euler(0, -)$ orthogonally. This proves the general case $n \in \mathbf{N}$.

□

Next we have the Type 2 periodic brake orbits.

Theorem 3.5.5. *(Type 2 periodic brake orbits) For all $m_3 > \epsilon_1$ and $n \in N$, there exists a T-periodic brake orbit with the following properties: The orbit starts at a brake time, then crosses the binary collision line $\{\theta = -\pi/2\}$ n times, then crosses the Euler collinear line $\{\theta = 0\}$, and then hits the binary collision line $\{\theta = \pi/2\}$ orthogonally at $t = T/4$, i.e., $(\theta(T/4), v(T/4)) = (\pi/2, 0)$. See the second row in figure 3.12.*
Remark. The orbits in Theorem 3.5.3 are Type 2 with $n = 1$.

Proof. For any $n \in N$, using the same arguments as in Theorem 3.5.4, one may show that part of Z can be followed to cross $Binary(-\pi/2, \pm)$ n times, and then form an arc, say Z_{III}, in $Euler(0, +)$ if n is odd, or in $Euler(-\pi, -)$ if n is even. The two endpoints

of the arc are at $(r, v) = (0, v_2)$ and $(0, v_3)$, where the branches of unstable manifolds γ and γ' for odd n (or γ_- and γ'_- for even n) cross the wall.

Then we use arguments similar to the last paragraph in Theorem 3.5.3. For odd n, part of Z_{III} can be followed to form an arc in $Binary(\pi/2, +)$ with endpoints at $v = v_1$ and v_4 or at v_4 and v_5. For even n, part of Z_{III} can be followed to form an arc, say Z_{IV}, in $Binary(-3\pi/2, -)$ with endpoints at $v = v_1$ and v_4 or at v_4 and v_5. Again $v_1 < 0$, $v_4 > 0$, and $v_5 < 0$, so there is a point on Z_{IV} with $v = 0$. Thus there is a point on Z that can be followed to cross $Binary(-\pi/2, \pm)$ n times, and then reach $Binary(\pi/2, +)$(for odd n) or $Binary(-3\pi/2, -)$(for even n) orthogonally. For even n, after translating the orbit by $\theta \to \theta + 2\pi$, we obtain an orbit that crosses $Binary(-3\pi/2, \pm)$ n times and reaches $Binary(\pi/2, -)$ orthogonally, as shown in figure 3.12(e). After reversing this orbit, we obtain the orbit described in the theorem. □

Next we have the Type 3 and 4 orbits.

Theorem 3.5.6. *For any $\epsilon_1 < m_3 < \epsilon_2$ and $n \in N$, there exists T-periodic brake orbits of the following two types:*

Type 3: The orbit stays in $\{w \geq 0\}$ until $t = T/2$. In a quarter of period, the orbit starts at a brake time, then crosses n binary collision lines, and then hits the Euler collinear line $\{\theta = (n-1)\pi\}$ orthogonally at $t = T/4$. (The orbits in Theorem 3.5.2 are both Type 1 and Type 3 with $n = 1$.)

Type 4: The orbit stays in $\{w \geq 0\}$ until $t = T/2$. In a quarter of period, the orbit starts at a brake time, then crosses n binary collision lines, then crosses the Euler collinear line $\{\theta = (n-1)\pi\}$, and then hits the binary collision line $\{\theta = \pi(2n-1)/2\}$ orthogonally at $t = T/4$. (The orbits in Theorem 3.5.3 are both Type 2 and Type 4 with $n = 1$.)

For both Type 3 and 4 orbits, between two consecutive binary collisions, the orbits always cross a Euler collinear line.

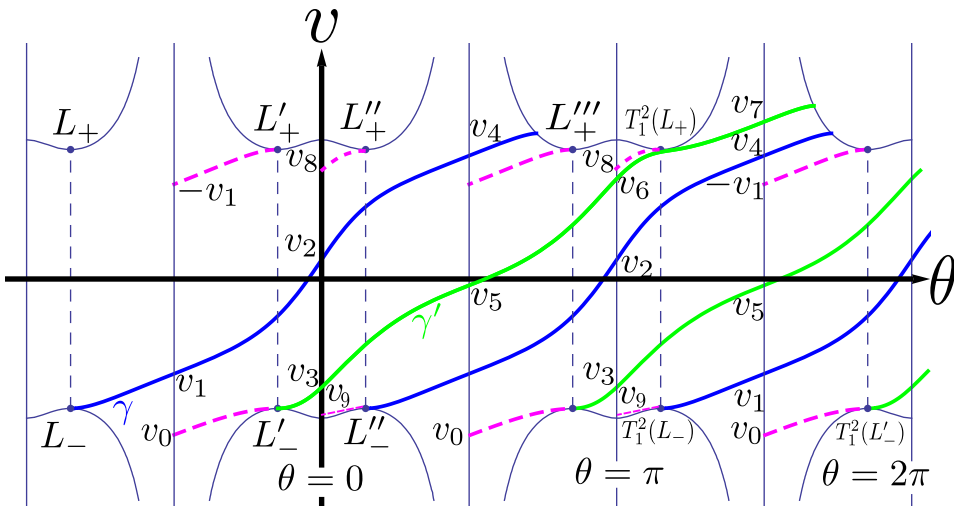

Figure 3.10: For $\epsilon_1 < m_3 < \epsilon_2$.

Proof. By Theorem 3.3.3, for $\epsilon_1 < m_3 < \epsilon_2$, both the branches γ and γ' remain in $\{w \geq 0\}$ at least until they cross two binary collision lines. The branch γ first intersects the binary collision line $\{\theta = -\pi/2\}$, say at $v = v_1$, then the Euler collinear line $\{\theta = 0\}$, say at $v = v_2$, and then the second binary collision line $\{\theta = \pi/2\}$, say at v_4. Also note that from symmetry, the intersection of the line $\{\theta = -\pi/2\}$ and the branch of $W^s(L'_+) \cap \{r = 0\}$ with $w \geq 0$ is at $v = -v_1$. On the other hand, the branch γ' intersects the Euler collinear line $\{\theta = 0\}$, say at $v = v_3$, then the binary collision line $\{\theta = \pi/2\}$, say at v_5, then the second Euler collinear line $\{\theta = \pi\}$, say at v_6, and then the second binary collision line $\{\theta = 3\pi/2\}$, say at v_7. Additionally, denote the intersections of the Euler collision line $\{\theta = 0\}$ with the $w > 0$ branches of $W^s(L''_+) \cap \{r = 0\}$, $W^s(L''_-) \cap \{r = 0\}$ by v_8 and v_9 respectively. We remark that by symmetry, $v_8 = -v_3$. Moreover, denote the intersection of $\theta = -\pi/2$ with the $w > 0$ branch of $W^s(L'_-) \cap \{r = 0\}$ by v_0. Theorem 3.3.3 implies that $v_9 < v_3 < 0 < v_2 < v_6 < v_8$, and that $v_0 < v_1 < v_5 < 0 < -v_1 < v_4 < v_7$. See figure 3.10.

Similar to the proofs for Type 1 and 2 orbits, we will follow part of the zero velocity curve Z to cross regions. The resulted image arcs in an Euler plane always satisfy some of the following conditions: (i) every point on the arc has $r > 0$ except the two endpoints, (ii.a) the endpoints are at $(r, v) = (0, v_2)$ and at $(r, v) = (0, v_3)$, (ii.b) the

endpoints are at $(r, v) = (0, v_3)$ and at $(r, v) = (0, v_6)$, (iii.a) the whole arc can be followed to reach the nearest Lagrange plane, and (iii.b) only part of the arc can be followed to reach the nearest Lagrange plane.

Consider the part of the energy manifold P_1 with $w \geq 0$. An arc in an Euler plane is said to be in *State 1* if conditions (i)(ii.a)(iii.a) are satisfied, in *State 2* if conditions (i)(ii.a)(iii.b) are satisfied, in *State 3* if conditions (i)(ii.b)(iii.a) are satisfied, and in *State 4* if conditions (i)(ii.b)(iii.b) are satisfied. Note that (iii.a) and (iii.b) are mutually exclusive conditions, and whichever condition (iii.a) or (iii.b) occurs depends on the relative position of the arc to the stable manifold of a certain Lagrange point. Specifically, if the arc is below the backward image of the stable manifold, then (iii.a) holds; if only part of the arc is below the backward image of the stable manifold, then (iii.b) holds.

One can show that for any $i \in \{1, 2, 3, 4\}$, a State i arc includes an arc that can be followed to reach the next Euler plane and forms a State j arc for some $j \in \{1, 2, 3, 4\}$. In particular, a State 1 arc includes an arc that can be followed to form a State 3 or 4 arc. A State 2 arc includes an arc that can be followed to form a State 1 or 2 arc. A State 3 arc includes an arc that can be followed to form a State 3 or 4 arc. A State 4 arc includes an arc that can be followed to form a State 1 or 2 arc.

Figure 11 illustrates the process of the proof. The reader may imagine that the collision manifold lies on the paper, while the positive $r-$direction points out of the paper. We will follow a State i arc across four regions, and the image arcs stand off of the paper except for their endpoints. Without loss of generality, we may assume the State i arc lies in $Euler(\pi, +)$, and the goal now is to construct part of the arc that can be followed across the four regions: $P_1 \cap \{\pi \leq \theta \leq \pi + \theta^*\}$, $P_1 \cap \{\pi + \theta^* \leq \theta \leq 3\pi/2\}$, $P_1 \cap \{3\pi/2 \leq \theta \leq 2\pi - \theta^*\}$, and $P_1 \cap \{2\pi - \theta^* \leq \theta \leq 2\pi\}$, to reach $Euler(2\pi, +)$. On the one hand, it is straightforward to cross a flowing-rightward region; the endpoints simply follow two of the branches γ', $T_1(\gamma)$, $T_1(\gamma')$, or $T_1^2(\gamma)$. On the other hand, to cross a region that is flowing-leftward in backward-time, one uses either the conditions (iii.a) or (iii.b) with the "roof-construction" as before; specifically, one considers the backward images of either $W^s(T_1^2(L_-))$ or $W^s(T_1^2(L'_-))$ intersecting with the image arc in $Euler(\pi, +)$ or $Binary(3\pi/2, +)$. The "first" intersection point is marked by a star ($\bigstar$), which divides the image arc into two pieces; one piece, which can be followed to

cross the next region, is marked with a tick ($\surd$). (Remark. Here, "first" is in the sense when one moves along the image arc starting from its endpoint that lies on the marked piece to the other endpoint.) Following the process shown in figure 3.11, for an arc of any state in $Euler(\pi, +)$, one may construct part of the arc that can be followed to reach the $Euler(2\pi, +)$ to form a State i arc for some $i \in \{1, 2, 3, 4\}$.

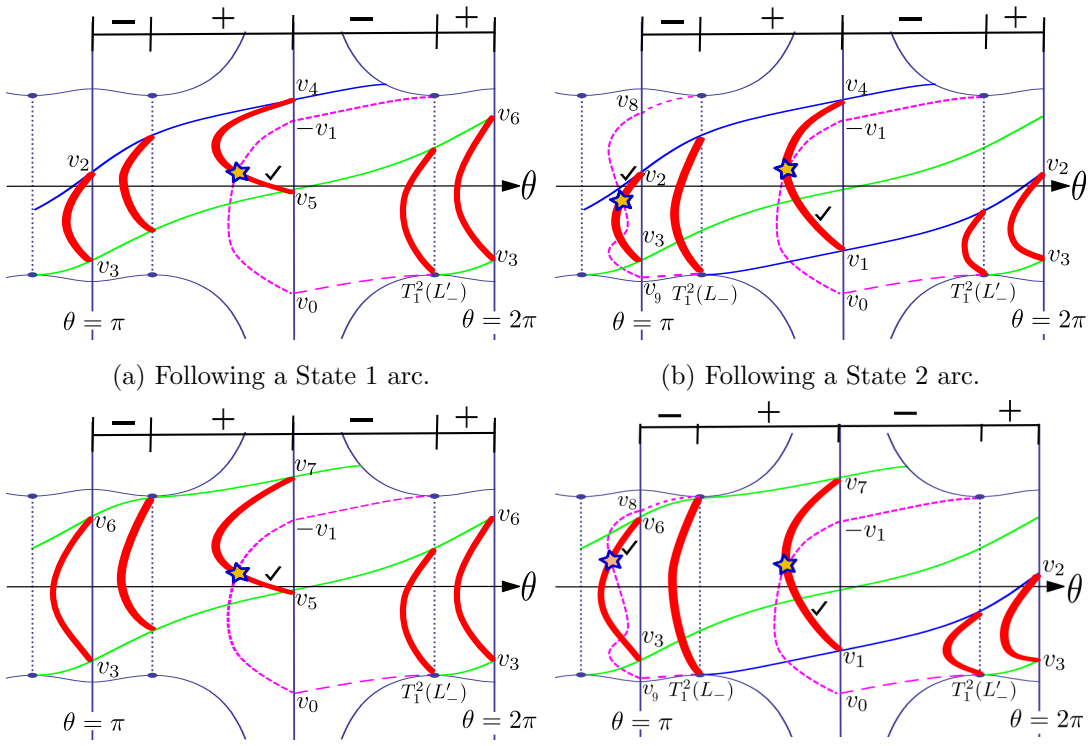

(a) Following a State 1 arc.

(b) Following a State 2 arc.

(c) Following a State 3 arc.

(d) Following a State 4 arc.

Figure 3.11: For Theorem 5.6. The figure shows the process to follow arcs of four states across regions. A region is marked with a positive sign (+) if it is flowing-rightward, and a negative sign (-) if it is flowing-leftward in backward-time. The image arc in each plane is represented by the thickest red solid curve. The backward images of certain stable manifolds are represented by the magenta dashed curves.

We now are ready to prove the existence of Type 3 and 4 periodic brake orbits. Again let Z be the zero velocity curve in region R_I. Following the arguments presented in the first six paragraphs of the proof for Theorem 3.5.3, we obtain an arc Z_{III} in the

right wall of R_{III}, connecting $(r, v, \theta) = (0, v_2, 0)$ with $(0, v_3, 0)$, and has $r < 0$ except at the endpoints. From the definition, Z_{III} is an arc of either State 1 or 2. Therefore, part of Z_{III} can be followed to the next Euler plane to form an arc of State i for some $i \in \{1, 2, 3, 4\}$. Inductively we may construct part of Z_{III} to stay in $\{w \geq 0\}$ and reach as many Euler planes as desired. The intersection of the image arc and the Euler plane forms an arc whose endpoints are either at $v = v_2 > 0$ and $v_3 < 0$ or at $v_3 < 0$ and $v_6 > 0$. In both cases, the image arc includes a point in the Euler plane with $v = 0$, which corresponds to a Type 3 periodic orbit by Lemma 3.5.1(ii). On the other hand, the intersection of the image arc and the binary collision plane forms an arc whose one endpoint is either at $v_1 < 0$ or at $v_5 < 0$, and the other endpoint is either at $v_4 > 0$ or at $v_7 > 0$; in every case, the image arc includes a point in the binary collision plane with $v = 0$, which corresponds to a Type 4 periodic orbit by Lemma 3.5.1(iii).

□

3.6 Finding More Periodic Brake Orbits

Now we use the condition (i) in Lemma 3.5.1 to find Type 5 and 6 periodic brake orbits. Unlike Type 1 to 4 orbits, these orbits are not symmetric with respect to any Euler collinear lines or binary collision lines when projected to the (r, θ)-plane. These orbits start with zero velocity and reach zero velocity again in half the period.

Theorem 3.6.1. *(Type 5 periodic brake orbits) Let $0 < m_3 < \epsilon_2$. For every pair of positive integers (i, j), there exists a periodic brake orbit with the following property: In a half period, the orbit starts at a brake time, then crosses the binary collision line $\{\theta = -\pi/2\}$ i times, then crosses the Euler collinear line $\{\theta = 0\}$, then crosses the binary collision line $\{\theta = \pi/2\}$ j times, and then reaches zero velocity. See figure 3.12.*

Proof. The main idea is to shoot from two different zero velocity curves, one in forward time and the other in backward time, to form two arcs in the plane $Euler(0, +)$, and show that the two arcs must intersect. An intersection point yields a connection between the two zero velocity curves, and the corresponding orbit is periodic according to Lemma 3.5.1(i)

In the proof of Theorem 3.5.4, for general $n \in N$, one shows that part of the zero

velocity curve in R_I, say S_n, can be followed to cross the two planes $Binary(-\pi/2, \pm)$ n times to reach $Euler(0, +)$ or $Euler(-\pi, -)$. Specifically, for odd n, we can construct S_n, which is a zero velocity curve contained in Z, such that its image, say Γ_n, forms an arc connecting $(r, v) = (0, v_2)$ and $(0, v_3)$ in $Euler(0, +)$; for even n, we can construct S_n, which is a zero velocity curve contained in Z, such that its image curve, say Γ_n, forms an arc connecting $(0, v_2)$ and $(0, v_3)$ in $Euler(-\pi, -)$. The endpoints of Γ_n always lie on the collision manifold, i.e., $r = 0$; from now on, we will omit writing the variables r, θ, w and only keep the variable v when there is no confusion.

We remark that $-v_3 \neq v_2$. This can be seen from the following argument. Figure 3.10 provides a correct picture for γ not only for $\epsilon_1 < m_3 < \epsilon_2$ but also for $0 < m_3 < \epsilon_2$. We note that $v_8 = -v_3$ by symmetry. If $-v_3 = v_2$, then $v_8 = v_2$, and γ becomes a connection orbit between L_- and L''_+, which is impossible for any mass ratio by Theorem 3.3.3.

We now prove the theorem for the case when both i and j are odd. In this case, both Γ_i and Γ_j are arcs in $Euler(0, +)$ connecting v_2 with v_3. Points on S_j can be followed to form Γ_j. Since the system is reversible, points on $R_2\Gamma_j$ can be followed to form R_2S_j. Note that $R_2\Gamma_j$ is an arc in $Euler(0, +)$ connecting $-v_3$ with $-v_2$; therefore, provided $-v_3 \neq v_2$, $R_2\Gamma_j$ and Γ_i must intersect. An intersection point yields an orbit connecting the two zero velocity curves S_i and R_2S_j. This proves the case when both i and j are odd. Furthermore, the case when both i and j are even can be proved similarly.

Next we prove the theorem for the case when i is odd and j is even. In this case, Γ_i is an arc in $Euler(0, +)$ connecting v_2 with v_3; S_j is a zero velocity curve in R_I such that all points on S_j cross $Binary(-\pi/2, \pm)$ j times, and then form Γ_j in $Euler(-\pi, -)$, connecting v_2 with v_3. Consider the translation of S_j by π, that is, T_1S_j; then all points on T_1S_j cross $Binary(\pi/2, \pm)$ j times and then form $T_1\Gamma_j$ in $Euler(0, -)$, connecting v_2 with v_3. The curve T_1S_j can be followed to form $T_1\Gamma_j$. Since the system is reversible, the arc $R_1T_1\Gamma_j$ can be followed to form $R_1T_1S_j$. Note that $R_1T_1\Gamma_j$ is an arc in $Euler(0, +)$ connecting $-v_3$ with $-v_2$; therefore, provided $-v_3 \neq v_2$, $R_1T_1\Gamma_j$ and Γ_i must intersect. An intersection point yields an orbit connecting the two zero velocity curves S_i and $R_1T_1S_j$. This proves the case when i is odd and j is even. Additionally, from the symmetry of the system, we obtain the case when i is even and j is odd.

□

Theorem 3.6.2. *(Type 6 periodic brake orbits) Let $\epsilon_1 < m_3$ and $m_3 \neq \epsilon_2$. For every pair of positive integers (i, j), there exists a periodic brake orbit with the following properties: In a half period, the orbit starts at a brake time, then crosses the binary collision line $\{\theta = -\pi/2\}$ i times, then crosses the binary collision line $\{\theta = \pi/2\}$, then crosses the binary collision line $\{\theta = 3\pi/2\}$ j times, and then reaches zero velocity. See figure 3.12.*

Proof. The proof is similar to the proof for Theorem 3.6.1; we show the existence of a point that connects two zero velocity curves. The major difference is that the target plane is now replaced by $Binary(\pi/2, +)$.

Now we recall the proof for Theorem 3.5.5 and define S'_n and Γ'_n as follows. To prove Theorem 3.5.5 for $m_3 > \epsilon_1$ and general $n \in N$, for odd n, one shows that part of Z, say S'_n, can be followed to cross $Binary(-\pi/2, \pm)$ n times and then form an arc, say Γ'_n, connecting v_1 with v_4 or v_4 with v_5 in $Binary(\pi/2, +)$. For even n, one shows that part of $T_1^2 Z$ (the translation of Z by $\theta \to \theta + 2\pi$), say S'_n, can be followed to cross $Binary(3\pi/2, \pm)$ n times and then form an arc, say Γ'_n, connecting v_1 with v_4 or v_4 with v_5 in $Binary(\pi/2, -)$.

We remark that $-v_1 \neq v_4$ and $-v_5 \neq v_4$. This can be seen from the following argument. Here we use the same notations as in figure 3.10. First, we show that $-v_1 \neq v_4$. Note that the $w > 0$ branch of $W^s(L'''_+) = T_1(W^s(L'_+))$ on the collision manifold intersects $\theta = \pi/2$ at $v = -v_1$. If $-v_1 = v_4$, then γ becomes a connection orbit between L_- and L'''_+; from Theorem 3.3.3, this is possible only when $m_3 = \epsilon_2$. Second, we show that $-v_5 \neq v_4$. Note that by symmetry, the $w > 0$ branch of $W^s(T_1^2(L_+))$ on the collision manifold intersects $\theta = \pi/2$ at $v = -v_5$. (This branch is not shown in figure 3.10). If $-v_5 = v_4$, then γ becomes a connection orbit between L_- and $T_1^2(L_+)$, which is impossible for any mass ratio.

Now we prove the theorem for the case when both i and j are odd. In this case, Γ'_i and Γ'_j are both arcs in $Binary(\pi/2, +)$ connecting either v_1 with v_4 or v_4 with v_5. Points on S'_i and S'_j can be followed to form Γ'_i and Γ'_j respectively. Since the system is reversible, points on $T_1 R_2 \Gamma'_j$ can be followed to form $T_1 R_2 S'_j$. Note that $T_1 R_2 \Gamma'_j$ is an arc in $Binary(\pi/2, +)$ connecting $-v_1$ with $-v_4$ or $-v_4$ with $-v_5$; therefore, provided $-v_1 \neq v_4$ and $-v_5 \neq v_4$, the arcs $T_1 R_2 \Gamma'_j$ and Γ'_i must intersect. An intersection point yields an orbit connecting the two zero velocity curves S'_i and $T_1 R_2 S'_j$

To prove the other cases, one may apply suitable transformations to S_i' and S_j' such that such that their image arcs intersect in $Binary(\pi, +)$ after the transformations. An intersection point yields a connection between two zero velocity curves, and hence yields a period orbits desired. In particular, when both i and j are even, one considers the intersection of $R_1T_1R_2\Gamma_i'$ and $R_1\Gamma_j'$. When i is odd and j is even, one considers the intersection of Γ_i' and $R_1\Gamma_j'$. Additionally, from the symmetry of the system, one obtains the case when i is even and j is odd.

□

Final remark about the stability properties. To study the stability of the periodic brake orbits, we have numerically computed the Floquet multipliers of the orbits in figure 3.12. The Floquet multipliers of a periodic orbit are the eigenvalues of the monodromy matrix of the orbit. By applying Roberts' technique [34], the monodromy matrix of a periodic orbit can be determined from the first quarter of the orbit for Type 1 to 4 orbits, and from the first half of the orbit for Type 5 and 6 orbits. All of the orbits (with three equal masses) in figure 3.12 are unstable. Specifically, their Floquet multipliers are: $1, 1, \lambda, 1/\lambda$, where λ is real, and $\lambda \gg 1$ for each orbit. The stability properties for other periodic brake orbits with various mass-ratios or with larger numbers of binary collisions are still unknown.

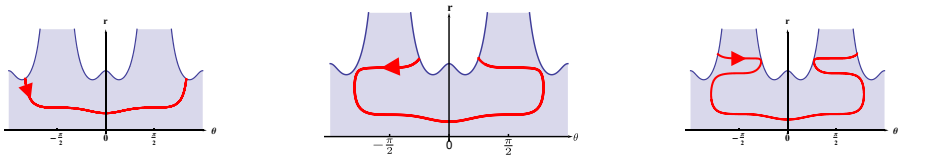

(a) Type 1 with $n = 1$ (b) Type 1 with $n = 2$ (c) Type 1 with $n = 3$

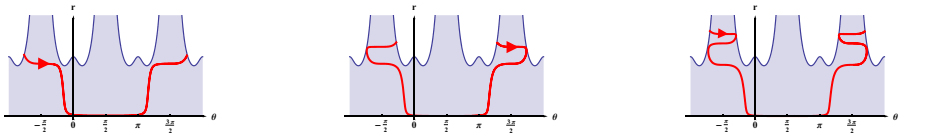

(d) Type 2 with $n = 1$ (e) Type 2 with $n = 2$ (f) Type 2 with $n = 3$

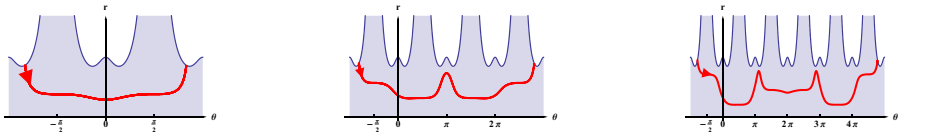

(g) Type 3 with $n = 1$ (h) Type 3 with $n = 2$ (i) Type 3 with $n = 3$

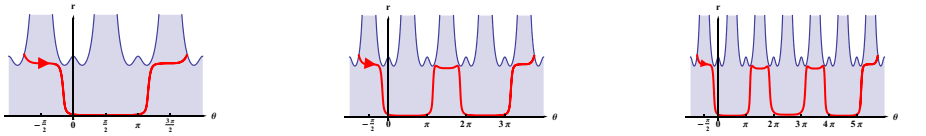

(j) Type 4 with $n = 1$ (k) Type 4 with $n = 2$ (l) Type 4 with $n = 3$

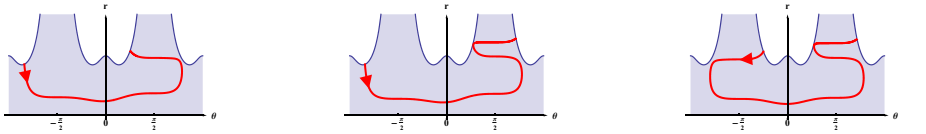

(m) Type 5: (i,j)=(1,2) (n) Type 5: (i,j)=(1,3) (o) Type 5: (i,j)=(2,3)

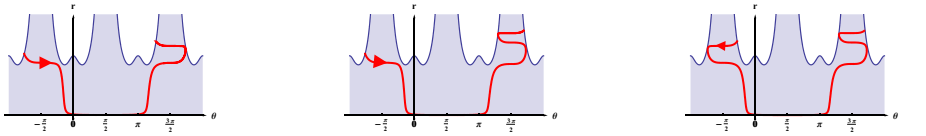

(p) Type 6: (i,j)=(1,2) (q) Type 6: (i,j)=(1,3) (r) Type 6: (i,j)=(2,3)

Figure 3.12: Six types of periodic orbits projected onto the (r, θ)-plane in the new coordinates. Every orbit starts with zero velocity. Only half of the period are plotted; each orbit will retrace its path in the other half period. All orbits are plotted with masses $m_1 = m_2 = m_3 = 1$.

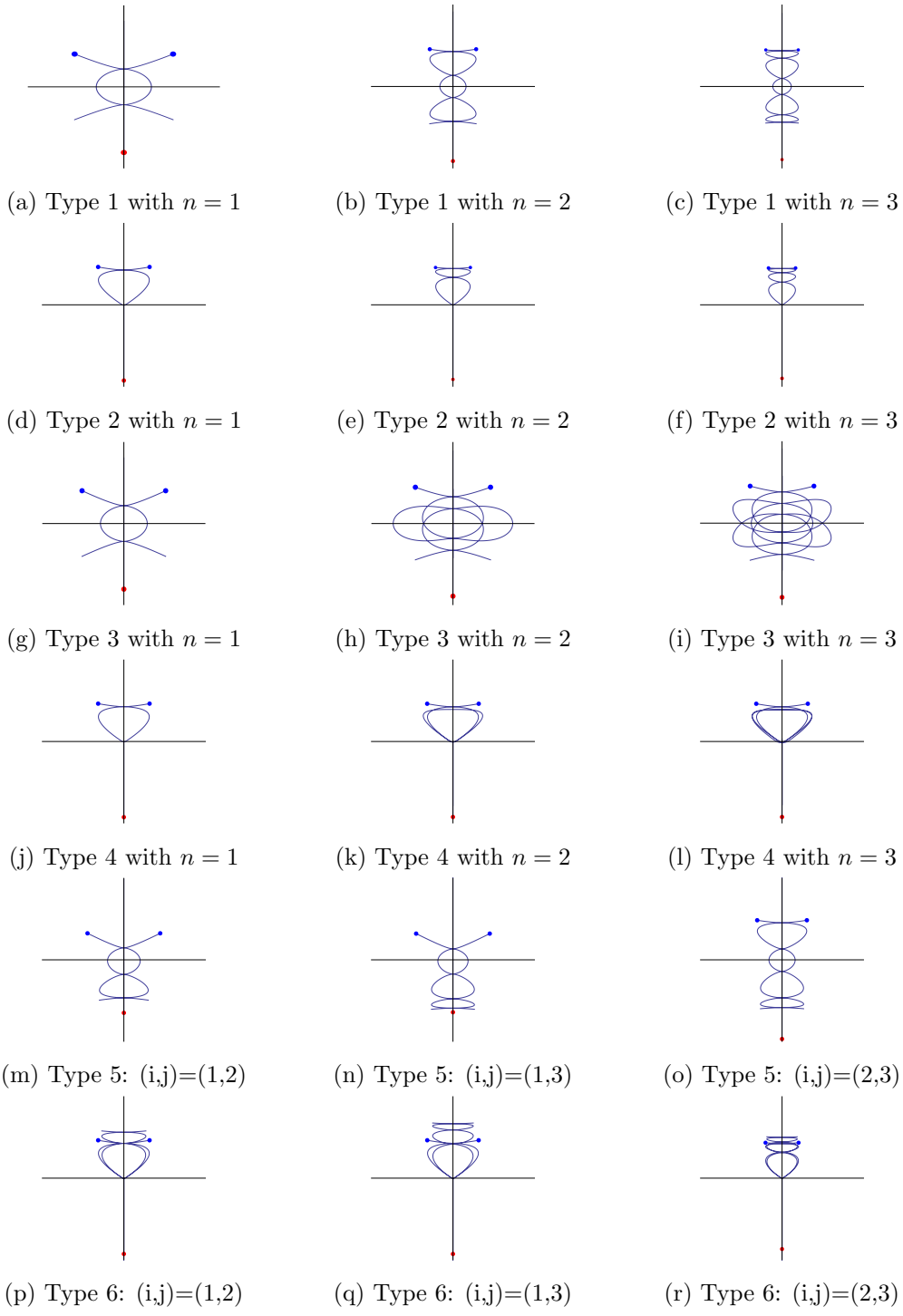

(a) Type 1 with $n = 1$ (b) Type 1 with $n = 2$ (c) Type 1 with $n = 3$

(d) Type 2 with $n = 1$ (e) Type 2 with $n = 2$ (f) Type 2 with $n = 3$

(g) Type 3 with $n = 1$ (h) Type 3 with $n = 2$ (i) Type 3 with $n = 3$

(j) Type 4 with $n = 1$ (k) Type 4 with $n = 2$ (l) Type 4 with $n = 3$

(m) Type 5: (i,j)=(1,2) (n) Type 5: (i,j)=(1,3) (o) Type 5: (i,j)=(2,3)

(p) Type 6: (i,j)=(1,2) (q) Type 6: (i,j)=(1,3) (r) Type 6: (i,j)=(2,3)

Figure 3.13: The orbits in figure 3.12 plotted in the configuration space.

Acknowledgements

The author would like to thank Professor Moeckel for his Mathematica notebook which gave this research a fun start, for guiding the author in the right direction, and for several helpful discussions. The author also thanks Richard Moeckel and Sean Vig for their numerical data of Type 1 to 4 orbits, which inspired the author to prove the existence of such orbits, and were used to plot figures 3.12 and 3.13. The author thanks the referees for their valuable comments that help to improve the manuscript. The research is partially supported by NSF grant DMS-1208908.

Chapter 4

Highly-Symmetric N-body Problems

We study three sub-problems of the N-body problem that have two degrees of freedom, namely the $n-$pyramidal problem, the planar double-polygon problem, and the spatial double-polygon problem. By extending the topological shooting arguments used in Chapter 2, we prove the existence of several families of symmetric periodic orbits, including "Schubart-like" orbits and brake orbits.[1]

4.1 Introduction

The Newtonian n-body problem studies the motion of n point masses moving in the Euclidean space, under the influence of their mutual gravitational attraction. The motion is determined by the system of differential equations:

$$\ddot{\mathbf{x}}_i = \sum_{j \neq i}^{n} m_j \frac{\mathbf{x}_j - \mathbf{x}_i}{|\mathbf{x}_j - \mathbf{x}_i|^3}, \quad \mathbf{x}_i \in \mathbf{R}^3,$$

where $\mathbf{x}_i$ and m_i represent the position and the mass of the i-th mass respectively.

One of the difficulties in studying the $n-$body problem is due to the large number of variables. Therefore, sub-problems of the $n-$body problem that have lower degrees of freedom, which are usually obtained by adding constraints on the configurations, have

[1] The content in this chapter has been published in [8].

received considerable attention. Two very popular examples are the collinear three-body problem and the isosceles three-body problem.

On one hand, a well-known periodic orbit in the collinear three-body problem is the so called Schubart orbit, formed by two equal masses $m_1 = m_2$ and another mass m_3, bouncing in between and having binary collisions with m_1, m_2 alternatively. This orbit was numerically found by Schubart [37]. Moeckel [26] and Venturelli [46] separately proved its existence by using topological shooting arguments and variational methods. On the other hand, in the isosceles three-body problem, Broucke found a symmetric periodic orbit [4], called Broucke orbit or a "Schubart-like" orbit, formed by two equal masses $m_1 = m_2$ whose positions are symmetric with respect to a fixed axes, along with a third mass m_3 that is moving up and down on the axes. See table 3.12(a) for the Broucke orbit. Broucke orbit has been proved to exist by Shibayama [40] and Martínez [18] separately. A "Schubart-like"(Broucke) orbit is similar to Schubart orbit in the sense that in one period, they both have two singularities due to binary collisions, and that when a binary collision occurs, the third mass reaches its maximum distance to the origin.

The motivation for this paper comes from the work of Martínez [18, 19] and Chen [7]. Martínez [18] studies certain Hamiltonian systems with two degrees of freedom and provides sufficient conditions for the existence of doubly symmetric "Schubart-like" periodic orbits (DSSP orbits) in these systems. These sufficient conditions are applied to three examples, namely the $n-$pyramidal problem, the $2n$-planar problem, and the double-polygon problem. However, the double-polygon problem fails one of these sufficient conditions. Recently, Martínez [19] extended her previous results. While the previously proved Schubart-like orbits have only one singularity in a half period (called 0-DSSP orbits), the orbits in the new paper have a sufficiently large number of singularities in a half period (called k-DSSP orbits), yet the existence proof requires one hypothesis that is verified only for several values of n. On the other hand, another six families of periodic orbits in the isosceles three-body problem are proved to be existed by using topological shooting arguments [7]. These are the so called brake orbits; that is, these orbits have zero initial velocity.

In this paper, we apply the framework from [7] to the following three problems:

the $n-$pyramidal problem, the planar double-polygon problem, and the spatial double-polygon problem. See table 4.2. First, the $n-$pyramidal problem is a spatial problem which consists of n masses whose configuration forms a planar regular $n-$gon, along with an additional mass lying on the vertical axes crossing the center of the $n-$gon. We remark that when $n = 2$, the $n-$pyramidal problem is identical to the planar isosceles three-body problem. Second, in the planar double-polygon problem, the configuration of the $2n$ bodies forms two regular $n-$gons in the plane. Third, in the spatial double-polygon problem, the configuration of the $2n$ bodies forms an anti-prism. We remark that the spatial double-polygon problem is a new example that has not appeared in [18, 19], and it is a special case of the dihedral n-body problem. The dihedral n-body problem is proposed by Ferrario and Portaluri in [14], where they find all central configurations and compute the dimensions of the stable/unstable manifolds, while the existence of periodic orbits with collision singularities has not been studied yet.

We prove the existence of several families of periodic orbits in the $n-$pyramidal problem and the spatial double-polygon problem. Representative orbits in the isosceles problem can be found in table 3.12. To picture orbits of the same types in other problems, for the $n-$pyramidal problem, one may imagine replacing the two symmetric bodies in the isosceles problem with n bodies lying on the vertices of a regular $n-$gon; for the spatial double-polygon problem, one furthermore replaces the third body with another n bodies lying on the vertices of another regular $n-$gon. As for the planar double-polygon problem, unfortunately, as in [18], there are difficulties to apply our arguments. Nonetheless, we complete Martínez's existence proof for 0-DSSP orbits, in which one of her three sufficient conditions fails, by showing that two of those conditions are enough to ensure the existence of 0-DSSP orbits. Existence of general k-DSSP orbits for the planar double-polygon problem are not proved here and will require further work. We summarize our conclusions in table 4.2.

Compared to Martínez's work [18, 19], we have found new families of periodic orbits, and our proofs are significantly simplified; we provide sufficient conditions that are looser and rigorously verified. Moreover, while the orbits in [18, 19] must have either one or a sufficiently large number of singularities, we prove the existence of periodic orbits for any positive number of singularities in a half period.

The paper is organized as follows. Section 2 introduces two coordinate systems,

both of which will be used in our proofs. Section 3 provides sufficient conditions for the existence of periodic brake orbits and Schubart-like orbit; it turns out that our sufficient conditions will be boiled down to the behaviours of two orbits. Section 4 proves theorems about the two orbits just mentioned. Finally, in Section 5, we apply our theorems to the three problems.

4.2 Two Coordinate Systems

Following the setting in Martínez's papers [18, 19], we consider Lagrangian systems with two degrees of freedom of the following form:

$$L(\mathbf{q}, \dot{\mathbf{q}}) = \frac{1}{2}\dot{\mathbf{q}}^T A\dot{\mathbf{q}} + \mathcal{U}(\mathbf{q}), \tag{4.1}$$

where $\mathbf{q}$ lies in an open set of $\mathbf{R}^2$, $A = diag(a_1, a_2)$ is a constant diagonal matrix with $a_1 > 0, a_2 > 0$, and $\mathcal{U}(\mathbf{q})$ satisfies certain assumptions that will be stated shortly.

Similar to [7], we will define two coordinate systems; one will be called Devaney's coordinates, and the other will be called the new coordinates.

4.2.1 Devaney and Martínez's Coordinates [18, 19]

Martínez generalizes Devaney's coordinate system (which uses McGehee-type coordinates [22]) for the isosceles problem to the Lagrangian system (4.2). In this subsection, we summarize the relevant results and the coordinate system used in [18, 19].

First, the size variable $r \geq 0$ is defined by $r^2 = \mathbf{q}^T A\mathbf{q}$. The shape variable ϕ is defined by $\bar{\mathbf{q}} = (\cos\phi, \sin\phi)$, where $\bar{\mathbf{q}} = \frac{1}{r}\sqrt{A}\mathbf{q}$ and $\|\bar{\mathbf{q}}\|^2 = \bar{\mathbf{q}}^T\bar{\mathbf{q}} = 1$.

Before introducing more variables, we state the assumptions that the potential function $\mathcal{U}(\mathbf{q})$ must satisfy as follows:

A.1 $U(\mathbf{q})$ is a homogeneous function of degree -1 such that $\mathcal{U}(\mathbf{q}) = V(\phi)/r$, where

$$V(\phi) = \frac{\beta_1}{\sin(\phi_b - \phi)} + \frac{\beta_2}{\sin(\phi - \phi_a)} + \widehat{V}(\phi),$$

with $\beta_1 > 0, \beta_2 \geq 0$ constants, where $\beta_2 = 0$ if and only if $\phi_b - \phi_a = \pi$, and $\widehat{V}(\phi) > 0$ is a smooth (at least $\mathcal{C}^3$) bounded function in ϕ_a, ϕ_b. Additionally, in the case $\phi_b - \phi_a < \pi$, we define $f(\phi) = \sin(\phi - \phi_a)\sin(\phi_b - \phi)$; in the case $\phi_b - \phi_a = \pi$,

we define $f(\phi) = \sin(\phi_b - \phi)$, so that $f(\phi)V(\phi)$ is bounded. Furthermore, the critical values of $V(\phi)$ is non-degenerate, that is, if $V'(\phi_*) = 0$, then $V''(\phi_*) \neq 0$.

A.2 $V(\phi)$ is symmetrical with respect to $\phi_m := (\phi_a + \phi_b)/2$.

A.3 $V(\phi)$ has exactly three critical points in (ϕ_a, ϕ_b). They are $\phi_L < \phi_m < \phi_R$.

Remark on A.1 The potential function $\mathcal{U}(\mathbf{q})$ has singularities at $r = 0$ and at $\phi = \phi_a, \phi_b$. Physically, $r = 0$ represents total collision of all masses, and $\phi = \phi_a$ and ϕ_b represent the partial collisions of certain masses, which will be referred to as $a-$collisions and $b-$collisions respectively.

Remark on A.3 Martínez [18] studies both the cases when $V(\phi)$ has either one or three critical points. The case when $V(\phi)$ has one critical point has been completely treated; therefore, we will omit this case.

In Devaney's coordinates, the Lagrangian becomes

$$L(r, \dot{r}, \phi, \dot{\phi}) = \frac{1}{2}\dot{r}^2 + \frac{1}{2}r^2\dot{\phi}^2 + \frac{1}{r}V(\phi).$$

Furthermore, we define the size velocity v by $v = r^{\frac{1}{2}}\dot{r}$ and the shape velocities w by $w = \dot{\phi}r^{3/2}\sqrt{\frac{f(\phi)}{V(\phi)}}$.

Let t be the original time scale and define

$$W(\phi) = f(\phi)V(\phi), \quad F(\phi) = \frac{f(\phi)}{\sqrt{W(\phi)}}.$$

After a change of time scale by $\frac{dt}{ds} = r^{\frac{3}{2}}F(\phi)$, the equations of the system become

$$\begin{aligned}
\frac{dr}{ds} =& rvF(\phi) \\
\frac{dv}{ds} =& F(\phi)(2hr - \frac{v^2}{2}) + \sqrt{W(\phi)} \\
\frac{d\phi}{ds} =& w \\
\frac{dw}{ds} =& -\frac{vw}{2}F(\phi) + \frac{W'(\phi)}{W(\phi)}(f(\phi) - \frac{w^2}{2}) + f'(\phi)(1 + \frac{f(\phi)}{W(\phi)}(2hr - v^2)),
\end{aligned} \tag{4.2}$$

where h is the energy of the system, and the energy equation is

$$\frac{w^2}{2f(\phi)} - 1 = \frac{f(\phi)}{W(\phi)}(rh - \frac{v^2}{2}).$$

The *energy manifold* (with $h = -1$) is defined as the set

$$\{(r, v, \phi, w) : r \geq 0, \phi_a \leq \phi \leq \phi_b, \frac{w^2}{2f(\phi)} - 1 = \frac{f(\phi)}{W(\phi)}(-r - \frac{v^2}{2})\}, \tag{4.3}$$

and the *collision manifold* is defined as the set

$$\{(r, v, \phi, w) : r = 0, \phi_a \leq \phi \leq \phi_b, \frac{w^2}{2f(\phi)} + \frac{f(\phi)}{W(\phi)}\frac{v^2}{2} = 1\}. \tag{4.4}$$

The collision manifold is a two-dimensional invariant manifold and is topologically a sphere with four holes. See figure 4.1. We note that the system of differential equations (4.2) no longer has singularities; the singularities due to partial collisions have been regularized, and the total collision singularity is replaced by the the collision manifold, an invariant set for the flow.

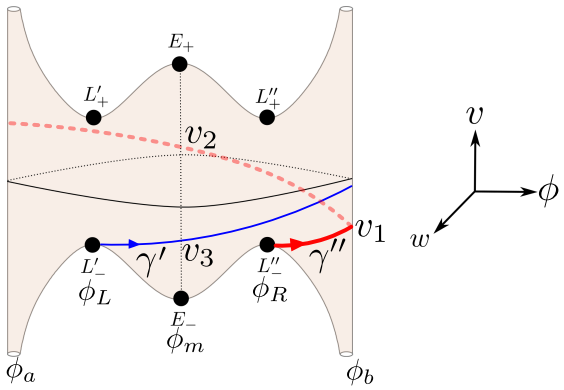

Figure 4.1: The collision manifold and the two branches γ', γ''.

The system 4.2 has exactly six equilibrium points: the Lagrange equilibria $L'_\pm = (0, \pm\sqrt{2V(\phi_L)}, \phi_L, 0)$, $L''_\pm = (0, \pm\sqrt{2V(\phi_R)}, \phi_R, 0)$, and the Euler equilibria $E_\pm = (0, \pm\sqrt{2V(\phi_m)}, \phi_m, 0)$. We call these equilibrium points Lagrange/Euler equilibria because they share the same hyperbolic properties with those equilibria in the isosceles three-body problem. When restricted to the triple collision manifold, both $W^u(L'_-)$ and $W^u(L''_-)$ are one-dimensional, while $W^u(E_-)$ is two-dimensional. We denote the branches of $W^u(L'_-)$ and $W^u(L''_-)$ that initially have $w \geq 0$ by γ' and γ'' respectively. When restricted to the energy manifold, all equilibria are hyperbolic, and $dim(W^s(L''_-)) = 2$, $dim(W^u(L''_-)) = 1$, $dim(W^u(E_-)) = 2$. Once we have $W^{s,u}(L''_-)$, we may find the stable and unstable manifolds of other equilibria by symmetries.

4.2.2 New Coordinates [24, 7]

The new coordinate system uses four variables: r,v,θ, and w. The size variable $r \geq 0$ and the size velocity v are defined the same as in Devaney's coordinates. That is, $r^2 = \mathbf{q}^T A\mathbf{q}$ and $v = r^{\frac{1}{2}}\dot{r}$. We write $\mathbf{q} = (q_1, q_2)$ and $\bar{\mathbf{q}} = 1/r\sqrt{A}\mathbf{q}$. The new shape variable θ is defined by $\bar{\mathbf{q}} = (c_1(\theta), c_2(\theta))$. In application, the choice of $(c_1(\theta), c_2(\theta))$ depends on the range of $\bar{\mathbf{q}}$. If $\bar{\mathbf{q}}$ lies on the half unit circle; that is, if $q_2 \in \mathbf{R}$, then we consider the stereographic projection of the segment $\{(0, \sin\theta), \theta \in \mathbf{R}\}$ from $(-1, 0)$ to the half unit circle, as shown in figure 4.2(a), and one obtains $(c_1(\theta), c_2(\theta)) = (\frac{\cos^2\theta}{1+\sin^2\theta}, \frac{2\sin\theta}{1+\sin^2\theta})$. If $\bar{\mathbf{q}}$ lies on the quarter unit circle in the first quadrant; that is, if $q_2 \geq 0$, then we consider the parallel projection of the segment $\{(0, \sin\theta), \theta \in \mathbf{R}\}$ along the direction $(1, 1)$ to the half unit circle, as shown in figure 4.2(b), and one obtains $(c_1(\theta), c_2(\theta)) = (\frac{\sqrt{\cos^2\theta+1}-\sin\theta}{2}, \frac{\sqrt{\cos^2\theta+1}+\sin\theta}{2})$. Note that we allow the variable θ to vary from $-\infty$ to ∞; this gives a multiple cover of the half unit circle or quarter circle, with branched points at the endpoints of circles which correspond to $a-$collision or $b-$collision singularities. In both cases, $c_1'(\theta)^2 + c_2'(\theta)^2 = \frac{\cos^2\theta}{c(\theta)}$ for some analytic function $c(\theta)$, with $c(\theta) > 0$ and $\frac{c'(\theta)}{\cos\theta\sin\theta}$ being analytic. Specifically, $c(\theta) = (1 + \sin^2\theta)^2/4$ for the first case, and $c(\theta) = 1 + \cos^2\theta$ for the second case. Finally, the shape velocity w is defined by $w = \dot{\theta}r^{3/2}\frac{\cos^2\theta}{c(\theta)}$.

Remark. The shape variable ϕ in Devaney's coordinates and the shape variable θ in the new coordinates are related by $(c_1(\theta), c_2(\theta)) = (\cos\phi, \sin\phi)$. There is no simple expression that relates the w variable in Devaney's coordinates with the w variable in the new coordinates.

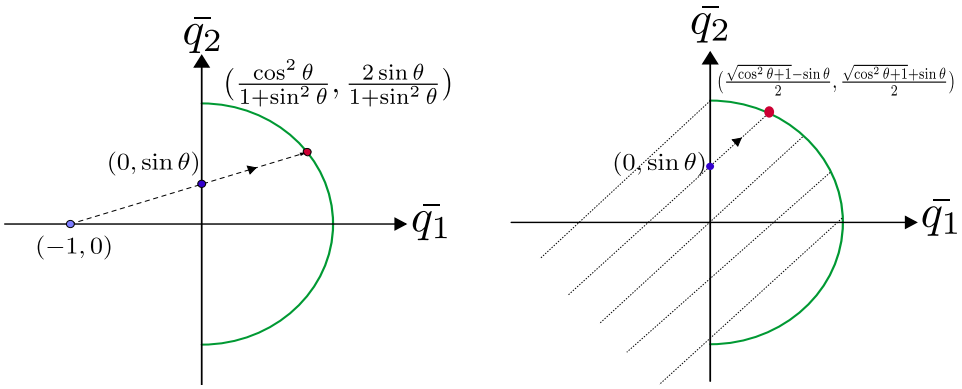

(a) $q_2 \in \mathbf{R}$. (b) $q_2 \geq 0$.

Figure 4.2: The shape variable θ.

In the new coordinates, the Lagrangian becomes

$$L(r, \dot{r}, \theta, \dot{\theta}) = \frac{1}{2}\dot{r}^2 + \frac{1}{2}r^2\dot{\theta}^2\frac{\cos^2\theta}{c(\theta)} + \frac{1}{r}V(\theta).$$

The energy equation becomes

$$\frac{1}{2}v^2\cos^2\theta + \frac{1}{2}w^2c(\theta) - \mathcal{W}(\theta) = rh\cos^2\theta,$$

where $\mathcal{W}(\theta) := \cos^2\theta V(\theta)$, h is the energy of the system, and with an abuse of notation, $V(\phi) = V(\theta)$.

After a change of time scale by $\frac{dt}{ds} = r^{\frac{3}{2}}\cos^2\theta$, the system of differential equations becomes

$$\begin{aligned}
\frac{dr}{ds} =& rv\cos^2\theta \\
\frac{dv}{ds} =& \frac{1}{2}v^2\cos^2\theta + w^2c(\theta) - \mathcal{W}(\theta) \\
\frac{d\theta}{ds} =& wc(\theta) \\
\frac{dw}{ds} =& \mathcal{W}'(\theta) - \frac{1}{2}vw\cos^2\theta + \cos\theta\sin\theta(2r + v^2 - \frac{1}{2}w^2\frac{c'(\theta)}{\sin\theta\cos\theta}).
\end{aligned} \tag{4.5}$$

The derivation of the system (4.5) can be found in the Appendix.

We remark that the singularities due to $a-$collision and $b-$collision have been regularized, since by our choice, $\mathcal{W}(\theta)$ and $\frac{c'(\theta)}{\cos\theta\sin\theta}$ appearing in equation (4.5) are both

analytic. Moreover, the total collision that corresponds to $r = 0$ has been blow-up to the collision manifold, which is an invariant set of the flow.

The *energy manifold* (with $h = -1$) is defined as the set

$$\mathcal{P}_1 = \{(r, v, \theta, w) : r \geq 0, \frac{1}{2}v^2 \cos^2\theta + \frac{1}{2}w^2 c(\theta) - \mathcal{W}(\theta) = -r\cos^2\theta.\}, \tag{4.6}$$

Notice that in the energy equation, $c(\theta) > 0$, and thus the variable w can be solved as a two-valued function of (r, v, θ). The energy manifold can be visualized as two copies (one with $w \geq 0$ and another one with $w \neq 0$) of its projection to the (r, v, θ)-space. See figure 4.3. The *collision manifold* is defined as the subset $P_1 \cap \{r = 0\}$, in which the flow is gradient-like with respect to the variable v, that is, $\frac{dv}{ds} \geq 0$.

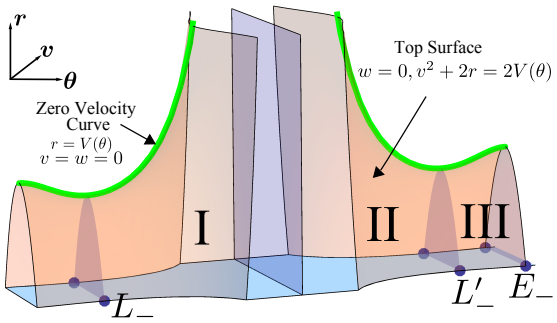

Figure 4.3: One copy of the projection of the energy manifold to the (r, v, θ)-space. The top surface, the floor surface, and the zero velocity curve are given by $w = 0$, $r = 0$, and $v = w = 0$ respectively.

Now we summarize the flow on the energy manifold. The equilibrium points of the system are at the Lagrange equilibria $(r, \theta, v, w) = (0, \pm\theta^* + k\pi, \pm v^*, 0)$ and the Euler equilibria $(r, \theta, v, w) = (0, k\pi, \pm\sqrt{2V(0)}, 0)$, where θ^* is the unique critical point of $V(\theta)$ for $\theta \in (0, \pi/2)$, $k \in Z$ and $v^* = \sqrt{2V(\theta^*)}$. Denote the equilibrium points that are relevant to our proofs by

$$L_\pm = (0, \theta^* - \pi, \pm v^*, 0), \quad L'_\pm = (0, -\theta^*, \pm v^*, 0), \quad E_\pm = (0, 0, \pm\sqrt{2V(0)}, 0).$$

The equilibrium points L_+ and L_- are connected by a homothetic orbit; so are L'_+ and L'_-. Also E_+ and E_- are connected by a homothetic orbit. When restricted to the

collision manifold, both $W^s(L_-)$ and $W^u(L_-)$ have dimension one, while $W^s(E_+)$ has dimension two. When restricted to the energy manifold P_1, $W^s(L_-)$ has dimension two, $W^u(L_-)$ has dimension one, and $W^s(E_+)$, which is contained in the collision manifold, has dimension two.

Next we divide a part of the energy manifold P_1 into several regions. Define

$$\begin{aligned} R_I =& P_1 \cap \{\theta \in [\theta^* - \pi, -\pi/2], w \geq 0\}, \quad Q_I = P_1 \cap \{\theta \in [\theta^* - \pi, -\pi/2], w \leq 0\}, \\ R_{II} =& P_1 \cap \{\theta \in [-\pi/2, -\theta^*], w \geq 0\}, \qquad Q_{II} = P_1 \cap \{\theta \in [-\pi/2, -\theta^*], w \leq 0\}, \\ R_{III} =& P_1 \cap \{\theta \in [-\theta^*, 0], w \geq 0\}. \end{aligned}$$

We call the planes $\theta = \theta^* - \pi$ and $\theta = -\pi/2$ the left and right walls of R_I respectively with similar definitions for the other regions. Now we summarize the properties of the flow in each region.

Lemma 4.2.1. *(i) Regions R_I, R_{III} are flowing-rightward. With the exception of the Lagrange homothetic orbits and orbits in the stable manifold of E_+, orbits cross theses regions as follows: every orbit beginning in the left wall of $R_I(R_{III})$ crosses region $R_I(R_{III})$ and exits at the right wall.*

(ii) Region R_{II} is flowing-leftward in backward-time. Except for the Lagrange homothetic orbits, any backward-time orbit beginning in the right wall of R_{II} can be followed back to the left wall. Furthermore, forward orbits beginning in the left wall of R_{II} either leave R_{II} through the right wall, leave R_{II} through the surface $\{w = 0\}$, or converge to one of the Lagrange restpoints $L'_\pm$ in the right wall. In other words, forward orbits would not stay in R_{II} forever unless they belong to $W^s(L'_\pm)$.

(iii) Region Q_I is flowing-rightward in backward-time. Except for the Lagrange homothetic orbit, every backward-time orbit beginning in the left wall of Q_I can be followed back to the right wall. Region Q_{II} is flowing-leftward; except for the Lagrange homothetic orbit, every forward orbit beginning in region Q_{II} crosses the region and exits at the left wall.

Proof. The proof for the case when the system of differential equations is given by the isosceles problem can be found in [24, 7], where their proof does not involve the formula

of $V(\theta)$. The two main ingredients of that proof are: (1) On the top surface of the energy manifold, $w = 0$, and $\frac{dw}{ds} = \cos^2\theta V'(\theta)$, so that an orbit cannot leave regions R_I or R_{III} through the top surface where $V'(\theta) \geq 0$. (2) The variable w has a uniform bound, since $w^2 \leq 2\mathcal{W}(\theta)/c(\theta)$ and both $\mathcal{W}(\theta)$ and $c(\theta)$ are bounded and non-zero. Let $\lambda := \sqrt{2r + v^2}$, then from (4.5), $\lambda\frac{d\lambda}{ds} = \frac{1}{2}vw^2c(\theta)$, $\frac{d\theta}{ds} = wc(\theta)$. Therefore, when reparametrized by θ, the quantity $|\frac{d\lambda}{d\theta}| \leq |\frac{1}{2}w|$ has a uniform bound.

Our systems have both these ingredients. Therefore, the lemma is true for our systems as well. □

We now list additional notations that will be used throughout the paper.

(Eulerian plane) : $Euler(\bar{\theta}, +) = \{(r, v, \bar{\theta}, w) : w \geq 0\}$, where $\bar{\theta} = k\pi$.

(Eulerian plane) : $Euler(\bar{\theta}, -) = \{(r, v, \bar{\theta}, w) : w \leq 0\}$, where $\bar{\theta} = k\pi$.

(Partial-collision plane) : $Partial(\bar{\theta}, +) = \{\theta = \bar{\theta}, w \geq 0\}$, where $\bar{\theta} = \pi/2 + k\pi$.

(Partial-collision plane) : $Partial(\bar{\theta}, -) = \{\theta = \bar{\theta}, w \leq 0\}$, where $\bar{\theta} = \pi/2 + k\pi$.

(The line $\theta = \bar{\theta}$) : $S(\bar{\theta}) = \{(r, v, \theta, w) \in P_1, v = 0, \theta = \bar{\theta}, w \geq 0\}$.

(Zero velocity curve) : $\mathcal{Z} = \{(r, v, \theta, w) \in P_1, v = w = 0\}$.

When considering the projection to the (r, θ)-plane, we will call the line $\theta = k\pi$ the *Eulerian line*, and the line $\theta = \pi/2 + k\pi$ the *partial-collision line* for any $k \in \mathbf{Z}$.

Moreover, the system (4.5) has symmetries. Let

$$\begin{aligned} &R_1 : (r, v, \theta, w) \to (r, -v, \theta, -w) \\ &R_2 : (r, v, \theta, w) \to (r, -v, -\theta, w) \\ &T_1 : (r, v, \theta, w) \to (r, v, \theta + \pi, w) \\ &\mathrm{Fix}(R_i) = \{(r, v, \theta, w) : R_i(r, v, \theta, w) = (r, v, \theta, w)\}, \quad i = 1, 2. \end{aligned} \tag{4.7}$$

Then $\varphi(t)$ be a solution to X if and only $R_i\varphi(-t)$ and $T_1\varphi(t)$ are solutions to X for $i = 1, 2$.

4.3 Theorems on the existence of periodic orbits

In [19], two families of Schubart-like periodic orbits, called $\mathcal{Z}-$family and $\mathcal{B}-$family, have been found but not completely rigorously proved. Here the letter $\mathcal{Z}$ stands for the

zero velocity curve and $\mathcal{B}$ stands for a partial collision: An orbit in the $\mathcal{Z}$-family has at least one point on the zero velocity curve; an orbit in the $\mathcal{B}$-family has at least one point belonging to the partial collision configuration. We remark that in the isosceles problem, $\mathcal{Z}-$family orbits are identical to type 1 periodic brake orbits in [7]; we will refer to this family as $\mathcal{Z}1$-family in this paper.

In this section, we provide theorems about the existence of $\mathcal{B}-$family, $\mathcal{Z}1-$family, and three additional families of periodic orbits: less-symmetric $\mathcal{B}-$family, $\mathcal{ZB}$-family, and $\mathcal{Z}5$-family. We now describe these orbits by their projection on the (θ, r)-plane. See table 3.12 for these orbits. We denote the period by T and the orbit by $\varphi(t) = (r(t), v(t), \theta(t), w(t))$. First, in a quarter of period, an orbit of $\mathcal{B}-$family starts from $\theta = -\pi/2$ with $v = 0$ and reaches an Eulerian line $\theta = 0$ or $\theta = -\pi$ orthogonally (i.e., $v = 0$) at $T/4$; before a quarter of period, the orbit may cross the line $\theta = -\pi/2$ arbitrary many times. The next quarter orbit is obtained by reflecting the first quarter orbit with respect to the line $\theta = \theta(T/4)$, and the second half orbit is obtained by reflecting the first half orbit with respect to the line $\theta = \theta(T/2)$. Next, we describe less-symmetric $\mathcal{B}-$family. An orbit in this family starts from $\theta = -\pi/2$ with $v = 0$ and reaches $\theta = \pi/2$ orthogonally (i.e., $v = 0$) at $T/2$; before a half period, the orbit crosses the line $\theta = -\pi/2$ at least once, then crosses the Eulerian line $\theta = 0$, and then crosses the line $\theta = \pi/2$ at least one. The second half orbit is obtained by reflecting the first half orbit with respect to the line $\theta = \theta(T/2)$. Next, an orbit in $\mathcal{ZB}-$family starts from the zero velocity curve and reaches a partial-collision line orthogonally at $T/2$. In the half period, the orbit crosses a partial collision line at least once, then crosses the Eulerian line, and then crosses another partial collision line at least once. The next half period is obtained by reflecting the first half orbit with respect to the line $\theta = \theta(T/2)$. Finally, an orbit in $\mathcal{Z}1-$family or $\mathcal{Z}5$-family starts at a brake time and reaches another brake time again at $t = T/2$, then the orbit retraces its first half orbit and reaches a brake time again at $t = T$; while orbits in $\mathcal{Z}1-$family cross the Eulerian line orthogonally at $T/4$, orbits in $\mathcal{Z}5-$family do not orthogonally cross any Eulerian lines or partial collision lines.

It may not be obvious at this point, but it will become clearer soon that the invariant manifolds of L_- and L'_- play a crucial role in the theorems.

Recall that the unstable manifold of L_- and L'_- are both one-dimensional and lie

on the collision manifold; we denote the branches of $W^u(L_-)$ and $W^u(L'_-)$ that initially have $w \geq 0$ by γ and γ' respectively. See figure 4.6(a). And whenever they are well-defined, we denote the $v-$coordinates of the intersections of γ with $\theta = -\pi/2$ and with $\theta = 0$ by v_1 and v_2 respectively, and that of the intersections of γ' with $\theta = 0$ by v_3. Furthermore, we denote the branches of $W^u(L_-)$, $W^u(L'_-)$ that initially have $w \leq 0$ by γ_-, γ'_- respectively. See figure 4.6(b). From symmetries, γ_- and γ'_- can be obtained by first reflecting γ and γ' with respect to the line $\theta = -\pi/2$ and then changing the positive values of w to negative values.

When restricted to the collision manifold, the stable manifold of L'_- is one-dimensional, and since R_{II} is flowing-leftward in backward-time, the branch that has $w \geq 0$ can be followed in backward-time to intersect $\theta = -\pi/2$ at, say $v = v_0$. When restricted to the energy manifold, the stable manifold of L'_- becomes two-dimensional, where the extra one dimension comes from the Lagrange homothetic orbit that connects L'_+ to L'_-.

(A crucial surface, Roof I) The "quadrant" of the surface $W^s(L'_-)$ that lies in R_{II} will be crucial to our proofs later. We will refer to this quadrant surface as Roof I. See figure 4.5(a) for this surface. One edge of Roof I is the Lagrange homothetic orbit connecting L'_+ to L'_-, and the other edge is the unstable branch of L'_- that lies in the collision manifold. Since region R_{II} is flowing-leftward in backward-time, Roof I can be followed to reach the left wall of R_{II}, intersecting with the wall $Partial(\pi/2, +)$ and forming a curve with two endpoints on the collision manifold. One endpoint arises from the stable branch of L'_+, and therefore it has $v = -v_1$; the other endpoint arises from the stable branch of L'_- that lies on the collision manifold, and therefore it has $v = v_0$.

(Roof II) Another surface that will also be crucial to our proofs is the "quadrant" of the surface $W^s(L_-)$ that lies in region Q_I. We will refer to the quadrant surface as Roof II. See figure 4.5(b). From symmetries, this surface can be obtained by first reflecting Roof I with respect to the plane $\theta = -\pi/2$ and then changing positive values of the w-coordinate to negative values.

We now are ready to prove the existence of periodic orbits.

Theorem 4.3.1. *If $v_1 < 0, v_2 > 0, v_3 < 0$, then there exists a T-periodic brake orbit of the following types:*

*(i) (**$\mathcal{Z}1-$family periodic orbits**). In a quarter of period, the orbit starts at a brake time, then crosses the partial collision line $\{\theta = -\pi/2\}$ k times, and then hits*

the Eulerian line orthogonally at $t = T/4$, i.e., $(\theta(T/4), v(T/4)) = (0, 0)$. See table 3.12(f).

(ii) ***($\mathcal{Z}5-$family periodic orbits).*** *Assume additionally, $v_2 \neq -v_3$. Let (i, j) be any pair of positive integers. In a half period, the orbit starts at a break time, then crosses the partial-collision line $\{\theta = -\pi/2\}$ i times, then crosses the Eulerian line $\{\theta = 0\}$, then crosses the partial-collision line $\{\theta = \pi/2\}$ j times, and then reaches zero velocity. See table 4.1(g).*

Proof. The case when the system is given by the isosceles three-body problem has been proved in theorem 5.4 and theorem 6.1 of [7]. The only three differences between those theorems and the theorem here are as follows. First, $\mathcal{Z}1-$family (respectively $\mathcal{Z}5-$family) periodic orbits here were called type 1 (respectively type 5) periodic brake orbits in [7]. Second, the statement of those theorems requires a condition on the mass of the third body, specifically, $0 < m_3 < \epsilon_2 \approx 2.661993$, which is used to ensure $v_1 < 0, v_2 > 0, v_3 < 0$, and additionally $v_2 \neq -v_3$ (for type 5 orbits). Here we replace that condition on m_3 by the condition $v_1 < 0, v_2 > 0$ and $v_3 < 0$. The third difference is only a change of naming; in that theorem, $\{\theta = -\pi/2\}$ is called a binary collision line, while we call the same line a partial collision line. After these modifications, that proof can be applied verbatim to prove our theorem here.

□

Theorem 4.3.2. ***($\mathcal{B}-$family Schubart-like orbits with $k = 0$).*** *If $v_1 < 0$ and $v_3 < 0$, then there exists a Schubart-like orbit with the following properties: In a quarter of period, the orbit starts at the partial-collision line $\theta = -\pi/2$, then hits the Eulerian line orthogonally at $t = T/4$, i.e., $(\theta(T/4), v(T/4)) = (0, 0)$. See table 4.1(a).*

Proof. Martínez's idea [18], expressed in the new coordinates, is to show that part of the line segment $S(-\pi)$ (which represents Eulerian shapes) can be followed to reach $\theta = -\pi/2$ (which represents partial-collision shapes) and form a continuous curve, whose one endpoint has $v > 0$ and the other endpoint has $v < 0$. Therefore, there is an orbit that starts with $\theta = -\pi, v = 0$ and hits $\theta = -\pi/2$ orthogonally (i.e. $v = 0$), which corresponds to a Schurbart-like periodic orbit. In contrast, we will shoot from the line segment $S(-\pi/2)$ and target to hit $\theta = 0$ orthogonally. Figure 4.4(a) illustrates the

idea of the proof. (**Remark.** Shooting from $S(-\pi)$ works fine in the new coordinates. Here we choose to shoot from $S(-\pi/2)$ simply because the proof will require fewer new notations and facilitate the proofs of further theorems.)

We start from $S(-\pi/2)$, whose one endpoint, say q_0, is in the collision manifold, and the other endpoint is at infinity. Our goal now is to construct part of $S(-\pi/2)$ that can be followed across region R_{II}. Note that by lemma 4.2.1(ii), region R_{II} is not flowing-rightward—not the entire $S(-\pi/2)$ can be followed across R_{II} under the flow. We consider Roof I surface, whose intersection with the left wall of R_{II} forms a curve with one endpoint having $(r, v) = (0, v_0)$ and the other endpoint having $(r, v) = (0, -v_1)$. Since $v_0 < 0 < -v_1$, $S(-\pi/2)$ and the curve just mentioned must intersect; we denote the first intersection by q_I. Let X_I be the part of $S(-\pi/2)$ that is between q_0 and q_I, then X_I can be followed across region R_{II} to reach the left wall of R_{III}, since Roof I serves as a trapping surface that prevents the image of X_I from leaving R_{II} through the surface $\{w = 0\}$. Furthermore, since region R_{III} is flowing-rightward, X_I can be followed further to cross region R_{III}, and then form an arc, called X_{II}, on the right wall of R_{III}. We now investigate the two endpoints of X_{II}. Denote the $v-$coordinate of the intersection of the orbit of q_0 with $\theta = 0$ by $\widehat{v}$. Since the flow in the collision manifold is gradient-like, $\widehat{v} > 0$. One endpoint of X_{II}, which arises from the orbit of q_0, has $v = \widehat{v}$. As for the other endpoint, orbits that start near a neighborhood of $q_I \in W^s(L'_-)$ will follow the orbit of q_I entering a neighborhood of L'_- and then follow the branch γ', and therefore the other endpoint of X_{II} is at $v = v_3 < 0$. Since $v_3 < 0 < \widehat{v}$, there exists a point on X_{II} that has $v = 0$, which corresponds to the desired periodic orbit. This completes the proof.

□

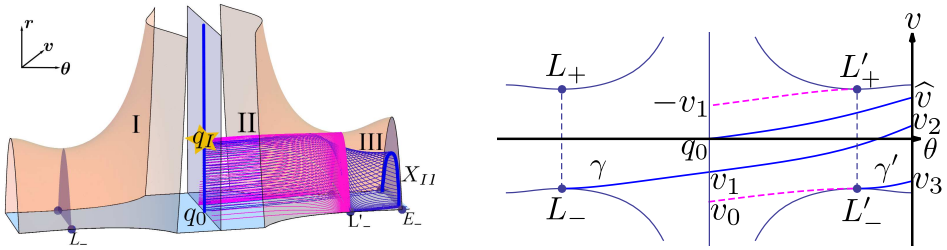

(a) The part of $S(-\pi/2)$ below Roof I can be followed across region R_{II}.

(b) The two branches γ, γ' and the orbit starting from q_0.

Figure 4.4: Illustration for the proof of Theorem 4.3.2

Theorem 4.3.3. ***($\mathcal{B}-$family Schubart-like orbits).*** *If $v_1 < 0, v_2 > 0, v_3 < 0$, then for any $k \in N$, there exists a Schubart-like orbit with the following properties: In a quarter of period, the orbit starts at the partial-collision line $\theta = -\pi/2$, then crosses the partial collision line $\{\theta = -\pi\}$ k times, and then hits one of the Eulerian lines $\theta = 0$ (if k is even) or $\theta = -\pi$ (if k is odd) orthogonally at $t = T/2$. See table 4.1(a)(b)(c).*

Proof. The proof of this theorem is quite similar to that of theorem 5.4 of [7].

The case $k = 0$ has been proved in theorem 4.3.2. We start with the case $k = 1$. Figure 4.5 illustrates the idea of the proof. Again we shoot from $S(-\pi/2)$. Recall that in the proof for the case $k = 0$, we choose X_I to be the part of $S(-\pi/2)$ that is below Roof I such that X_I can be followed across R_{II}. Now for the case $k = 1$, we construct X'_I to be the part of $S(-\pi/2)$ that is above Roof I such that X'_I can **not** be followed across R_{II}. Specifically, let p_I be the last intersection of $S(-\pi/2)$ with the Roof I, and let X'_I be the part of X_I that is between p_I and infinity. Then points on X'_I will not cross R_{II}; instead, they leave R_{II} through the top boundary surface $\{w = 0\}$, then enter Q_{II}, and then reach the left wall of Q_{II}, forming an arc, say X_{II}. One of the endpoints of X_{II} has $v = v_1$, which arise from γ'_-, and the other endpoint is at infinity. To construct the part of X_{II} that can cross region Q_I, which is flowing-rightward in backward-time, we consider Roof II, whose intersection with $Partial(-\pi/2, -)$ forms an arc whose endpoints are at $v = v_0$ and at $v = -v_1$. Let X'_{II} be the part of X_{II} that is below the arc just mentioned, than X'_{II} can be followed across region Q_{II}, since Roof II serves as a trapping surface here. Points on X'_{II} can furthermore reach $Euler(-\pi, -)$, forming an arc, say X_{III}, whose endpoints are at $(r, v) = (0, v_2)$ and $(r, v) = (0, v_3)$.

This proves the case $k = 1$.

If instead of considering X'_{II}, we consider X''_{II} to be the part of X_{II} that is above Roof II, then X''_{II} will leave Q_I through the top surface $\{w = 0\}$, enter R_I, and reach the right wall of R_I, forming an image curve on $Partial(\pi/2, +)$, with the endpoints at $(r, v) = (0, v_1)$ and infinity respectively. The situation now is quite similar to that when we have $S(-\pi/2)$ — we obtain a curve that connects the collision manifold and infinity. By considering the relative position of the image curves with respect to Roof I or II, one may construct part of the image curves that travels between $\{w \geq 0\}$,$\{w \geq 0\}$ as many times as desired and then forms a curve on $Euler(0, +)$ or $Euler(-\pi, 0)$, with the endpoints at $v = v_2 > 0$ and $v_3 < 0$. This proves the general case $k \in \mathbf{N}$.

□

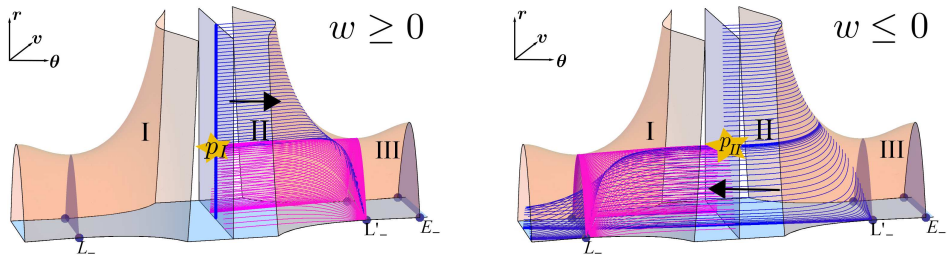

(a) Points above Roof I will leave R_{II} through the surface $\{w = 0\}$.

(b) Points below Roof II will cross Q_I and then reach $Euler(-\pi, -)$.

Figure 4.5: This figure illustrates the proof of Theorem 4.3.4.

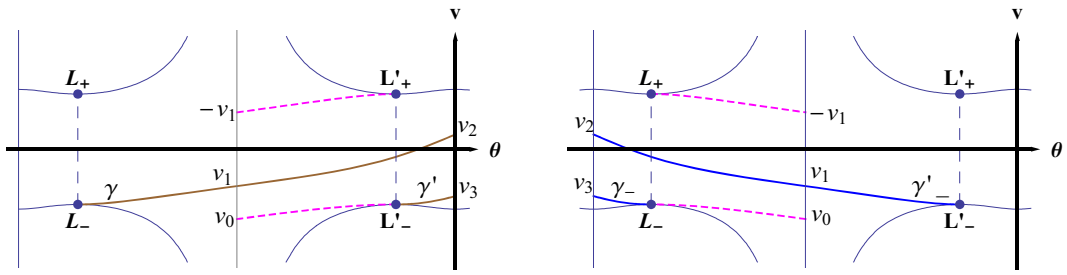

(a) $w \geq 0$. (b) $w \leq 0$.

Figure 4.6: The branches γ,γ' lie in $w \geq 0$, while the branches γ_-,γ'_- lie in $w \leq 0$.

Theorem 4.3.4. ***(Less-symmetric $\mathcal{B}-$family Schubart-like orbits).*** *Assume $v_1 < 0, v_2 > 0, v_3 < 0$, and $v_2 \neq -v_3$. For every pair of positive integers (i, j), there exists a Schubart-like orbit with the following property: In a half period, the orbit starts with $i+1$ partial-collisions, then crosses the Eulerian line, followed by $j+1$ continuous partial-collisions. See table 4.1(d).*

Proof. The proof is quite similar to the proof of theorem 6.1 of [7].

Here we only prove the case when i is even and j is odd; the other cases can be proved similarly. In the proof of theorem 4.3.3, for even i, we construct a subset of $S(-\pi/2)$, say S_i, that can be followed to cross $Partial(-\pi/2, \pm)$ i times to reach $Euler(0, +)$, and form a curve, say Γ_i, having endpoints at $v = v_2, v_3$ in the collision manifold. For odd j, we construct a subset of $S(-\pi/2)$, say S_j, that can be followed to cross $Partial(-\pi/2, \pm)$ j times to reach $Euler(-\pi, -)$, and form a curve, said Γ_j, having endpoints at $v = v_2, v_3$ in the collision manifold. Recall that the system has symmetries R_1, R_2, and T_1 as defined in (4.7). By symmetries and reversibility, $R_1T_1\Gamma_j$ can be followed to cross $Partial(\pi/2, \pm)$ $j-1$ times to form $R_1T_1S_i$. The curve $R_1T_1\Gamma_j$ lies on $Euler(0, +)$, with its endpoints at $(r, v) = (0, -v_2)$ and $(0, -v_3)$. Since $v_2 > 0, v_3 < 0$, and $v_2 \neq -v_3$, the two curves Γ_i and $R_1T_1\Gamma_j$ must intersect. An intersection point yields the desired orbit.

□

Theorem 4.3.5. ***($\mathcal{ZB}-$family Schubart-like orbits).*** *Assume $v_1 < 0, v_2 > 0, v_3 < 0$, and $v_2 \neq -v_3$. For every pair of positive integers (i, j), $i, j \geq 1$, there exists a periodic orbit with the following property: In a half period, the orbit starts at a brake time, then crosses the partial-collision line $\{\theta = -\pi/2\}$ i times, then crosses the Eulerian line, then crosses the partial-collision line $\{\theta = \pi/2\}$ j times, and then hits the partial-collision line $\{\theta = \pi/2\}$ orthogonally. See table 4.1(e).*

Proof. Here we prove the case when both i and j are odd; the other cases can be proved similarly. The proof is almost the same as that of theorem 4.3.4; only the curve S_i is constructed differently. In the proof of type 1 periodic brake orbits, which is theorem 5.4 of [7], we construct a part of the zero velocity curve $\mathcal{Z}$, say S_i, that can be followed to cross $Partial(-\pi/2, \pm)$ i times to reach $Euler(0, +)$, and form a curve, say Γ_i, having endpoints at $v = v_2, v_3$ in the collision manifold. Therefore, the curve $R_1T_1S_j$ constructed in theorem 4.3.4, which also lies on $Euler(0, +)$ with its endpoints at $v = -v_2, -v_3$, must intersect Γ_i. An intersection point yields the desired orbit. □

We end this section with another family of periodic orbits in the equal-mass isosceles three-body problem. See table 4.1(h)(i). These orbits are numerically founded by shooting from $S(-\pi/2)$ and targeting to hit $\theta = \pi/2$ or $\theta = -3\pi/2$ orthogonally but not orthogonally hitting an Euler line. We are unable to prove their existence at this moment. The difficulty is not to prove the existence of orbits that hit two partial-collision lines orthogonally, but is to distinguish them from $\mathcal{B}-$family orbits.

4.4 The Behaviours of γ and γ'

From the previous section, we can see that the two branches γ and γ' play a crucial role in the existence proofs of periodic orbits. Recall that we denote the v-coordinates of the intersections of γ with $\theta = -\pi/2$, $\theta = 0$ by v_1, v_2 respectively, and that of γ' with $\theta = 0$ by v_3. See figure 4.6(a). Since regions R_I and R_{III} are flowing rightward, v_1 and v_3 are always well-defined. As for v_2, it is well-defined provided $v_1 < 0$; this can be seen by considering the stable branches of L' and L'_- which trap γ in between, and hence γ crosses region II.

While the new coordinates facilitate the proofs for the existence theorems of periodic

orbits, it is, however, easier to estimate the branches γ and γ' in Devaney's coordinates. The branch γ' in the new corresponds to γ' in the Devaney's coordinates, and hence the identical notations. On the other hand, the translation of the branch γ in the new coordinate, i.e., $T_1\gamma$, corresponds to γ'' in Devaney's coordinates. Therefore, studying γ,γ' in the new coordinates is equivalent to studying γ'',γ' in Devaney's coordinates.

We will provide sufficient conditions that guarantee $v_1 < 0, v_3 < 0$, along with a lower bound for v_1 that guarantees $v_2 > 0$. In the case when $V(\phi)$ has exactly three critical points at $\phi = \phi_L, \phi_m, \phi_R$, Martínez's conditions are as follows [18, 19]:

$$\cos(\phi_b - \phi)\widehat{V}(\phi) - \sin(\phi_b - \phi)\widehat{V}'(\phi) > 0, \quad \phi \in [\phi_R, \phi_b] \tag{M1}$$

$$3V(\phi_R) - 2V(\phi_m) > 0, \tag{M2}$$

$$G(\phi) := \frac{1}{\phi_R - \phi_m} - \frac{\phi - \phi_m}{2}\sqrt{\frac{2(\phi_R - \phi)}{\phi_R - \phi_m}} + 2\frac{V'(\phi)}{V(\phi_m)} > 0, \quad \phi \in [\phi_m, \phi_b] \tag{M3}$$

$$\text{The orbit } \phi(t; P_m) \text{ runs up to } B_b^+(B_a^+) \text{ for positive time,} \tag{M4}$$

where $P_m = (r, v, \phi, w) = (0, 0, \phi_m, +)$ lies on the collision manifold, and B_a^+, B_b^+ represent two of the four holes of the collision manifold that have $v \geq 0$. Specifically, Martínez's existence proof of Schubart-like periodic orbits that have only one singularity in a half period requires conditions (M1,M2,M3), and the existence proof of Schubart-like periodic orbits that have many singularities requires an additional condition (M4). However, not every condition has been successfully verified. For the planar double-polygon problem, the condition (M3) fails, and the condition (M2) is not rigorously proved. (In [18], it is proved that (M2) is true for n large enough and numerically verified only for $3 \leq n \leq 50$.) In [19], the condition (M4) is not proved but only supported by numerical evidence in all her three problems.

In contrast, in the same setting, our conditions are as follows:

$$\phi_a = -\pi/2, \phi_b = \pi/2, W'(\phi) \leq 0, \quad \phi \in [0, \frac{\pi}{2}) \tag{N1}$$

$$V(\phi_R) - (\sin^2 \frac{\phi_R - \phi_m}{2}) V(\phi_m) > 0 \tag{N2}$$

$$\text{In addition to } (N1), \ |\frac{W'(\phi)}{W(\phi)}| \leq \frac{4}{5} \text{ for } \phi \in [\frac{\pi}{4}, \frac{\pi}{2}) \tag{N3}$$

$$\text{Replace } |\frac{W'(\phi)}{W(\phi)}| \leq \frac{4}{5} \text{ in (N3) by the condition in Lemma 4.1(iv)} \tag{N3'}$$

$v_2 \neq -v_3$, or equivalently,

$$\gamma \text{ is not a heteroclinic connection between } L_- \text{ and } T_1(L_+), \tag{N4}$$

where $S_n = \sum_{k=1}^{n} \csc \pi k/n$. We remark that the conditions (M1) and (N1) are equivalent when $\phi_a = -\pi/2, \phi_b = \pi/2$; this is apparent from the proof for proposition 1 in [18]. We also remark that, in our examples, the condition (N2) is looser than (M2), since we will show that $\phi_R - \phi_m \leq \pi/4$.

In the following lemmas, we will show that the condition (N1) implies $v_1 < 0$, that (N2) implies $v_3 < 0$, and that the condition (N3) or (N3') implies $v_2 > 0$. As a result, the conditions (N1,N2) ensure the existence of $\mathcal{B}-$family Schubart-like periodic orbits with $n = 0$. The conditions (N1,N2,N3 or N3') ensure the existence of $\mathcal{B}-$family and $\mathcal{Z}1-$family periodic orbits. If moreover, $v_2 \neq -v_3$, then there exist $\mathcal{ZB}-$family, less-symmetric $\mathcal{B}-$family, and $\mathcal{Z}5-$family periodic orbits.

Lemma 4.4.1. *Assume $\phi_a = -\pi/2$, $\phi_b = \pi/2$, and $\phi_R \in (0, \pi/4]$. Then*

(i) ***(N1)*** *If $W'(\phi) \leq 0$ in $[0, \frac{\pi}{2})$, then $v_1 < 0$.*

(ii) ***(N3)*** *If moreover, $\alpha := \frac{4}{5} \geq |\frac{W'(\phi)}{W(\phi)}|$ for $\phi \in [\frac{\pi}{4}, \frac{\pi}{2})$, then $\beta\sqrt{W(\pi/2)} < v_1 < 0$, where $\beta = -1.32$.*

(iii) Furthermore, (ii) implies that $v_2 > 0$.

(iv) ***(N3')*** *If the condition for (ii) does not hold, let $g_3(\phi)$ be the solution of (4.14). If $g_3(\pi/2) \geq \beta$, then $v_2 > 0$.*

Proof. Following [18], we introduce a new variable $g = \frac{v}{\sqrt{W(\phi)}}$. When restricted to the

collision manifold, the differential equations become

$$\begin{aligned}
\dot{g} &= 1 - \frac{g^2}{2}\cos\phi - \frac{gw}{2}\frac{W'(\phi)}{W(\phi)} \\
\dot{\phi} &= w \\
\dot{w} &= -\frac{gw}{2}\cos\phi - \sin\phi(1 - \cos\phi g^2) + \frac{W'(\phi)}{W(\phi)}(\cos\phi - \frac{w^2}{2}),
\end{aligned} \tag{4.8}$$

and the collision manifold becomes

$$\frac{w^2}{2\cos\phi} - 1 = -\frac{1}{2}\cos\phi g^2. \tag{4.9}$$

Note that the equation of the collision manifold (4.9) is independent of $W(\phi)$, and the differential equation (4.8) is not necessary gradient-like with respect to g.

Using the equation for collision manifold, one finds that $\dot{g} = \frac{w^2}{2\cos\phi} - \frac{gw}{2}\frac{W'(\phi)}{W(\phi)}$, and hence

$$\begin{aligned}
\frac{dg}{d\phi} &= \frac{w}{2\cos\phi} - \frac{g}{2}\frac{W'(\phi)}{W(\phi)} \\
&= \pm\sqrt{\frac{1}{2\cos\phi} - \frac{g^2}{4}} - \frac{g}{2}\frac{W'(\phi)}{W(\phi)},
\end{aligned}$$

where we take the + sign when $w \geq 0$ and the − sign when $w < 0$.

Before reaching $\phi = \pi/2$, the unstable branch γ'' stays in $\{w \geq 0\}$, and it satisfies the differential equation

$$\begin{aligned}
\frac{dg}{d\phi} &= \sqrt{\frac{1}{2\cos\phi} - \frac{g^2}{4}} - \frac{g}{2}\frac{W'(\phi)}{W(\phi)} \\
\lim_{\phi\to\phi_R} g(\phi) &= -\sqrt{2\sec\phi_R}.
\end{aligned} \tag{4.10}$$

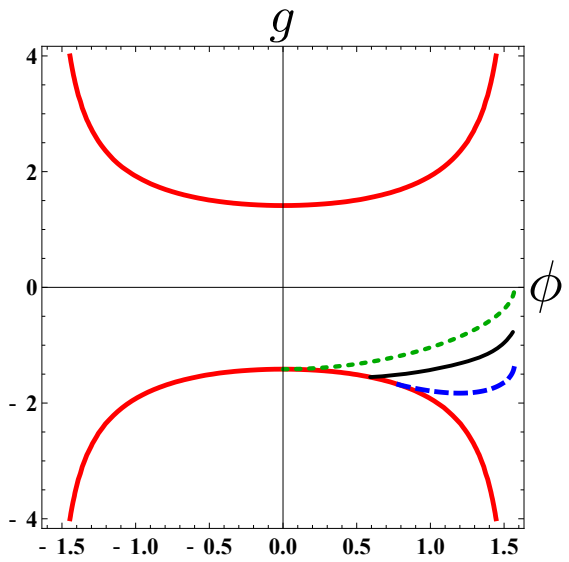

Figure 4.7: The black solid curve is γ''. The green dotted curve and the blue dashed curve are the solutions to (4.11) and (4.12) respectively.

We study γ'' by comparing it with the solutions to the following two differential equations, see figure 4.7.

$$\begin{aligned} \frac{dg_1}{d\phi} &= \sqrt{\frac{1}{2\cos\phi} - \frac{g_1^2}{4}} \\ g_1(0) &= -\sqrt{2}. \end{aligned} \tag{4.11}$$

$$\begin{aligned} \frac{dg_2}{d\phi} &= \sqrt{\frac{1}{2\cos\phi} - \frac{g_2^2}{4}} + \alpha\frac{g_2}{2}, \quad \text{where} \quad \alpha = \frac{4}{5} \\ g_2(\frac{\pi}{4}) &= -\sqrt{2\sqrt{2}}. \end{aligned} \tag{4.12}$$

For equation (4.11), one can find the solution explicitly; the solution is $g_1(\phi) = -\sqrt{2\cos\phi}$, and hence $g_1(\pi/2) = 0$. The branch γ'' cannot cross the solution to (4.11) before it reaches $\phi = \pi/2$, since the slope $\frac{dg}{d\phi}$ of (4.10) is strictly less than that of (4.11) when $g < 0$ and $\frac{W'(\phi)}{W(\phi)} < 0$. Therefore, $v_1 < g_1(\pi/2) = 0$. This proves (i).

Now we prove (ii). For equation (4.12), after a numerical integration, we find that $g_2(\pi/2) := \beta_1 \approx -1.315705 > \beta$. Therefore, provided that $|\frac{W'(\phi)}{W(\phi)}| \leq \alpha := \frac{4}{5}$ for $\phi \in [\pi/4, \pi/2)$ and that $\frac{W'(\phi)}{W(\phi)} \leq 0$ for $\phi \in [0, \pi/2)$, the curve γ'' stays above the solution

of (4.12) at least until it reaches $\phi = \pi/2$, since

$$\alpha\frac{g}{2} \le -\frac{g}{2}\frac{W'(\phi)}{W(\phi)} \le 0.$$

Therefore, the intersection of γ'' and $\phi = \pi/2$ has $\beta < g(\pi/2) < 0$. Recovering the variable v by using the relation $v = g\sqrt{W(\phi)}$, one obtains $\beta\sqrt{W(\pi/2)} < v_1 < 0$. This proves (ii).

Next, we prove (iii). We follow γ'' from $\phi = \pi/2$ to $\phi = 0$. Note that along this segment of γ'', we have $w \le 0$. For the sake of contradiction, assume $v \le 0$, which is equivalent to that $g \le 0$. Then $\frac{dg}{d\phi} = -\sqrt{\frac{1}{2\cos\phi} - \frac{g^2}{4}} - \frac{g}{2}\frac{W'(\phi)}{W(\phi)}$ is negative, hence $0 \ge g(\phi) \ge g(\pi/2) > \beta = -1.32$ along the part of γ'' where ϕ goes from $\phi = \pi/2$ to $\phi = 0$.

We then have

$$\begin{aligned} g(0) &= g(\frac{\pi}{2}) + \int_{\pi/2}^{0} \frac{dg}{d\phi} d\phi \\ &= g(\frac{\pi}{2}) + \int_{0}^{\frac{\pi}{2}} \sqrt{\frac{1}{2\cos\phi} - \frac{g^2}{4}} + \frac{g}{2}\frac{W'(\phi)}{W(\phi)} d\phi \\ &\ge g(\frac{\pi}{2}) + \int_{0}^{\frac{\pi}{2}} \sqrt{\frac{1}{2\cos\phi} - \frac{g^2}{4}} d\phi \\ &\ge \beta + \int_{0}^{\frac{\pi}{2}} \sqrt{\frac{1}{2\cos\phi} - \frac{\beta^2}{4}} d\phi \\ &\approx -1.32 + 1.379875 > 0. \end{aligned} \tag{4.13}$$

This contradicts to our assumption that $g \le 0$. So this implies that γ'' intersects $g = 0$, i.e., $v = 0$, before it reaches $\phi = 0$. Therefore, $v_2 > 0$.

Finally, if the condition in (ii) does not hold, we compare γ'' with the solution of the initial value problem,

$$\begin{aligned} \frac{dg_3}{d\phi} &= \sqrt{\frac{1}{2\cos\phi} - \frac{g_3^2}{4}} - \frac{g_3}{2}\frac{W'(\phi)}{W(\phi)} \\ g_3(\pi/4) &= -\sqrt{2\sqrt{2}}. \end{aligned} \tag{4.14}$$

In the interval when ϕ increases from $\pi/4$ to $\pi/2$, the solution of (4.14) stays below γ'', since they satisfy the same differential equation and $g(\pi/4) \ge g_3(\pi/4)$. Therefore, if $g_3(\pi/2) \ge \beta$, then by using the same argument for (iii), one proves that $v_2 > 0$.

□

Remarks on lemma 4.4.1:

(a) **A lower bound for v_1:** For the $n-$pyramidal problem and the spatial double-polygon problem, from the definition of $W(\phi)$, one may easily verify that $W(\pi/2) = S_n/4$. Then lemma 4.4.1(ii) immediately implies that $v_1 > \beta\sqrt{S_n}/2$. This lower bound will not be used in this paper but might be useful for future research.

(b) **On loosening the condition for (N3):** When n is sufficiently large (specifically, $n \geq 4$ for the $n-$pyramidal problem and $n \geq 10$ for the spatial double-polygon problem), the constant $\alpha = 4/5$ is an upper bound for $|\frac{W'(\phi)}{W(\phi)}|$. If one chooses a larger upper bound, for example, $\alpha = 1$, then one would obtain a larger value of β_1, and the contradiction argument from equation (4.13) may fail.

Lemma 4.4.2. ***(N2)*** *If $V(\phi_R) > (\sin^2 \frac{\phi_R - \phi_m}{2})V(\phi_m)$, then $v_3 < 0$.*

Proof. Along the branch γ'', from equation (4.2), we have

$$\frac{dv}{d\phi} = \frac{1}{2}\sqrt{2V(\phi) - v^2}. \tag{4.15}$$

If $v_3 \geq 0$, this implies that γ'' reaches $v = 0$ before it reaches $\phi = \phi_m$, which implies that along γ'', when the variable v varies from $-v_L = -\sqrt{2V(\phi_L)} = -v_R$ to 0, the total variation of the variable ϕ is less then $\phi_m - \phi_L$, so

$$\begin{aligned}
\phi_R - \phi_m = \phi_m - \phi_L \geq \triangle\phi &= \int_{-v_L}^{0} \frac{2}{\sqrt{2V(\phi) - v^2}} dv \\
&\geq \int_{-v_L}^{0} \frac{2}{\sqrt{2V(\phi_m) - v^2}} dv \\
&= 2\arcsin(\frac{v_L}{\sqrt{2V(\phi_m)}}) = 2\arcsin(\sqrt{\frac{2V(\phi_R)}{2V(\phi_m)}}),
\end{aligned}$$

which makes a contradiction to the assumption $V(\phi_R) - \sin^2 \frac{\phi_R - \phi_m}{2} V(\phi_m) > 0$.

□

4.5 Three Applications

4.5.1 The n-pyramidal problem.

The n-pyramidal problem consists of n equal masses $m_1 = m_2 = \cdots = m_n = 1$ along with an additional mass $m_{n+1} = \mu$. The n equal masses always lie in some horizontal plane $z = z_1$ and equally spaced in a circle centered at the origin with radius q_1, forming a regular $n-$polygon, while m_n moves up and down on the $z-$axis. We denote the signed distance between m_{n+1} to the plane $z = z_1$ by q_2. See table 4.2 for the configuration. Note that the planar isosceles problem is the special case of the $n-$pyramidal problem when $n = 2$.

Following Martínez [18], the Lagrangian is given by

$$L(q_1, q_2, \dot{q_1}, \dot{q_2}) = \sum_{k=1}^{n-1} \frac{1}{4q_1 \sin l_k} + \frac{\mu}{\sqrt{q_1^2 + q_2^2}} + \frac{1}{2}(\dot{q_1}^2 + \frac{\mu}{n+\mu}\dot{q_2}^2), \tag{4.16}$$

where $l_k = \pi k/n$, and $q_1 \geq 0, q_2 \in \mathbf{R}$. In Devaney's coordinates, the variables r, ϕ are defined by

$$r^2 = q_1^2 + \frac{\mu}{n+\mu}q_2^2, \quad q_1 = r\cos\phi, \quad q_2 = r\sqrt{\frac{n+\mu}{\mu}}\sin\phi, \quad r \geq 0, \quad \phi \in (-\frac{\pi}{2}, \frac{\pi}{2}),$$

and as a consequence,

$$V(\phi) = \frac{S_n}{4\cos\phi} + \frac{\mu}{\sqrt{1 + (n/\mu)\sin^2\phi}}, \quad \text{where} \quad S_n = \sum_{k=1}^{n-1} \csc l_k, l_k = \pi k/n.$$

Martínez has located the critical points of $V(\phi)$ in the following lemma.

Lemma 4.5.1. *[18]*

1. *If $2 \leq n < 473$, then $V(\phi)$ has three non-degenerate critical points: a maximum at $\phi = 0$ and two minima at $\pm\phi_R$, where*

$$\tan^2\phi_R = \frac{\mu}{n+\mu}((\frac{4n}{S_n})^{2/3} - 1).$$

2. *If $n \geq 473$, then $V(\phi)$ has a unique non-degenerate critical point at $\phi = 0$.*

In [18], the conditions (M1,M2,M3) have been successfully verified, and therefore the existence of $\mathcal{B}-$family periodic orbits with $k = 0$ is proved. We remark that the conditions (M1,M2) imply our conditions (N1,N2), which also ensure the existence of $\mathcal{B}-$family periodic orbits with $k = 0$.

To prove the existence of other families of periodic orbits, we now are left to verify the condition (N3), which ensures $v_2 > 0$. However, in the case $n = 2$, that is, in the isosceles problem, the behavior of γ and γ' with respect to the mass ratio has be carefully analyzed [41, 42, 7]. It is shown that $v_2 > 0$ if and only if the mass ratio μ satisfies $0 < \mu < \epsilon_2 \approx 2.661993$. In other words, the condition (N3) can not hold for general μ. **From now on, we restrict our study to the case $\mu = 1$.** We will verify the condition (N3) for $n \geq 4$.

We first show that $\phi_R \in (0, \pi/4]$. From the previous lemma,

$$\tan^2 \phi_R = \frac{1}{n+1}((\frac{4n}{S_n})^{2/3} - 1) \leq \frac{1}{n+1}((\frac{4n}{n-1})^{2/3} - 1) \leq \frac{1}{n+1}(8^{2/3} - 1) \leq 1.$$

Therefore, $\phi_R \in (0, \pi/4]$ for $n \geq 2$.

Second, we study the function $\frac{W'(\phi)}{W(\phi)}$. See figure 4.8(a) for its graph. We have $W(\phi) = \frac{S_n}{4} + \frac{\cos\phi}{\sqrt{1+n\sin^2\phi}} > 0$. By the monotonicity of $\sin\phi$ and $\cos\phi$, it is apparently that $W'(\phi) \leq 0$ and $\frac{W'(\phi)}{W(\phi)} \leq 0$ in $[0, \pi/2)$.

Third, we show that for $n \geq 4$, $|\frac{W'(\phi)}{W(\phi)}| \leq \frac{4}{5}$ for $\phi \in [\pi/4, \pi/2)$. We compute $W'(\phi) = -\frac{(n+1)\sin\phi}{(1+n\sin^2\phi)^{3/2}}$ and $W''(\phi) = -\frac{(n+1)\cos\phi}{(1+n\sin^2\phi)^{5/2}}(1 - 2n\sin^2\phi)$, so in the interval $(0, \pi/2)$, the critical point of $W'(\phi)$ is at $\phi_* = \arcsin(\sqrt{\frac{1}{2n}}) < \frac{\pi}{4}$ and $W'(\phi) \leq 0$ is increasing in $(\phi_*, \pi/2)$. Therefore, $|W'(\phi)| \leq W'(\pi/4)$ in $[\pi/4, \pi/2)$.

On the other hand, clearly $W(\phi) \geq \frac{S_n}{4}$. Therefore,

$$|\frac{W'(\phi)}{W(\phi)}| \leq |W'(\frac{\pi}{4})|\frac{4}{S_n} = \frac{2(n+1)}{(2+n)^{3/2}}\frac{4}{S_n} < \frac{4}{5} \quad \forall\phi \in [\frac{\pi}{4}, \frac{\pi}{2}), n \geq 4.$$

This verifies the condition (N3) for $n \geq 4$. For $n = 2, 3$, the condition (N3) does not hold, so we verify the condition (N3') in Lemma 4.4.1(iv) instead. Let $g_3(\phi)$ be the solution to (4.14). After a numerical integration with Mathematica, we found that $g_3(\pi/2) \approx -1.2328676, -0.9930229 \geq \beta$ for $n = 2, 3$ respectively. This implies that $v_2 > 0$.

As a remark, the condition (N2) can be easily verified as follows. We have $V(0) = \frac{S_n}{4} + 1 < \frac{S_n}{4} + S_n = \frac{5}{4}S_n$ and $V(\phi_R) \geq \frac{S_n}{4}$. Therefore, $V(\phi_R) \geq V(0)/5 \geq \sin^2(\pi/8)V(0)$.

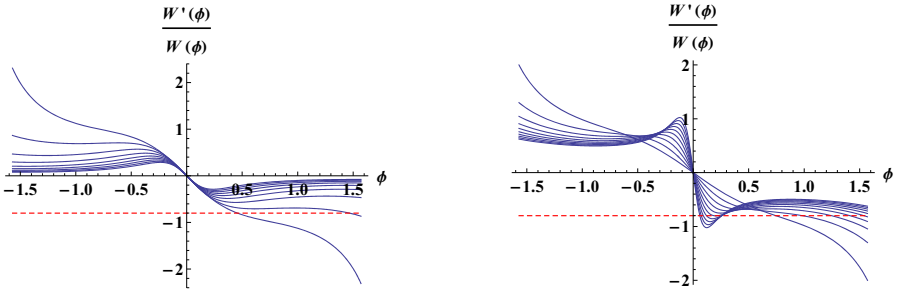

(a) The $n-$pyramidal problem (b) The spatial double-polygon problem

Figure 4.8: Graph of $\frac{W'(\phi)}{W(\phi)}$ for the equal-mass $n-$pyramidal problem and the spatial double-polygon problem with $2 \leq n \leq 10$. As n increases, $\frac{W'(\pi/2)}{W(\pi/2)}$ increases. The horizontal dash line is $\frac{W'(\phi)}{W(\phi)} = -\frac{4}{5}$

Finally, we formally state the conclusion.

Theorem 4.5.2. *In the planar isosceles three-body problem, let $m_1 = m_2 = 1$. For any m_3 in an open interval including $m_3 = 1$, in addition to the six types of periodic brake orbits (including $\mathcal{Z}1-$famly and $\mathcal{Z}5-$family) proved in [7], there exist $\mathcal{B}-$family, less-symmetric $\mathcal{B}-$family, and $\mathcal{ZB}-$family periodic orbits.*

For any $2 \leq n < 473$ with any positive mass μ in the $n-$pyramidal problem, there exists a Schubart-like orbit in the $\mathcal{B}-$family with $n = 0$.

For any $2 \leq n < 473$, in the equal-mass $n-$pyramidal problem, there exist $\mathcal{B}-$family and $\mathcal{Z}1-$family periodic orbits. If moreover, the hypothesis $v_2 \neq -v_3$ is true, then there exist $\mathcal{Z}5-$family, less-symmetric $\mathcal{B}-$family, and $\mathcal{ZB}-$family periodic orbits.

4.5.2 The spatial double-polygon problem.

The spatial double-polygon problem consists of $2n$ equal masses, $n \geq 2$. The configurations form two twisted regular $n-$gons of the same size in two different non-fixed horizontal planes $z = \pm q_2$, centered on the $z-$axis. We denote the distance between a vertex to the $z-$axis by q_1. When projected to the $xy-$plane, the two $n-$gons are different by a rotation angle of $2\pi/n$. See figure 4.9.

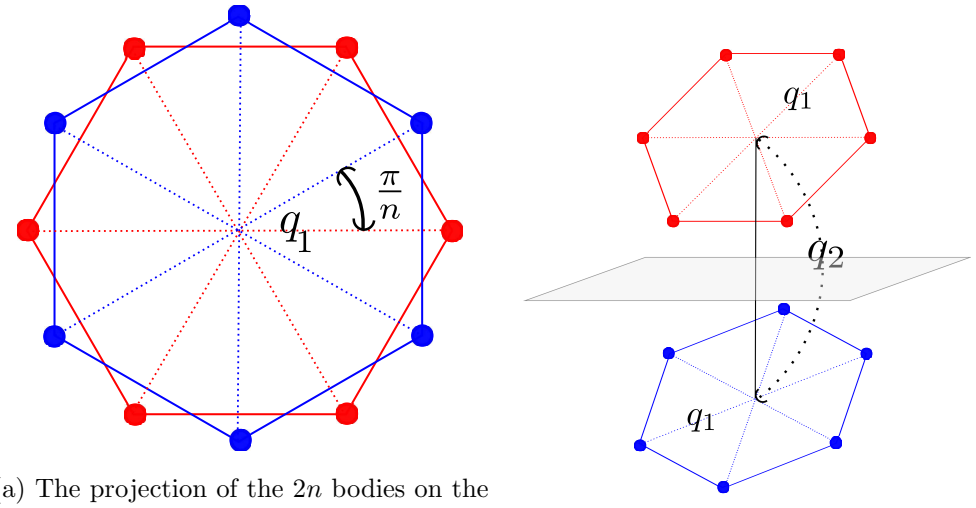

(a) The projection of the $2n$ bodies on the xy-plane.

(b) The configuration of the $2n$ bodies.

Figure 4.9: The spatial double-polygon problem

The Lagrangian is given by

$$L(q_1, q_2, \dot{q}_1, \dot{q}_2) = \frac{1}{2}\left(\sum_{k=1}^{n-1} \frac{1}{2q_1 \sin l_k} + \sum_{k=1}^{n} \frac{1}{\sqrt{(2q_1 \sin \frac{l_{2k-1}}{2})^2 + q_2^2}}\right) + \frac{1}{2}\left(\dot{q_1}^2 + \frac{\dot{q_2}^2}{4}\right),$$

where $l_k = \pi k/n$.

In Devaney's coordinates, write $(q_1, q_2) = r(\cos\phi, 2\sin\phi)$. Then

$$\begin{aligned} V(\phi) &= \frac{1}{2}\left(\sum_{k=1}^{n-1} \frac{1}{2\cos\phi \sin l_k} + \sum_{k=1}^{n} \frac{1}{\sqrt{(2\cos\phi \sin \frac{l_{2k-1}}{2})^2 + 4\sin^2\phi}}\right) \\ &= \frac{S_n}{4}\frac{1}{\cos\phi} + \frac{1}{4}\sum_{k=1}^{n}\frac{1}{\sigma_k}, \end{aligned} \tag{4.17}$$

where $S_n = \sum_{k=1}^{n-1} \csc l_k$, $\sigma_k = (1 - c_k^2\cos^2\phi)^{1/2}$, and $c_k = \cos\frac{\pi}{2n}(2k-1)$.

Lemma 4.5.3. *$V(\phi)$ has exactly three critical points in $(-\pi/2, \pi/2)$, all of which are non-degenerate. They are at $\phi = -\phi_R, 0, \phi_R$, where $\phi_R \in (0, \pi/4)$.*

Proof.

$$\begin{aligned} V'(\phi) &= \frac{S_n}{4}\sec\phi\tan\phi - \frac{1}{4}\sum_{k=1}^{n}\frac{c_k^2}{\sigma_k^3}\cos\phi\sin\phi \\ &= \frac{S_n}{4}\sin\phi\cos\phi(h(\phi) - g_n(\phi)), \end{aligned} \tag{4.18}$$

where $h(\phi) = \sec^3\phi$ and $g_n(\phi) = \frac{1}{S_n}\sum_{k=1}^{n}\frac{c_k^2}{\sigma_k^3}$.

Obviously $\phi = 0$ is a critical point of $V(\phi)$. To show that $V(\phi)$ has exactly one critical point ϕ_R in $(0, \pi/2)$ and that $\phi_R \in (0, \pi/4)$, we will show that $g_n(\phi)$(resp. $h(\phi)$) is a decreasing (resp. increasing) function of $\phi \in (0, \pi/2)$, that $h(0) < g(0)$, and that $h(\pi/4) > g(\pi/4)$.

Since $\cos\phi$ is strictly decreasing in $(0, \pi/2)$, the increasing or decreasing properties of $h(\phi)$ and $g_n(\phi)$ are obvious. Now we show that $h(0) < g(0)$. Note that $h(0) = 1$, and that to show $g(0) > 1$ is equivalent to show that $\sum_{k=1}^{n}\frac{c_k^2}{(1-c_k^2)^{3/2}} > S_n$. Actually, the left-hand side of this inequality is much greater than the right-hand side. It is straightforward to verify the case when $n = 1, 2$. For $n \geq 3$, by using the two relations: $\cot^2\frac{\pi}{2n} \geq n$ for $n \geq 3$ and $\sin\frac{\pi}{2n} < \sin\frac{\pi}{n}(k-1)$ for $k = 2, \cdots, n$, a very rough estimate will prove this inequality as follows:

$$\sum_{k=1}^{n}\frac{c_k^2}{(1-c_k^2)^{3/2}} \geq \frac{c_1^2}{(1-c_1^2)^{3/2}} = (\cot^2\frac{\pi}{2n})\frac{1}{\sin\frac{\pi}{2n}} \geq \frac{n}{\sin\frac{\pi}{2n}} > \sum_{k=1}^{n-1}\frac{1}{\sin\frac{\pi}{n}(k)} = S_n.$$

Now we show that $h(\pi/4) > g(\pi/4)$. We have $h(\pi/4) = 2\sqrt{2}$.

$$g_n(\frac{\pi}{4}) = \frac{1}{S_n}\sum_{k=1}^{n}\frac{c_k^2}{(1-\frac{1}{2}c_k^2)^{3/2}} \leq \frac{1}{S_n}\sum_{k=1}^{n}\frac{c_k^2}{(1/2)^{3/2}} = \frac{2\sqrt{2}}{S_n}\sum_{k=1}^{n}c_k^2 = \frac{2\sqrt{2}}{S_n}\frac{n}{2} \leq 2\sqrt{2},$$

where we use the fact $S_n = \sum_{k=1}^{n-1}\frac{1}{\sin\frac{\pi}{n}(k)} \geq n-1$ at the last step.

Finally we show non-degeneracy. Since

$$V''(\phi) = \frac{S_n}{4}(\cos 2\phi(h(\phi) - g_n(\phi)) + \frac{1}{2}\sin 2\phi(h'(\phi) - g_n'(\phi))),$$

$V''(0) = \frac{S_n}{4}(h(0) - g(0)) < 0$, and $V''(\phi_*) = \frac{S_n}{8}\sin 2\phi_*(h'(\phi_*) - g_n'(\phi_*))) > 0$.

□

Now we study the function $\frac{W'(\phi)}{W(\phi)}$. See figure 4.8(b) for its graph.

Lemma 4.5.4.

(i) ***Condition (N1)*** $\frac{W'(\phi)}{W(\phi)} \leq 0$ *for* $\phi \in [0, \pi/2)$.

(ii) ***Condition (N2)*** *Let* $n \geq 10$. *Then* $|\frac{W'(\phi)}{W(\phi)}| \leq \frac{4}{5}$ *for* $\phi \in [\pi/4, \pi/2)$.

Proof. Since $W(\phi) = \frac{S_n}{4} + \frac{\cos\phi}{4}\sum_{k=1}^n \frac{1}{\sigma_k}$, we have $4W'(\phi) = -\sin\phi\sum_{k=1}^n \frac{1}{\sigma_k^3}$. Clearly, $W(0) = \pi/4$, $W'(\phi) \le 0$ and $W(\phi) > 0$ in $[0, \pi/2)$.

We then show that $4|W'(\phi)| \le \delta n/\pi$ for $\phi \in [\pi/4, \pi/2)$, where $\delta = 3.83$. We write

$$4|W'(\phi)| = \sum_{k=1}^n \frac{\sin\phi}{(1 - c_k^2\cos^2\phi)^{3/2}}, c_k = \cos\frac{\pi(2k-1)}{2n},$$
$$f_\phi(x) = f(x;\phi) := \frac{\sin\phi}{(1-\cos^2 x\cos^2\phi)^{3/2}},$$

then $f_\phi(x)$, as a function of x, is Riemann integrable over the interval $[0, \pi/2]$. Since $f_\phi(x)$ is decreasing in $[0, \pi/2]$ and increasing in $[\pi/2, \pi]$, we have

$$\frac{\pi}{n}\sum_{k=1}^n f_\phi(\frac{2k-1}{2n}\pi) + \frac{\pi}{n}f_\phi(\frac{\pi}{2}) \le \int_0^\pi f_\phi(x)dx := h(\phi),$$

where the expression on the left-hand side equals the lower Riemann sum of the integral.

To find the maximum of $h(\phi)$, we write

$$f(x;\phi) = -\frac{d}{d\phi}\frac{\cos\phi}{\sqrt{1-\cos^2 x\cos^2\phi}}.$$
$$\begin{aligned}\frac{1}{2}h(\phi) &= \int_0^{\frac{\pi}{2}} f(x;\phi)dx = -\frac{d}{d\phi}\int_0^{\frac{\pi}{2}} \frac{\cos\phi}{\sqrt{1-\cos^2 x\cos^2\phi}}dx \\ &= -\frac{d}{d\phi}\cos\phi K(\cos^2\phi) = \frac{1}{\sin\phi}E(\cos^2\phi) \\ &= E(-\cot^2\phi),\end{aligned}$$

where the elliptic integrals are defined by

$$K(m) = \int_0^{\frac{\pi}{2}} \frac{1}{\sqrt{1-m\cos^2\theta}}d\theta, \quad E(m) = \int_0^{\frac{\pi}{2}} \sqrt{1-m\sin^2\theta}d\theta,$$

and we use the fact that

$$\frac{dK(m^2)}{dm} = \frac{E(m^2)}{m(1-m)} - \frac{K(m^2)}{m}.$$

Therefore, the maximum of $h(\phi)$ in $[\pi/4, \pi/2)$ is at $h(\pi/4) = 2E(-1) \approx 3.82 < \delta$.

This implies that $4|W'(\phi)| \le \delta n/\pi$. On the other hand, $4W(\phi) \ge S_n$. Therefore,

$$|\frac{W'(\phi)}{W(\phi)}| \le \frac{\delta}{\pi}\frac{n}{S_n} < \frac{4}{5}, \tag{4.19}$$

provided $\frac{S_n}{n} > \frac{5\delta}{4\pi} > 1.524$. The numerical estimate of the sequence S_n/n is included in Appendix.

□

We still need to prove that $v_2 > 0$ in the case $2 \le n \le 9$, when the condition (N3) is either untrue or not verified. First, the case $n = 2$ is the so called tetrahedral 4-body problem, in which the flow on the collision manifold has been studied in [11], where its theorem 1 implies that $v_2 > 0$. As for the cases left, we have verified the condition (N3') stated in lemma 4.4.1(iv). We compute the value of $g_3(\pi/2)$, where g_3 is the solution of (4.14). The result is summarized in the following table. One sees that $g_3(\pi/2) \ge \beta_1 = -1.32$ for $3 \le n \le 9$. This implies that $v_2 > 0$.

n	2	3	4	5	6	7	8	9
$g_3(\pi/2)$	-1.41124	-1.28340	-1.21070	-1.16294	-1.12866	-1.10259	-1.08191	-1.06499

Lemma 4.5.5. ***(N3)*** *Let $n \ge 2$. Then $V(\phi_R) \ge \sin^2 \frac{\phi_R - \phi_m}{2} V(\phi_m)$.*

Proof. Since $\phi_R \in (0, \pi/4)$, $\phi_m = 0$ and $\sin^2 \frac{\phi_R - \phi_m}{2} \sin^2 \le \frac{\pi}{8} \le \frac{1}{4}$, it is sufficient to show that $4V(\phi_R) \ge V(0)$.

Clearly, from (4.17), $4V(\phi_R) \ge S_n$. When $n = 2$, $4V(\phi_R) \ge S_n = 1$ and $V(0) = \frac{1+2\sqrt{2}}{4} < 1$, so $4V(\phi_R) \ge V(0)$. We then consider the case when $n \ge 3$.

Write

$$4V(0) = S_n + \sum_{k=1}^{n} \frac{1}{\sin \frac{\pi}{2n}(2k-1)} = \sum_{k=1}^{n-1} s_k + \sum_{k=1}^{n} a_k,$$

where $s_k = \csc \frac{\pi}{n} k \ge 0$ and $a_k = \csc \frac{\pi}{2n}(2k-1) \ge 0$.

It is sufficient to show that $a_k \le 2s_k$ for $k = 1, \cdots, n-2$ and that $a_{n-1} + a_n < 3s_{n-1}$. Since if these two conditions are true, then $\sum_{k=1}^{n} a_k < 3 \sum_{k=1}^{n-1} s_k = 3S_n$, and therefore $4V(0) < 4S_n$. This implies that $4V(\phi_R) \ge V(0)$.

Now we show that $a_k \le 2s_k$ for $k = 1, \cdots, n-2$.

$$\begin{aligned} 0 \le \frac{a_k}{s_k} &= \frac{\sin \frac{2k}{2n}\pi}{\sin \frac{2k-1}{2n}\pi} = \frac{\sin \frac{2k-1}{2n}\pi \cos \frac{\pi}{2n} + \cos \frac{2k-1}{2n}\pi \sin \frac{\pi}{2n}}{\sin \frac{2k-1}{2n}\pi} \\ &= \cos \frac{\pi}{2n} + \cos \frac{(2k-1)\pi}{2n} \frac{\sin \frac{\pi}{2n}}{\sin \frac{2k-1}{2n}\pi} \le 2. \end{aligned}$$

Finally, we show that $a_{n-1} + a_n < 3s_{n-1}$. Since $\frac{a_n}{s_{n-1}} = 2\cos\frac{\pi}{2n} \leq 2$ and $\frac{a_{n-1}}{s_{n-1}} = \sin\frac{2\pi}{2n}\csc\frac{3\pi}{2n} < 1$ when $n \geq 3$, therefore, $a_{n-1} + a_n < 3s_{n-1}$.

□

Finally, we formally state the conclusion.

Theorem 4.5.6. *In the equal-mass spatial double-polygon problem, when $n \geq 2$, there exist $\mathcal{B}-$family and $\mathcal{Z}1-$family periodic orbits. If moreover, the hypothesis $v_2 \neq -v_3$ is true, then there exist $\mathcal{Z}5-$family, less-symmetric $\mathcal{B}-$family, and $\mathcal{ZB}-$family periodic orbits as well.*

4.5.3 The planar double-polygon problem

The configurations of the planar double-polygon problem consist of two regular $n-$gons centered both at the origin and different by a rotation of angle $\frac{2\pi}{2n}$. We denote the distance between any vertex on the two polygons to the origin by q_1 and q_2 respectively. See table 4.2.

The Lagrangian of this system is

$$L(q_1, q_2, \dot{q_1}, \dot{q_2}) = \frac{S_n}{4}(\frac{1}{q_1} + \frac{1}{q_2}) + \sum_{k=1}^{n}\frac{1}{r_k} + \frac{1}{2}(\dot{q_1}^2 + \dot{q_2}^2), \tag{4.20}$$

where $r_k^2 = q_1^2 + q_2^2 - 2q_1q_2\cos l_{2k-1}$.

Note that q_1 and q_2 are non-negative. So we define the size variable by $r^2 = q_1^2 + q_2^2$ and the shape variable $\theta \in (-\infty, \infty)$ by

$$q_1 = r\frac{\sqrt{\cos^2\theta + 1} - \sin\theta}{2}, \quad q_2 = r\frac{\sqrt{\cos^2\theta + 1} + \sin\theta}{2}.$$

Then

$$L(r, \dot{r}, \theta, \dot{\theta}) = \frac{1}{2}\dot{r}^2 + \frac{1}{2}r^2\dot{\theta}^2\frac{\cos^2\theta}{1 + \cos^2\theta} + \frac{1}{r}V(\theta),$$

where $V(\theta) = \frac{S_n}{2}\frac{\sqrt{\cos^2\theta+1}}{\cos^2\theta} + \sum_{k=1}^{n}\frac{1}{\sqrt{1-\cos^2\theta\cos l_{2k}}}$.

In Devaney's coordinates, clearly $\phi_a = 0, \phi_b = \pi/2$, and Martínez [18] has shown that $V(\phi)$ has a unique critical point at $\phi = 0$ if $n = 2$. Moreover, if $n \geq 3$, then $V(\phi)$ has three non-degenerate critical points $\phi_L < \phi_m < \phi_R$, $\phi_m = \pi/4$, and $\phi_R \in (\pi/4, \arctan(2))$.

To prove the existence of Shubart-like orbits, Martínez has successfully verified the conditions (M1,M2); however, the condition (M3) fails. Nonetheless, the conditions (M1,M2) imply our conditions (N1,N2), which are sufficient to guarantee the existence of Schubart-like periodic orbits.

To furthermore prove the existence of other periodic orbits, we need to show that $v_2 > 0$. However, for $3 \leq n \leq 20$, we numerically study the two important branches γ, γ' as shown in figure 4.10, and find that $v_2 < 0$ and $v_3 < 0$. So our shooting arguments do not work here. Nonetheless, the figure suggests that γ and γ' can reach $\theta = \pi/2$ and that their intersections with $\theta = \pi/2$ have $v_4 > 0$ and $v_5 < 0$ respectively. This suggests the existence of another type of periodic orbits, namely type 2 periodic brake orbits, by Theorem 5.5 of [7]. At this point we are unable to prove that $v_4 > 0, v_5 < 0$ rigorously; we leave it for further investigation.

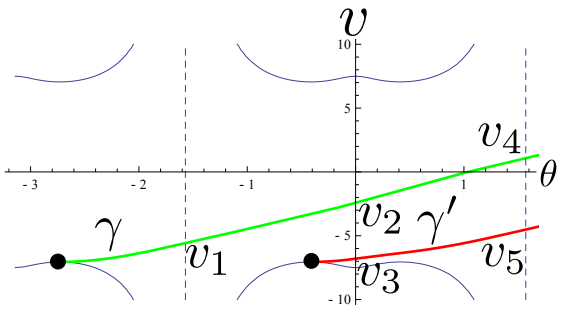

Figure 4.10: The branches γ, γ' for the planar double-polygon problem with $n = 10$.

Finally, we formally state the conclusion.

Theorem 4.5.7. *In the equal-mass planar double-polygon problem, when $n \geq 3$, there exists a Shubart-like orbit in $\mathcal{B}-$family with $k = 0$.*

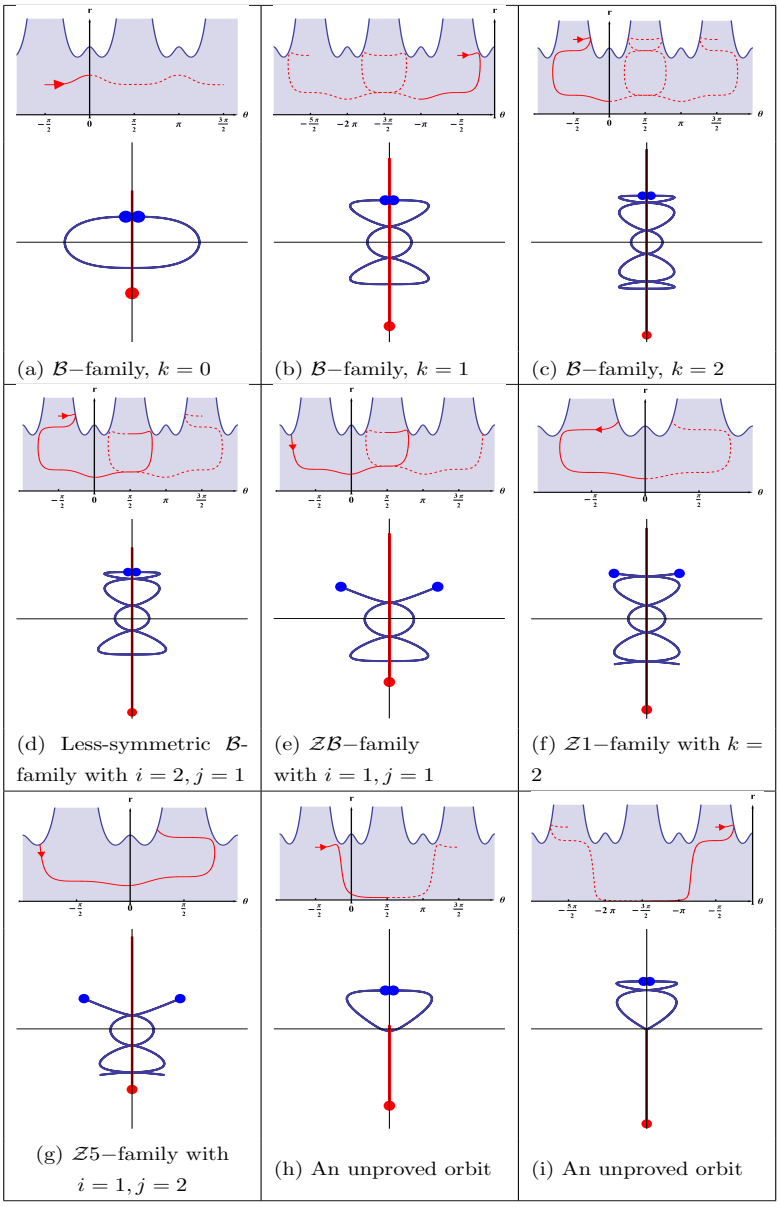

(a) $\mathcal{B}-$family, $k=0$ (b) $\mathcal{B}-$family, $k=1$ (c) $\mathcal{B}-$family, $k=2$

(d) Less-symmetric $\mathcal{B}$-family with $i=2, j=1$ (e) $\mathcal{ZB}-$family with $i=1, j=1$ (f) $\mathcal{Z}1-$family with $k=2$

(g) $\mathcal{Z}5-$family with $i=1, j=2$ (h) An unproved orbit (i) An unproved orbit

Table 4.1: Periodic orbits and their projection in the $(\theta, r)-$plane. For the projection in the $(\theta, r)-$plane, the fundamental domain of each orbit is plotted in solid curve; one may obtain the full orbit by symmetries.

The problem (all equal-mass)	n-pyramidal problem	Spatial double-polygon problem	Planar double-polygon problem
Number of masses	$n+1$	$2n$	$2n$
The configuration	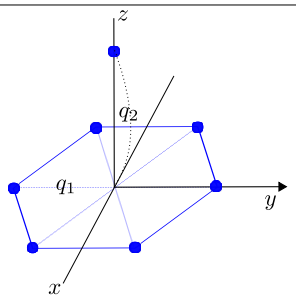	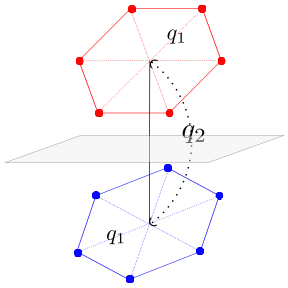	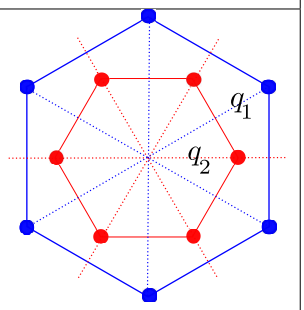
$V(\phi)$ has three critical points	when $2 \leq n < 473$	when $n \geq 2$	when $n \geq 3$
$v_1 < 0$	true	true	true
$v_2 > 0$	true	true	not true in general
$v_3 < 0$	true	true	true
Martínez (M1)	proved in [18]	not verified; new problem	proved in [18]
Martínez (M2)	proved in [18]	not verified; new problem	proved in [18]
Martínez (M3)	verified in [18]	not verified; new problem	(M3) fails
Martínez (M4)	computed in [19] only for some n	not verified; new problem	computed in [19] only for some n
Condition (N1)	holds	holds	not applicable
Condition (N2)	holds, since (M2) holds	holds	holds, since (M2) holds
Condition (N3)	proved true for $n \geq 4$	numerically true for $n \geq 7$ proved true for $n \geq 10$	not applicable
Condition (N3')	numerically verified for $n = 2, 3$	case $n = 2$ is treated in [11] numerically verified here for $3 \leq n \leq 9$	not applicable
Orbits proved to exist	$\mathcal{B}-$family $\mathcal{Z}1-$family	$\mathcal{B}-$family $\mathcal{Z}1-$family	$\mathcal{B}-$family with $k = 0$
Additional families if (N4) holds	Less-symmetric $\mathcal{B}-$family $\mathcal{Z}5-$family $\mathcal{ZB}-$family	Less-symmetric $\mathcal{B}-$family $\mathcal{Z}5-$family $\mathcal{ZB}-$family	none is proved
Other cases (unequal-mass):	(1) Isosceles three-body problem. $m_1 = m_2 = 1, m_3 = \mu$, for $\epsilon_1 \approx 0.379 < \mu < \epsilon_2 \approx 2.662$, there exist Type 1 to 6 periodic brake orbits, $\mathcal{B}-$family, $\mathcal{ZB}-$family, and less-symmetric $\mathcal{B}-$family Schubart-like periodic orbits. (2) n-pyramidal problem. $m_1 = m_2 \cdots = m_n = 1, m_{n+1} = \mu$, for any $\mu < 0$, there exists a $\mathcal{B}-$family Schubart-like orbit with $k = 0$.		

Table 4.2: Summary of Results

4.6 Appendix

The appendix includes the properties of the series S_n/n.

We recall that $S_n = \sum_{k=1}^{n-1} \csc \frac{\pi}{n} k$. The series S_n has been carefully analyzed in [25], where the authors provided an asymptotic expansion of $S_n/4$ for n large:

$$\frac{S_n}{4} \approx \frac{n}{2\pi}(\gamma + \log \frac{2\pi}{n}) - \frac{\pi}{144n} + \frac{7\pi^3}{86400n^3} - \frac{31\pi^5}{7620480n^5} := \tilde{A}_n, \tag{4.21}$$

where $\gamma \approx 0.5772156649$ is the Euler-Mascheroni constant, and the approximation has a relative error less than 10^{-6} for $n \geq 47$. Letting $F(n) := \frac{\tilde{A}_n}{n}$, then $F(n)$ is an increasing function. Martínez [18] has numerically computed some values of $\frac{S_n}{4n}$ and $F(n)$, which provide a strong evidence that S_n/n should be an increasing sequence.

In this paper, we have assumed the fact that $\frac{S_n}{n} > 1.524$ for $n \geq 10$ in (4.19).

Acknowledgments

The author thanks the anonymous referee, Richard Moeckel, and Regina Martínez for their critical reading of this paper and their valuable comments. This research was supported by NSF grant DMS-1208908.

References

[1] A. Albouy and V. Kaloshin, Finiteness of central configurations of five bodies in the plane, *Ann. of Math.*, **176** (2012), 535–588.

[2] G. D. Birkhoff, The restricted problem of three bodies, *Rend. Circolo. Mat. Palermo*, **39** (1915), 255–334.

[3] S. Bolotin, Libration motions of natural dynamical systems, *Vestnik Moskov Univ. Ser. I. Mat. Mekh.*, **6** (1978), 72–77.

[4] R. Broucke, On the isosceles triangle configuration in the planar general three body problem, *Astron. Astrophys.*, **73** (1979), 303–313.

[5] H. Bruns, Über die integrale des vielkörper-problems, *Acta Math.*, **11** (1887), 25–96.

[6] K.-C. Chen, Existence and minimizing properties of retrograde orbits to the three-body problem with various choices of masses, *Ann. of Math.*, **167** (2008), 325–348.

[7] N.C. Chen, Periodic brake orbits in the planar isosceles three-body problem, *Nonlinearity*, **26** (2013), 2875–2898.

[8] N.C. Chen, Symmetric periodic orbits in three sub-problems of the N-body problem, *Discrete Contin. Dyn. Syst. Ser. B.*, **19** (2014), 1523–1548.

[9] A. Chenciner and R. Montgomery, A remarkable periodic solution of the three body problem in the case of equal masses, *Ann. of Math.*, **152** (2000), 881–901.

[10] A. Chenciner and A. Venturelli, Minima de lintégrale daction du problème newtonien de 4 corps de masses égales dans $\mathbf{R}^3$: orbites "hip-hop", *Celestial Mech. Dynam. Astronom.*, **77** (2001), 139–152 (2001).

[11] J. Delgado and C. Vidal, The tetrahedral 4-body problem, *J. Dynam. Differential Equations*, **11** (1999), 735–780.

[12] R. Devaney, Triple collision in the planar isosceles three body problem, *Invent. Math.*, **60** (1980), 249–267.

[13] D. Ferrario and S. Terracini, On the existence of collisionless equivariant minimizers for the classical n-body problem, *Invent. Math.*, **155** (2004), 305–362.

[14] D. Ferrario and A. Portaluri, On the dihedral n-body problem, *Nonlinearity*, **21** (2008), 1307–1321.

[15] M. Hampton and R. Moeckel, Finiteness of relative equilibria of the four-body problem, *Invent. Math.*, **163** (2006), 289–312.

[16] C. Liu and D. Zhang, Seifert conjecture in the even convex case, *Comm. Pure Appl. Math.*, (2014).

[17] A. Lyapunov, Problème général de la stabilité du mouvement, *Ann. Math. Studies*, **17**, Princeton Univ. Press. Princeton N J, (1947). (Reproduction of 1892 monograph)

[18] R. Martínez, On the existence of doubly symmetric "Schubart-like" periodic orbits, *Discrete Contin. Dyn. Syst. Ser. B*, **17** (2012), 943–975.

[19] R. Martínez, Families of double symmetric 'Schubart-like' periodic orbits, *Celest. Mech. Dyn. Astr.*, **117** (2013), 217–243.

[20] J. Mather and R. McGehee, *Solutions of the collinear four body problem which become unbounded in finite time*, in "Lecture Notes in Physics" (ed. J. Moser), Berlin-New York, Springer-Verlag, (1975), 575–597.

[21] R. McGehee, Von Zeipel's theorem on singularities in celestial mechanics, *Expositiones Mathematicae*, **4** (1986), 335–345.

[22] R. McGehee, Triple collision in the collinear three-body problem, *Invent. Math.*, **27** (1974), 191–227.

[23] K. R. Meyer, Periodic solutions of the N-body problem, *Lectures on Celestial Mechanics*, **1719**, Springer-Verlag, New York, (1971).

[24] R. Moeckel, R. Montgomery and A. Venturelli, From brake to syzygy, *Arch. Ration. Mech. Anal.*, **204** (2012), 1009–1060.

[25] R. Moeckel and C. Simó, Bifurcation of spatial central configurations from planar ones, *SIAM J. Math. Anal.*, **26** (1995), 978–998.

[26] R. Moeckel, A topological existence proof for the Schubart orbits in the collinear three-body problem, *Discrete Contin. Dyn. Syst. Ser. B*, **10** (2008), 609–620.

[27] R. Montgomery, Infinitely many syzygies, *Arch. Ration. Mech. Anal.*, **164** (2002), 311–340.

[28] R. Montgomery, The zero angular momentum, three-body problem: all but one solution has syzygies, *Ergod. Theory Dyn. Syst.*, **27** (2007), 1933–1946.

[29] J. K. Moser, Regularization of Kepler's problem and the averaging method on a manifold, *Comm. Pure Appl. Math.*, **23** (1970), 609–635.

[30] P. Painlevé, Leçons sur la théorie analytique des équations différentielles: professées à Stockholm (septembre, octobre, novembre 1895), Paris: Hermann, (1897).

[31] H. Poincaré, *Les methodés nouvelles de la mécanique céleste*, Gauthier-Villars, Paris, (1892).

[32] P. Rabinowitz, Periodic solutions of hamiltonian systems: a survey, *SIAM J. Math. Anal.*, **13** (1982), 343–352.

[33] P. Rabinowitz, Periodic solutions of hamiltonian systems, *Comm. Pure Appl. Math.*, **31** (1978), 157–184.

[34] G. Roberts, Linear stability analysis of the figure-eight orbit in the three-body problem *Erg. the. and Dyn. Syst.*, **27** (2009), 1947–1963.

[35] O.R. Ruiz, *Existence of Brake-Orbits in Finsler Mechanical Systems*, U.C. Berkeley thesis in Mathematics, (1975).

[36] D. S. Schmidt, Periodic solutions near a resonant equilibrium of a Hamiltonian system, *Celest. Mech.*, **9** (1974), 91–103.

[37] J. Schubart, Numerische Aufsuchung periodischer Lösungen im Dreikörperproblem, *Astron. Nachr.*, **283** (1956), 17–22.

[38] C. L. Siegel and J. K. Moser, *Lectures on Celestial Mechanics*, Springer-Verlag, New York, (1971).

[39] M. Shibayama and K. Yagasaki, Heteroclinic connections between triple collisions and relative periodic orbits in the isosceles three-body problem *Nonlinearity*, **22** (2009), 2377–2403.

[40] M. Shibayama, Minimizing periodic orbits with regularizable collisions in the n-body problem, *Arch. Ration. Mech. Anal.*, **199** (2011), 821–841.

[41] C. Simó, *Analysis of triple collision in the isosceles problem*, in "Classical Mechanics and Dynamical Systems" (eds. R L Devaney and Z H Nitecki), New York: Marcel Dekker, (1981), 203–224.

[42] C. Simó and R. Martínez, Qualitative study of the planar isosceles three-body problem, *Celest. Mech. Dyn. Astr.*, **41** (1987), 179–251.

[43] C. Simó, New families of solutions in N-body problems, in "European Congress of Mathematics Vol. I", volume 201 of Progr. Math., 101–115, Birkhäuser, Basel, 2001.

[44] S. Smale, Mathematical problems for the next century, *Math. Intelligencer*, **20** (1998), 7–15.

[45] E.W. C., van Groesen, Analytical mini-max methods for Hamiltonian brake orbits of prescribed energy, *J. Math. Anal. Appl.*, **132**,(1988), 1–12.

[46] A. Venturelli, A variational proof of the existence of von Schubarts orbit, *Discrete Contin. Dyn. Syst. Ser. B*, **10** (2008), 699-717.

[47] A. Weinstein, Periodic orbits for convex Hamiltonian systems, *Ann. of Math. (2)*, **108** (1978), 507–518.

[48] Z. Xia, The existence of noncollision singularities in newtonian systems, *Ann. of Math. (2)*, **135** (1992), 411–468.